ORIGIN OF POROSITY IN CAST METALS.

A Thesis
submitted for the Degree of
Doctor of Philosophy
under Special Regulations.

by

JOHN CAMPBELL, M.A.(Cantab.), M.Met.(Sheffield).

Department of Industrial Metallurgy,
University of Birmingham.

February 1967.

PAGE NUMBERING AS ORIGINAL

SYNOPSIS

A literature survey on the whole field of pore formation is assembled into the form of a general theory of the causes of porosity in castings. The conventionally accepted modes of feeding are assessed: liquid-, mass-, and interdendritic-feeding; and two further mechanisms are proposed: burst- and solid-feeding. The latter is investigated theoretically using various flow models: elastic-plastic, viscous, creep and Bingham flow. A new theory is proposed for the origin of layer porosity in castings. Experimental work on a wide variety of alloys: Al-Cu, Fe-C, Complex Ni- and Co-base alloys, cast both in air and in vacuum are investigated for the effect of section thickness, taper, and mould and metal temperatures. The formation of porosity appears to change from a non-nucleation to a nucleation mechanism as section thickness increases. A new method of interpreting radiographs based upon a longitudinal line count reveals that solid feeding becomes important in reducing porosity at high mould temperatures. Experiments on the effect of composition of an alloy on porosity cast doubt on the widely accepted theory that the presence of non-equilibrium eutectic liquid reduces porosity, but indicate that the non-equilibrium freezing range of the alloy may be the critical parameter. The effect of pressure on porosity is investigated utilising pressures below atmospheric; the results are inadequately explained by current theories and are discussed in terms of the nucleation and growth of pores; the effect would also appear to have considerable industrial potential for reducing porosity in vacuum cast components.

ACKNOWLEDGEMENTS.

The author is indebted to his supervisor, Dr. V. Kondic, for much helpful criticism and for the reading of this manuscript; to Dr. G.E.J. Bennett for discussions on the thermodynamic aspects of this work; to Professor P. Chadwick and Dr. G.W. Rowe for help with plasticity problems; to Professor E.C. Rollason for the provision of the facilities of the Aitchison Laboratory; to the Ministry of Aviation for financial support of part of the work, and to the University of Birmingham for the grant of a Research Fellowship.

CONTENTS

FIGURES.

TABLES.

LIST OF SYMBOLS

A	Area
a_i	Length of side of cubic inclusion
a_c, a_o	activity of carbon, oxygen
a , a_o	radius of liquid core ; unstrained.
α, α_S, α_L	solidification shrinkage; volumetric contraction in solid and liquid states
α'	$(\alpha/1 - \alpha)$ approximately equal to α
b	ext. radius of a spherical or cylindrical casting
c	radius of plastic zone
C, C_S, C_L C_o, C_c, C_i	Concentration of a solute, in a solid, in a liquid, original concentration in a liquid, critical concentration of inclusion material (wt. fraction)
C_{max}	maximum at a solidification front
γ, γ_{LS}, γ_S	surface energy between phases: liquid-vapour; liquid-solid; solid-vapour
d	distance of bubble centre from the liquid-solid interface (Fig. 21a.)
d_o	Radius of liquid-solid interface of spherical casting at the instant of cut-off of supply of feeding liquid
E	Young's modulus
ϵ	Strain
f_L	fraction of residual liquid
ϕ	$(2 - \cos\theta)(1 + \cos^2\theta)/4$
G_L, G_S	bulk modulus of liquid and solid
g	acceleration due to gravity
H	Latent heat of fusion
h	Plank's constant (taken as 6.62×10^{-27} cgs)
K_S, K_L	Solubility or Sievert's constant for solid and liquid
K	Boltzmann constant (taken as 1.33×10^{-16} cgs)
L	width of pasty zone
L'	Function of length and width of flow channel
λ	Heat Flow Constant $q'(T_f - T_o)/H\rho_S(\pi q)^{\frac{1}{2}}$
M	Mass of a casting
M_L, M_i	Molecular Weight of liquid, inclusion
m	mass
m_1, m_2	wetting parameter equal to $\cos\theta_1$ and $\cos\theta_2$ respectively

η	viscosity of solid
μ	viscosity of liquid
N	Avogadro's Number (taken as 6.02×10^{23})
n	number of channels/unit area (= 1/(Dendrite Arm Spacing)^2)
n_i	number of inclusions/mole of liquid
$P_a, P_b, P_e, P_f, P_f', P_g, P_i, P_m, P_s, P_v$	Pressure: applied at liquid surface; burst threshold; external acting on a bubble surface; fracture of liquid; fracture at solid-liquid interface; total due to gas; internal acting on a bubble surface; maximum pressure to which melt has been subjected; due to shrinkage; vapour pressure (usually at the freezing point of the liquid).
Q_{Total}	Total heat content of metal-mould system.
Q	Activation Energy
q	thermal diffusivity of mould
q'	thermal conductivity of mould
R	Gas Constant
R_v	radius of the perimeter of a forced vortex
r, r^*, r_i, r_v	radius: critical radius of a bubble; minimum radius of an inclusion; radius of the core of a forced vortex
$\rho, \rho_i, \rho_L, \rho_S, \rho_W$	density of porous solid, inclusion, liquid (normally at its freezing point), sound solid, water.
s_1, s_2	specific heat of metal; mould
$\dot{s}$	shear strain rate
$T, T_e, T_f, T_i, T_L, T_m, T_o, T_p, T_s$	Temperature: of eutectic reaction; freezing; metal-mould interface, liquidus; mould; ambient; pouring; solidus
ΔT_f, ΔT_s	Freezing range Equilibrium = $(T_L - T_S)$, Non-equilibrium = $(T_L - T_e)$; Superheat = $(T_e - T_L)$ or $= (T_p - T_f)$
$t, t_s, \Delta t$	time; solidification time after casting; solidification interval (temp. between T_L and T_s)
Γ	the circulation of a vortex; a measure of its intensity
τ, τ_c	shear stress, critical (or yield) shear stress
τ_o	tortuosity factor (value between 1 and 2).
θ	contact angle
V, V_o	Volume; original volume of a trapped liquid region
v	velocity
x	length variable
Y	yield stress
z	proportionality constant (various)

INTRODUCTION.

The phenomena surrounding the origin of porosity in cast metals are inadequately understood in detail so the first part of this work is devoted to a scientific analysis of the mechanisms involved. The problem of porosity is approached throughout as a nucleation-and-growth phenomenon.

The experimental approach recorded in the remainder of this work has aimed to provide some critical measurements of the effects of the main variables on porosity since there is a dearth of experimental data in this field, particularly for thin investment castings, from which empirical solutions for dealing with immediate production problems could be obtained.

Regarding the theoretical background to this work some introductory explanation may be helpful.

An important concept used in this work is negative pressure. This is equivalent to a tensile stress in the residual liquid of a casting and provides part of the driving force for both the nucleation and the growth processes of a pore (dissolved gas in the liquid provides the rest of the driving force). Negative pressures have been generated in controlled experiments on liquids by many ways[202] and is a well-known condition giving rise to cavitation in sea water on a ship's propeller, and during the rarefaction cycle of an ultrasonic wave passing through a liquid. Hydrostatic tension is also a well-known cause of pores in the solid state: during the final stages of testing of a tensile specimen of a ductile metal, localised deformation occurs which causes the stress system in the specimen to depart from its simple uniaxial form and to become triaxial, resulting in the nucleation and growth of cavities.

A general view of the origin of microporosity which is widely recorded in the literature[203-205] is that pores

form simply by shrinkage and subsequently fill with gas which prevents further liquid healing the pores. However this is fundamentally incorrect for as will be shown later, shrinkage alone is unlikely to nucleate a pore, and secondly, if gas is present at all then elementary thermodynamics and kinetics demand that the gas phase must contribute to the nucleation process. Finally, once the pore has nucleated and expanded to reduce the elastic energy of the liquid-solid mass, then under normal conditions the pore will not fill with liquid again since this process would again raise the free energy of the system (the strain energy which must be supplied to the casting can easily be shown to be vastly in excess of the surface energy of the pore which would be destroyed).

In considering the difficulties of feeding liquid through a dendrite mesh many authors[205] invoke terms such as 'capillary forces'. An application of elementary physics will demonstrate that such forces are fictitious since before bubble nucleation no free surfaces exist, and after nucleation the freezing liquid invariably exhibits a zero contact angle towards the solid phase so again flow is unhindered by surface phenomenon[220]. Flow is impeded of course by viscous forces as will be discussed later.

On these grounds therefore, the above mentioned theories of porosity formation will not be further considered in the present work, and instead a fresh approach will be put forward.

A field of pore formation which is beyond the scope of the present work is of the initiation of pores under the high gas pressures resulting from various chemical reactions, particularly in mould-metal reactions, resulting in surface and subsurface blowholes. Also deserving

mention is the paper by Flinn[206] on the qualitative evaluation of the susceptibility of various alloys to shrinkage defects but this is an empirical test which is not easy to explain and again not really relevant to this work.

SECTION 1.

DISCUSSION ON TERMINOLOGY.

1.1. Gas and Shrinkage Porosity.

Throughout this work no distinction will be drawn between porosity due to gas and that due to shrinkage[13]. Both are cooperative in their effects upon nucleation growth and final size of a pore. The exact contribution of each will vary as a result of many factors, particularly the gas content of the solidifying liquid. Dissolved gases cannot be entirely eliminated from liquids.

1.2. Macroporosity.

Although it is feasible that a large cavity in a poorly fed casting could be the result of excessive gas content of the melt, most metals are degassed tolerably effectively prior to casting, and the final size of a large cavity in a skin freezing metal (i.e., a metal having negligible freezing range) is in general due to shrinkage. In a long freezing range alloy freezing under similar conditions, a rather more extensive spongy volume of completely interconnected interdendritic cavities results, bearing some resemblance to severe microporosity. However, the cavity is better described as a macropore (since it is a single cavity) whose morphology has been dictated by the growth of the surrounding solid. Gating and feeding methods are the normal means for controlling the extent of macroporosity.

1.3. Microporosity.

Microporosity is often arbitrarily defined as being porosity which is invisible to the naked eye on a polished section, although colonies of micropores may be seen. However, all grades of pore sizes between macro- and micro-porosity are found, and there is no difference in principle between the nucleation and growth of either. Nevertheless, some differentiation is possible since the

phenomenon occurs exclusively in alloys having a finite freezing range, and in general it is not possible to greatly reduce the percentage porosity due to micropores by conventional feeding. Several forms of microporosity may be distinguished:

1.3.1. Centre line Shrinkage.

In parallel or plate-like sections the porosity is found to be concentrated along the centre line. This form of microporosity is not confined to long freezing range alloys (ΔT_f = 200°C or more) but is in fact accentuated in alloys of intermediate or short freezing range (ΔT_f = 10 to 50°C). Of all forms of micro-porosity, this variety is most closely related to macro-porosity, and thus greatly accentuated by deficiencies in feeding, and exhibiting a large degree of interconnection between pores on the centre line. Since the effect derives directly from solidification geometry dictated by the shape of the casting, the remedy is to be found in geometrical terms: a tapered section greatly reduces centre line shrinkage[7], while unidirectional solidification[8] reduces it very much further.

1.3.2. Layer Porosity.

Commonly observed in sections of light alloys[9] although occasionally revealed in semi-microradiographs of steels. The pores are found to be concentrated in layers parallel to the supposed position of the isotherms in the solidifying mass, and are broadly distributed over the casting section.

1.3.3. Interdendritic Porosity.

Very fine pores, mutually isolated, and broadly distributed over the casting section resulting from micro-regions of trapped liquid between secondary dendrite arms.

2. A GENERAL THEORY OF PORE FORMATION.

2.1. Non-Nucleation.

Fox[248] and some later authors[247-8] suppose that the residual interdendritic liquid drains from the dendrite mesh, leaving a network of interconnected pores which closely resemble the characteristic interdendritic appearance of microporosity when observed in section. This theory presupposes the prior existence of a free liquid surface, such as at an ingot top (in which case the so-called microporosity is merely an extension of the primary pipe) or adjacent to a previously formed macropore; in fact anywhere where the solidus isotherm intersects a free surface of the casting at a late stage in freezing. As the internal pressure in the casting falls, the liquid which is still present at the surface of the casting will be sucked into the interior to compensate for the contraction on solidification. The final result is a labyrinth of interconnected channels emerging in surface pinholes. Clearly, alloys of long freezing range will be particularly prone to the formation of porosity by this mechanism, especially in thin sections, at at 'hot spots' such as re-entrant angles (no metal-mould reaction need be invoked to explain the occurrence of pinholes at such locations, as is also suggested by Chalmers[11]).

Air entering, for instance, a steel casting in this manner would not be expected to oxidise (or decarburise) much more than the entrance to the pinhole, since the oxygen would be rapidly used up. Much of the nitrogen would probably also be absorbed 'en route' so that the internal porosity would contain nearly pure argon (and perhaps carbon monoxide) thus preserving the characteristic unoxidised appearance of the central porosity.

2.2 HOMOGENEOUS NUCLEATION.

The condition for bubble stability in a liquid is expressed by the relation

$$P_i - P_e = 2\gamma / r \qquad \ldots.(1)$$

where P_i and P_e are the internal and external pressures respectively acting on the bubble surface. The term $2\gamma / r$ gives the value of the pressure difference across a spherical interface having an energy of γ per unit area, and a radius r.

P_i is the sum of the partial pressures of all the gases and vapours contained in the bubble

$$P_i = \Sigma P_g \qquad \ldots.(2)$$

where for steel $\Sigma P_g = P_{CO} + P_{H_2} + P_{N_2} + P_{H_2O} + P_{CO_2} + P_{Fe}$ etc.

In a liquid at rest, the external pressure, P_e, is the sum of the metallostatic head, P_d, the applied pressure at the liquid surface, P_a (usually 1 atmosphere, or close to zero if in vacuum) and the reduction in pressure due to solidification shrinkage, $-P_s$, Thus

$$P_e = P_a + P_d - P_s \qquad \ldots.(3)$$

substituting (2) and (3) into (1) and re-arranging

$$(P_i - P_e) = (\Sigma P_g + P_s) - (P_a + P_d) = 2\gamma / r \qquad \ldots.(4)$$

Because of the negative sign, it is clear that an increase in $(P_d + P_a)$ tends to suppress bubble formation (although P_d is normally negligible - a pressure of 1 atmosphere is equivalent to a depth of 1.3 m. of liquid steel, or 3.8 m. of liquid Al)(which is a widely appreciated fact often exploited for this purpose by casting under a high applied pressure.) Since P_s is negative and increases negatively the contributions of gas and shrinkage are seen to be additive and to encourage bubble formation.

The bubble nucleation process has generally been approached in terms of the maximum negative pressure that a liquid can withstand before rupture occurs (i.e. a bubble forms) in the liquid. This tensile

strength of the liquid is known as its fracture pressure, P_f, Blake[3] and Wakeshima[4] give critical reviews of some of the theoretical attempts at estimating this quantity; they may be broadly divided into two categories (a) various methods based upon equations of state, particularly Van der Waal's equation, and (b) the nucleation theories. Other theories based on viscosity considerations by Briggs et al.[58] and on energy density considerations by Thorndike[58b] are carefully assessed by Blake who finds the former to be erroneous and the latter to be insufficient.

(a) It was thought that the a/v^2 term from the Van der Waal's equation $(P+ a/v^2)(v - b) = RT$ represented an 'intrinsic pressure' due to the mutual attraction of the molecules of the liquid, and which must be exceeded before fracture could occur. Estimates of this quantity based upon critical constants, and other phenomena such as heat of vapourisation and compressibility all yield values of the order of 10^4 atmospheres for water. In order to obtain more reasonable values, Temperley[5] has argued that P_f is not given by the intrinsic pressure but by the minimum on the Van der Waal's isothermals. Using again critical constants, vapour pressure and compressibility, P_f for water works out at 1000, 6,800, and 1400 atmospheres respectively[4]. a wide spread.

(b) The nucleation theories consider the detailed atomic mechanism of fracture of the liquid. Following Fisher's treatment[3], a definite quantity of work is associated with the reversible formation of a bubble in the interior of a liquid. The creation of a spherical volume of radius r requires work equal to $(4/3)\pi r^3 P_e$. The creation of the liquid-vapour interface requires work equal to $4\pi r^2\gamma$ and the work required to reversibly fill the bubble with vapour (or gas) of pressure P_i is negative and equal to $-(4/3)\pi r^3 P_i$. The net energy required is therefore

$$W = 4\pi r^2\gamma + (4/3)\pi r^3 (P_e - P_i)$$

The variation of W with r can be shown to have a maximum

$$W^* = 16\pi\gamma^3/3 P_f^2$$

corresponding to the critical radius

$$r^* = 2\gamma/P_f$$

where P_f is now the critical value of $(P_e - P_i)$. Bubbles with radii less than r* require free energy for further growth, while those with radii larger than r* grow freely with decreasing free energy. Since bubbles grow as the result of statistical thermal fluctuations of atoms, it is evident that small bubbles with radii less than r* will usually disappear. Only exceptionally will a long chain of favourable energy fluctuations produce a bubble with radius exceeding r*. When this rare event does happen however, the bubble will grow, tending to promote the equalisation of the external and internal pressures.

From the theory of nucleation and reaction rates, Fisher finds that there exists a well defined pressure threshold at which super-critical bubbles will appear in finite time. This is

$$P_f = -\left[\frac{16\pi}{3kT} \cdot \frac{\gamma^3}{\ln (NkT/h)}\right]^{\frac{1}{2}}$$

This statement of Fisher's result neglects a term involving the activation energy for viscous flow of the liquid, which he assumes will be less than 10 k cal/mol for rather fluid liquids. Thus this formula represents the lowest possible strengths from Fisher's theory since if the activation energy for viscous flow is assumed to be 10 k cal/mol, then some 13% increases in these values result[4].

Frenkel[8a] outlines a crude approach (which is heavily criticised by Blake[3]) which gives

$$P_f = -2\gamma/\delta$$

where δ is of the order of an interatomic distance in the liquid. The resulting fracture pressures are, of course, very high (about 10^4 atmospheres for water) and are likely to represent an upper limit to P_f values.

Furth[8b] considers only average-sized embryonic bubbles in the liquid which leads/also therefore to an expression yielding high values for P_f

$$P_f = -\frac{8}{9}\left[\frac{\pi}{K} \cdot \frac{\gamma^3}{T}\right]^{\frac{1}{2}}$$

TABLE 1

Fracture Pressures
(Atmospheres)

Liquid	Surface Tension ergs/cm.	Temp. °K	Furth[18]	Modified Doring[4]	Fisher[3]	Bernath[6]	Maximum Observed[40]
Helium	0.35	1.7	21.3	6.16	6.25	5.09	
Ethyl Ether	17	300	541	161	158	113	
Benzene	29	300	1,210	358	352	284	150
Acetic Acid	28	300	1,150	331	325	262	288
Water	72	300	4,740	1,320	1,380	1,120	270
Mercury	490	300	84,000	23,500	23,100	19,900	425
Aluminium	850	933	108,600	31,300	30,500	25,700	
Copper	1300	1356	170,800	49,100	48,000	40,500	
Iron	1850	1800	252,000	72,300	70,800	60,000	
Rhenium	2700	3430	321,000	91,600	90,500	76,000	

More sophisticated approaches by Kagan[8c] and Döring[7] result in the same formula for P_f but are criticised by Wakeshima[4] on the grounds that the perfect gas law is assumed for the vapour in the bubble. This author produces a modified Döring equation assuming that the vapour in the bubbles is at a constant pressure, although the equation below is not given explicitly in Wakeshima's paper

$$P_f = -\left[\frac{32\,\pi}{3\,kT} \cdot \frac{\gamma^3}{\ln\,(2\gamma\,N^2/\pi m}\right]^{\frac{1}{2}}$$

From quite different considerations showing that the frequency of nucleus formation depends upon the molecular latent heat of vapourisation, Bernath[6] finds a relation which requires a trial-and-error solution for P_f since this quantity appears also inside the logarithm:

$$P_f = -\left[\frac{9.06}{kT} \cdot \frac{\gamma^3}{\ln \frac{(1.45\,\rho\,N^2\,\gamma^2)}{P_f\,(M^3\,RT)^{\frac{1}{2}}} \cdot \frac{H}{kT}}\right]^{\frac{1}{2}}$$

For most liquids between temperatures about 100 and 2000°C the formulae due to Fürth, modified Döring, Fisher and Bernath become approximately

$$P_f = -A\,(\gamma^3/T)^{\frac{1}{2}}$$

where A is respectively about 134, 38.4, 37.7 and ∿32, when pressure is in atmospheres, temperature in °K, and surface tension in dynes/cm. The reduced form of Fisher's equation is used throughout this paper, although for comparison, the fracture pressures of a wide range of liquids are given in Table 1.

Although the nucleation theories are likely to describe reality a good deal closer than an approach from any of the equations of state, and certainly the agreement amongst the more refined theories is good, yet they are all open to criticism since they all assume relation (1) which may well be inaccurate for bubbles of atomic dimensions (the critical embryonic radius lies between 2 and 5 atomic radii for practically all liquids) since apart from the fact that

such bubbles may approximate poorly to a spherical form, causing r to be uncertain and the whole theoretical model to be ill-founded, more important still, for bubbles smaller than about 10-50 atomic radii surface tension is progressively reduced and may become negligible for bubbles of one atom radius.

This variation of surface tension with radius is investigated theoretically by several authors[193-200] but is critically applied to bubble nucleation only by Wakeshima[4] who produces some modified values of P_f deduced from van der Waal's equation. These P_f values are chosen for modification because of a 'maximum' and 'minimum' pressure concept which arises in his analysis which are tentatively identified with the turning points on the van der Waal isotherms. This attempt to apply this analogy in a consistent way unfortunately neglects the fact that the equation of state approach can never yield accurate P_f values since also the maximum pressure term disappears from the equations anyway it would obviously be better to introduce a minimum pressure as derived from one of the better nucleation theories. The application of Wakeshima's analysis is complicated, however, and is not pursued here - modified values would possibly be a factor of 2 lower. P_f values calculated direct from Fisher's formula are used throughout this work. Although the P_f

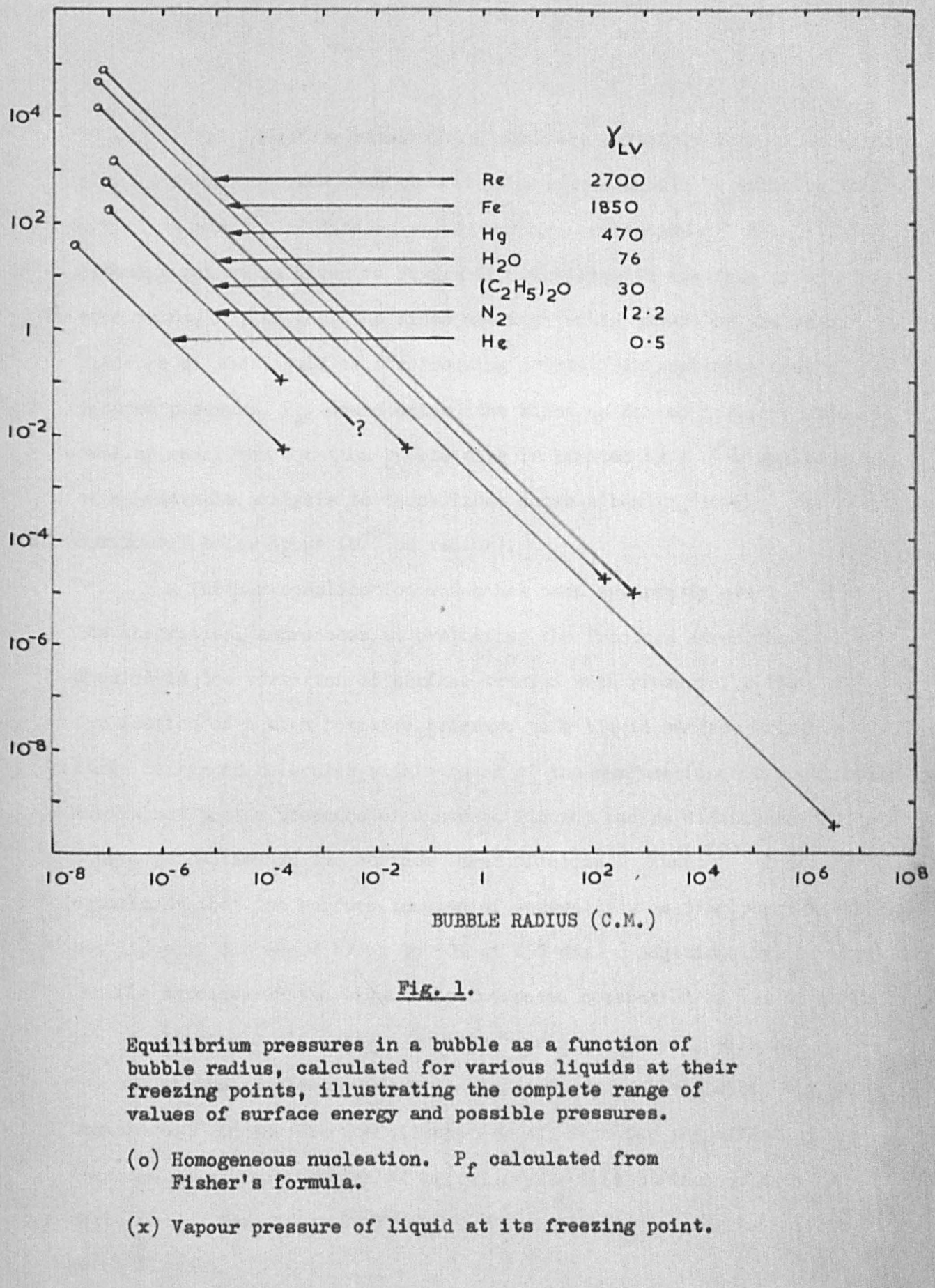

Fig. 1.

Equilibrium pressures in a bubble as a function of bubble radius, calculated for various liquids at their freezing points, illustrating the complete range of values of surface energy and possible pressures.

(o) Homogeneous nucleation. P_f calculated from Fisher's formula.

(x) Vapour pressure of liquid at its freezing point.

values may be therefore rather high, they are certainly correct to within about a factor of five, and the relative values should be quite reliable.

A summary of data on a wide variety of liquids at their freezing points is given in Figure 1. The liquids are free of external constraint, P_e, so that the lines are limited in extent by the vapour pressure of the liquid at its freezing point. An application of a reduced pressure, P_e, would extend the lines as far as desired. Towards smaller radii the equation bubble size is limited by r^* (An application of Wakeshima's analysis to these lines shows a bending towards the horizontal below about 10^{-6} cm radius).

A further complication which has been apparently overlooked in the theoretical approaches at evaluating the fracture strengths of liquids is the variation of surface tension with pressure. The application of a high positive pressure to a liquid surface brings a large number of molecules within reach of the surface (and is practically equivalent to the presence of a second liquid) and so diminishes the net inward attraction on the surface layer of atoms. Kundt[9] found by experiment that the surface tension of several low melting point liquids was linearly decreased by up to 50% at 150 atm. Additionally, at high tensile stresses in the liquid the increased separation of the atoms in the liquid should also reduce surface tension. Thus P_f will be reduced whether nucleation occurs solely due to either gas or shrinkage. In the absence of experimental data for the effect of pressure on surface tension of liquid metals this refinement is neglected. The effect is likely to be more important for low melting point liquids.

It follows from the above considerations that the condition for homogeneous nucleation in the liquid is

$$P_e - P_i = P_f \qquad \ldots(11)$$

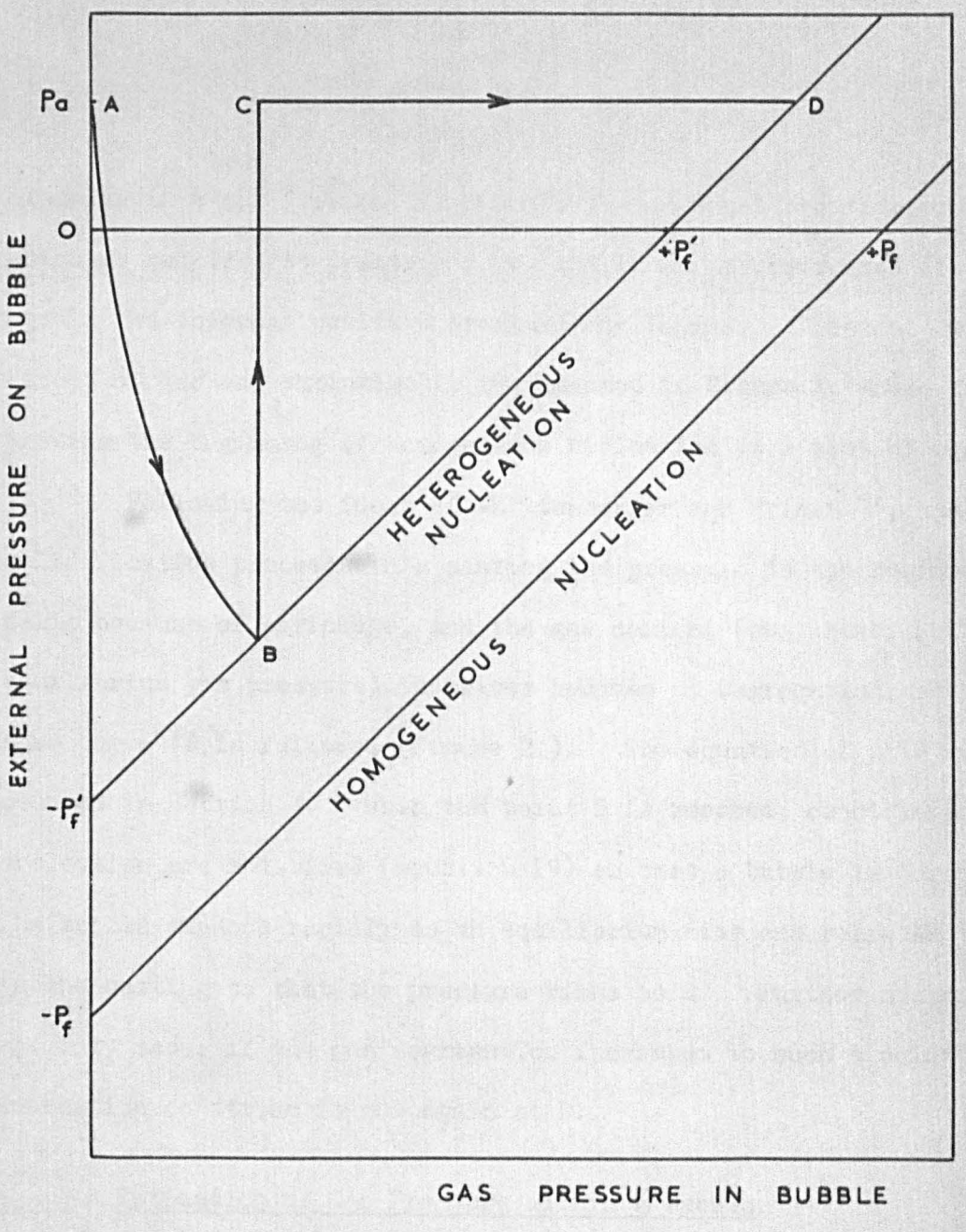

Fig. 2.

Schematic representation of the cooperative effects of gas and shrinkage on the nucleation of pores.

Adapted from Whittenberger and Rhines.

which becomes, since P_a and P_d of equation (4) are often negligible

$$P_g + P_s = P_f \qquad \ldots(12)$$

Clearly, in a gas-free melt P_f equals the external negative pressure which is required to create a pore, and in an unconstrained liquid P_f equals the internal positive pressure due to gas. This cooperative effect of gas and shrinkage is represented in Figure 2. where the line showing the beginning of homogeneous nucleation is a plot of equation (12).

Following the ideas of Whittenberger and Rhines[2]; as solidification proceeds in a casting the pressure in the residual liquid falls because of shrinkage, and the gas content (and therefore the equilibrium gas pressure) increases because of segregation, so that some curve AB is followed (Figure 2.). The equation of this curve is deduced in Section 3. When the point B is reached, conditions for nucleation are satisfied (equation 19) so that a bubble is formed. The bubble expands rapidly to an equilibrium size and relieves the stress in the casting so that the pressure rises to C. Further nucleation can now only occur if the gas segregation increases to such a point that the nucleation condition is met again at D.

2.2.1 Estimation of Gas Pressure within a Bubble.

Considering the segregation of gases in a little more detail: The rejection of various solutes by an advancing planar solidification front is represented schematically in Figure 7., and some partition coefficients, K, for gases in metals are given in Table II. (the scatter in the solubility data is rather large so that some coefficients are probably only accurate to within a factor of 2). The peak concentration at the interface C_{max} is related to the concentration in the bulk of the liquid, Co, by the well known equation

$$C_{max} = C_o/K$$

Hydrogen and nitrogen are seen to be concentrated by a factor of 2 or 3 for most metals, although hydrogen in aluminium is increased by 10 times.

TABLE II.

Solubilities of Gases in Metals at the Melting Point

(at 1 atm. pressure)

Metal	Solid	Liquid	Reference	K
		Hydrogen (cc/100 g)		
Al	0.036 0.062 0.050	0.69 0.77 0.43	41 42 43 44	0.1
Mg	15 19	33 41 27	45 46 47	0.5
Cu	1.90 1.53	5.17 5.42 5.46	48 49 50 51	0.30
Fe	6.5 13.36	 20.4 26.7 30.2 25.6 27.7 (1600°C) 29.8 (1600°C)	52 53 54 55 51 56 57	0.5
Co	6.7	 19.5 22.4 (1600°C) 23.2 (") 24.5 (")	59 51 56 57 60	0.34
Ni	13.7	 41.0 44.0	61 51 60	0.3
		Nitrogen (wt.%)		
Fe	0.0122	 0.446 0.40	62 63 64	0.3
		Oxygen (wt.%)		
Fe	0.0324	 0.17 0.17 0.18	65 66 67 68	0.19

TABLE III.

Data for the estimation of equilibrium gas pressure in contact with molten iron
(Pressure in atm.)

Gas	Reaction	Law	Effect of Temperature	Ref.
H_2	$2\,H = H_2$	$P_{H_2}^{\frac{1}{2}} = [wt.\%H]/K$	$\log K = -\frac{1670}{T} - 1.68$	69
N_2	$2\,N = N_2$	$P_{H_2}^{\frac{1}{2}} = [wt.\%N]/K$	$\log K = -\frac{188.1}{T} - 1.246$	63
O_2	$2\,O = O_2$	No data available since pressures immeasurably low		70
CO	$C + O = CO$	$P_{CO} = K.\ a_c \cdot a_o$	$\log K = \frac{1160}{T} + 2.00$	71
CO_2	$CO + O = CO_2$	$P_{CO_2} = K\,(P_{CO} \cdot a_o)$	$\log K = \frac{8718}{T} - 4.762$	71
H_2O	$2H + O = H_2O$	$P_{H_2O} = [wt.\%H]^2[wt.\%O]/K$	$\log K = -\frac{10390}{T} - 0.19$	72
H_2S	$2H + S = H_2S$	$P_{H_2O} = [wt.\%H]^2[wt.\%S]/K$	$\log K = -\frac{11.9}{T} - 1.93$	70
SO_2	$S + 2O = SO_2$	$P_{S_2O} = [wt.\%S]\,[wt.\%O]^2/K$	$\log K = -\frac{293}{T} + 2.8$	70

TABLE IV.

Approximate Maximum Equilibrium Gas Pressures attainable at a plane solidification front in liquid iron.

Gas	Pressure (atm.)
N_2	30
H_2	4
CO	440
SO_2	3×10^{-3}
H_2S	6×10^{-2}
H_2O	10
CO_2	530
O_2	0.00

The height of the concentration peak may be considerably lowered by the nucleation of a second phase. The maximum concentration is therefore that required to homogeneously nucleate this phase: for oxygen in liquid iron, for instance, FeO inclusions are thought to homogeneously nucleate at about 0.2 wt. % O_2 [10]. Using in each case the maximum concentration of solutes which may be found at a solidification front, and using the relations in Table III, Table IV has been compiled to show the maximum attainable equilibrium pressures in contact with liquid iron (the activities of carbon and oxygen are taken as 1, corresponding to a saturated solution). The most important gases are clearly CO_2 and CO* which emphasises the importance of efficient deoxidation, but H_2O and N_2 are not negligible, and H_2 is not so important as is so often assumed. Its importance would increase in properly deoxidised melts. The maximum total pressure is in the region of 1000 atmospheres - considerably lower than the 70,000 atmospheres required for homogeneous nucleation.

This value for the internal gas pressure, P_g, does not require a reduction due to the curvature of the bubble surface, for as Doring points out, the increased vapour pressure of a very small droplet of liquid predicted by the Thomson-Gibbs equation should be properly interpreted as resulting from the increased pressure on the liquid phase, not from the curvature of the surface. Thus in a bubble the internal gas pressure is independent of the radius, but does vary with the external pressure, P_e, according to

$$\ln\left(\frac{P_\infty}{P_g}\right) = \frac{M}{RT\rho}\ (P_\infty - P_e)$$

where P_∞ is the "normal" gas pressure, and ρ and M the density and molecular weight respectively of the liquid.

If, instead of plotting gas pressure, gas concentration were plotted in Figure 2., then for a simple diatomic gas in solution the line

* Footnote: The pressures of other gases may be somewhat increased if account is taken of the 3 (rather than 1) dimensional nature of solidification. Turkdogan [26] indicates how the solute concentration may be calculated (by equations analogous to our equation 20) although he omits the important correction (equation 21) in the case of wide freezing range alloys. In any case, however, the approach leads to infinite concentrations as solidification becomes complete so that it is not clear what concentrations are actually obtained

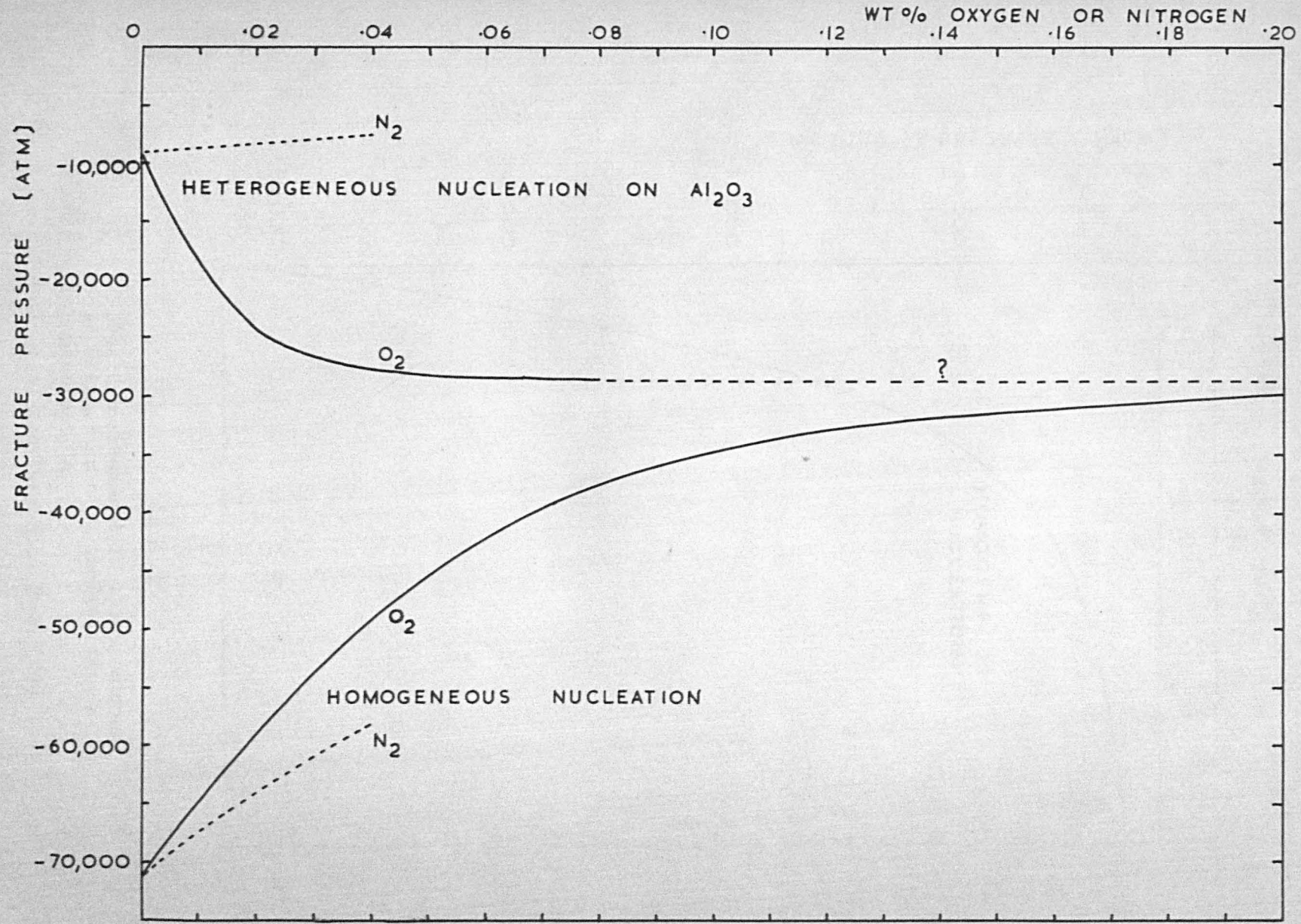

Fig. 3.

Fracture pressure of liquid iron as a function of oxygen and nitrogen contents.

(Calculated from data taken from references 73-76)

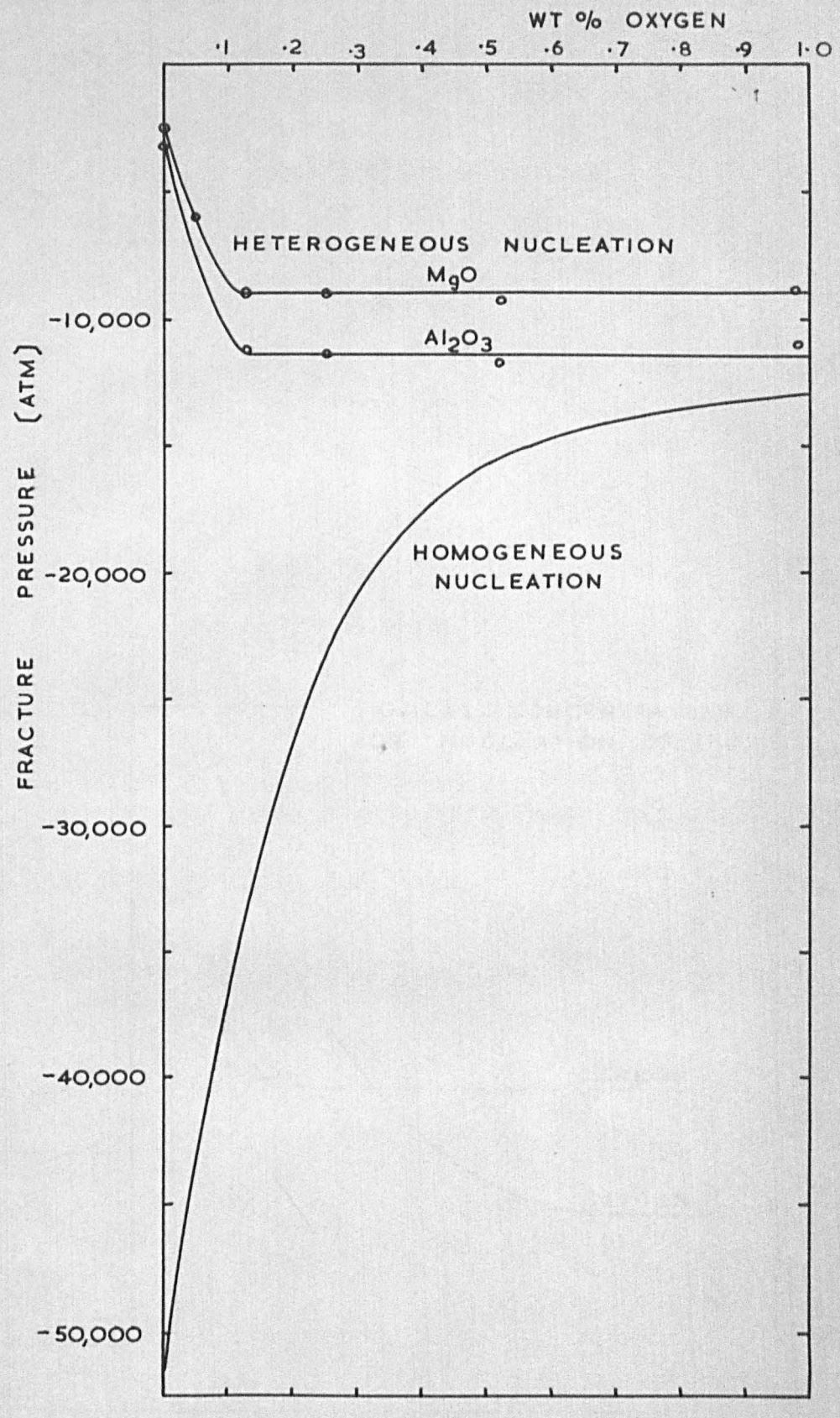

Fig. 4.

Fracture pressures in liquid copper as a function of dissolved oxygen concentration.

(Calculated from data from (77)

representing the threshold of nucleation would become a parabola (in contrast with the straight line proposed schematically by Whittenberger and Rhines[2]) because of Sievert's Law

$$P_g^{\frac{1}{2}} = [C] / K_s$$

Such considerations apply to a simple system such as hydrogen in liquid iron. With surface active gas, however, the surface tension is reduced causing P_f to be a function of gas content as is demonstrated in Figures 3. and 4.

Estimation of the Maximum Shrinkage Pressure.

The author has shown elsewhere[39] that the maximum possible negative pressure in a casting of pure iron is in the region of -1,500 atmospheres because of plastic collapse of the casting under the internal tension.

Thus it seems that neither gas nor shrinkage alone, nor even in combination can meet the very stringent conditions defined by equation (12) so that homogeneous nucleation does not seem to be a feasible mechanism for the creation of pores in iron castings. Similar considerations show that this conclusion applies to aluminium castings, and perhaps to castings in any metal.

2.3 HETEROGENEOUS NUCLEATION.

It is believed that nucleation of bubbles occurs at certain preferred sites in the liquid. These sites may consist of the boundary of the liquid with a solid, a second immiscible liquid, or a gas phase. These are discussed in turn.

2.3.1 Solid Inclusions.

Following Fisher's treatment[3] of heterogeneous nucleation, a bubble at the interface of the solid and liquid phases assumes the shape shown in Fig. 8A γ_{LV}, γ_{SV} and γ_{SL} represent the liquid-vapour, solid-vapour and solid-liquid interfacial energies respectively. The value of d corresponding to a minimum energy can be seen to be

$$d/r = -\cos\theta = (\gamma_{SL} - \gamma_{SV})/\gamma_{LV} \qquad \ldots(13)$$

where θ is the normal contact angle measured by a sessile drop technique. Considering the maximum value of the energy required to produce a bubble of critical size leads to a value of the fracture pressure, P_f', at the interface

$$P_f' = -\left(\frac{16\pi}{3kT} \cdot \frac{\gamma_{LV}^3 \phi}{\ln (6N^{2/3} kT/h)}\right)^{\frac{1}{2}} \qquad \ldots(14)$$

where $$\phi = (2-\cos\theta)(1+\cos\theta)^2/4 \qquad \ldots(15)$$

Equation (14) differs from (8) in that a factor of $\phi^{\frac{1}{2}}$ has been introduced and the number of interface atoms $6N^{2/3}$ (assuming that the liquid is bounded by the solid in the form of a cubical container) appears in place of N in the logarithm. Thus

$$\frac{P_f'}{P_f} = \phi^{\frac{1}{2}} \left(\frac{\ln N\, kT/h}{\ln 6N^{2/3}\, kT/h}\right)^{\frac{1}{3}} \qquad \ldots(16)$$

or approximately for temperatures between 1000°C and 2000°C

$$\frac{P_f'}{P_f} = 1.12\,\phi^{\frac{1}{2}} \qquad \ldots(17)$$

A plot of equation 17 is given in Figure 9. We may further modify equation 14 by assuming that one mole of liquid contains a

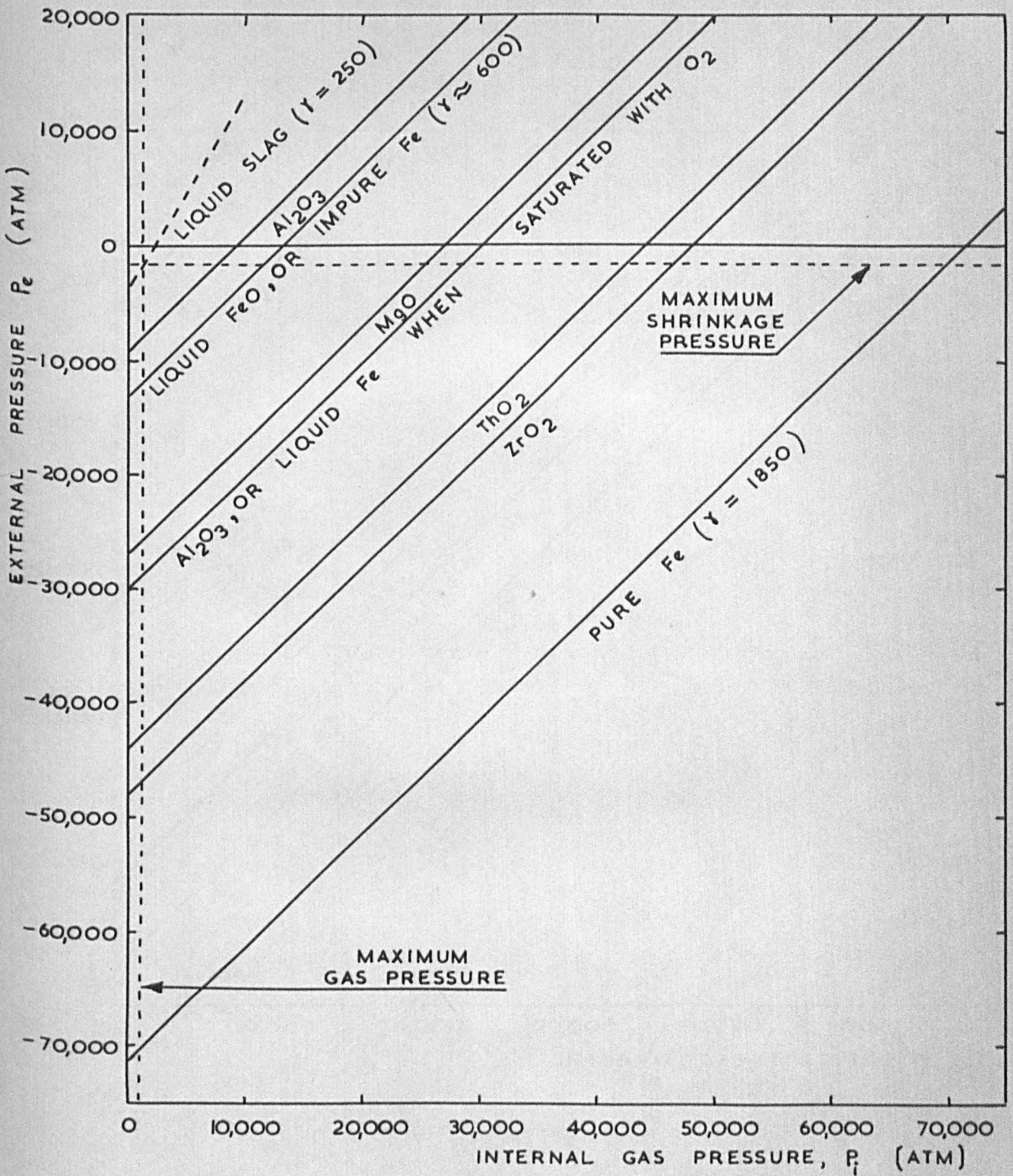

Figure 6.

Conditions for pore nucleation in liquid iron, heterogeneously on solid inclusions, and homogeneously in liquid iron and liquid inclusions. (Values for surface energy, γ, in ergs/cm^2).

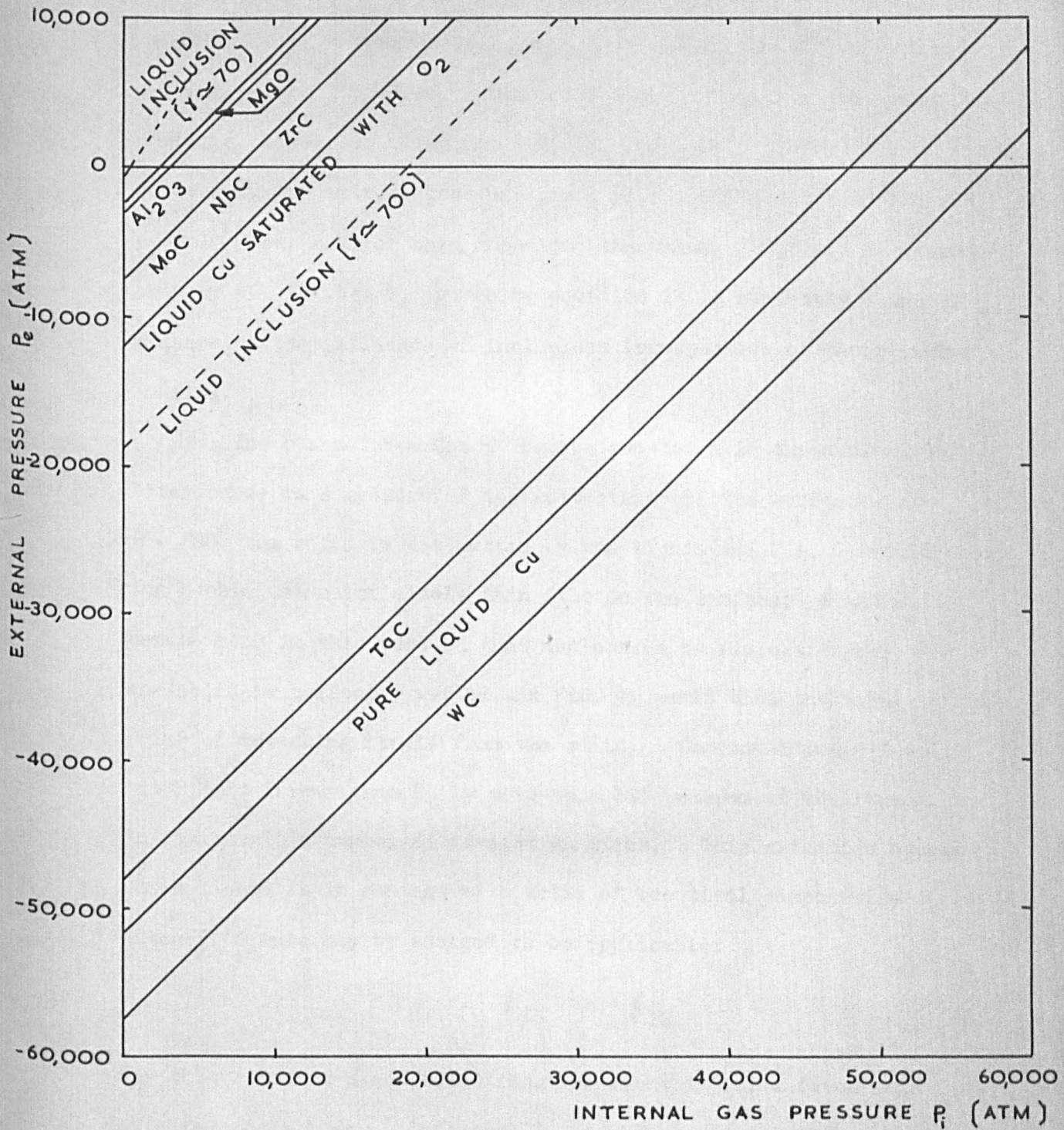

Fig. 7.

Conditions for pore nucleation in liquid copper, heterogeneously on solid inclusions, and homogeneously in liquid copper and liquid inclusions.

concentration C_i of inclusion material. If the inclusions are cubical and of average side a_i and if M_L and M_i are the molecular weights of the liquid and inclusions respectively then the total number of interface atoms now is $6\,(c_i\, M_L/a_i \rho_i^{1/3})(N/M_i)^{2/3}$. However in the extreme case of $c_i = 1$ (i.e. 100% inclusion) and $a_i = 10^{-8}$ cm (smaller than one atom) the value of P_f' is decreased only by 9%, so that P_f' given by equation 14 is evidently a useful measure of the influence of inclusions irrespective of their number or size.

The parameter - Cos θ (often denoted m in the nucleation literature) is a measure of the wettability of the surface: if $\theta = 180^\circ$ the solid is not wetted by the liquid and Fig. 8A would show the bubble as an infinitely thin film on the surface; ϕ and P_f' become zero in this case so that nucleation is easiest. For $\theta = 0^\circ$ the solid is perfectly wetted and Fig. 8A would show the bubble on the point of detaching itself from the solid. Correspondingly $\phi = 1$, but P_f' is larger than P_f by more than 10% because of the reduction in the possible number of cavitation sites. This situation occurs where liquid is in contact with solid of identical composition since Antonoff's rule may be assumed to be applicable:

$$\gamma_{SV} - \gamma_{LV} = \gamma_{LS} \qquad \ldots(18)$$

For this reason a plane solidification front is NOT a favourable site for nucleation. Chalmers[11] reaches an identical conclusion by a rather more qualitative approach. The quantity ϕ would have to decrease to less than 0.80 ($\theta > 65^\circ$) before nucleation becomes favourable (i.e. $P_f' \leqslant P_f$) on solid surfaces (Fig. 9.).

Some measured values of surface energies and contact angles are tabulated in the appendix. Using this data Figures 6 and 7 have been derived, although it is clear that some of the contact angle measurements are very unreliable (c.f. TiC inclusions in liquid iron). The line representing the threshold of heterogeneous nucleation in Figures 2, 6 and 7 is defined by the equation

$$P_g + P_s = P_f' \qquad \ldots(19)$$

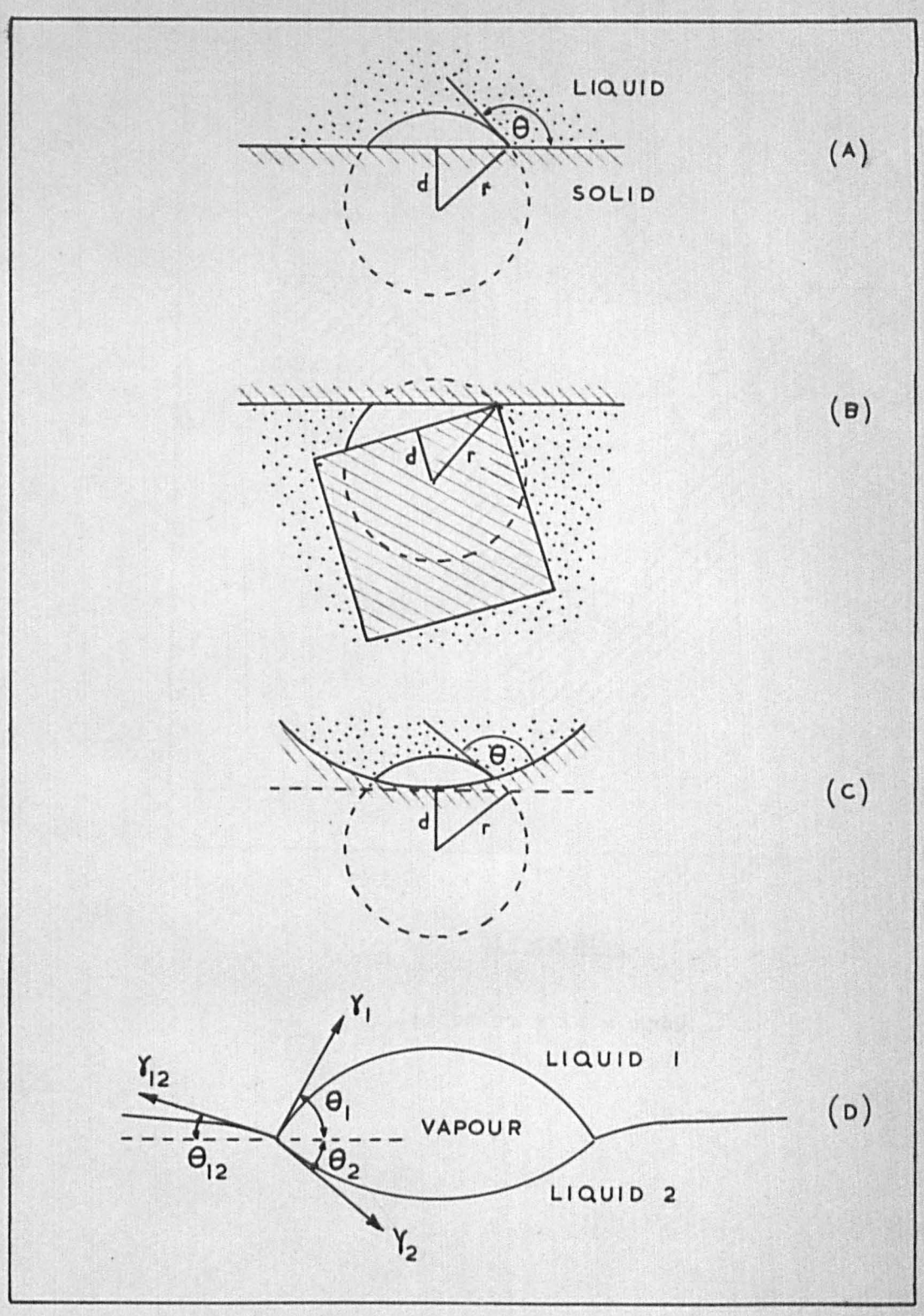

Fig. 8.

Heterogeneous nucleation at various interfaces.

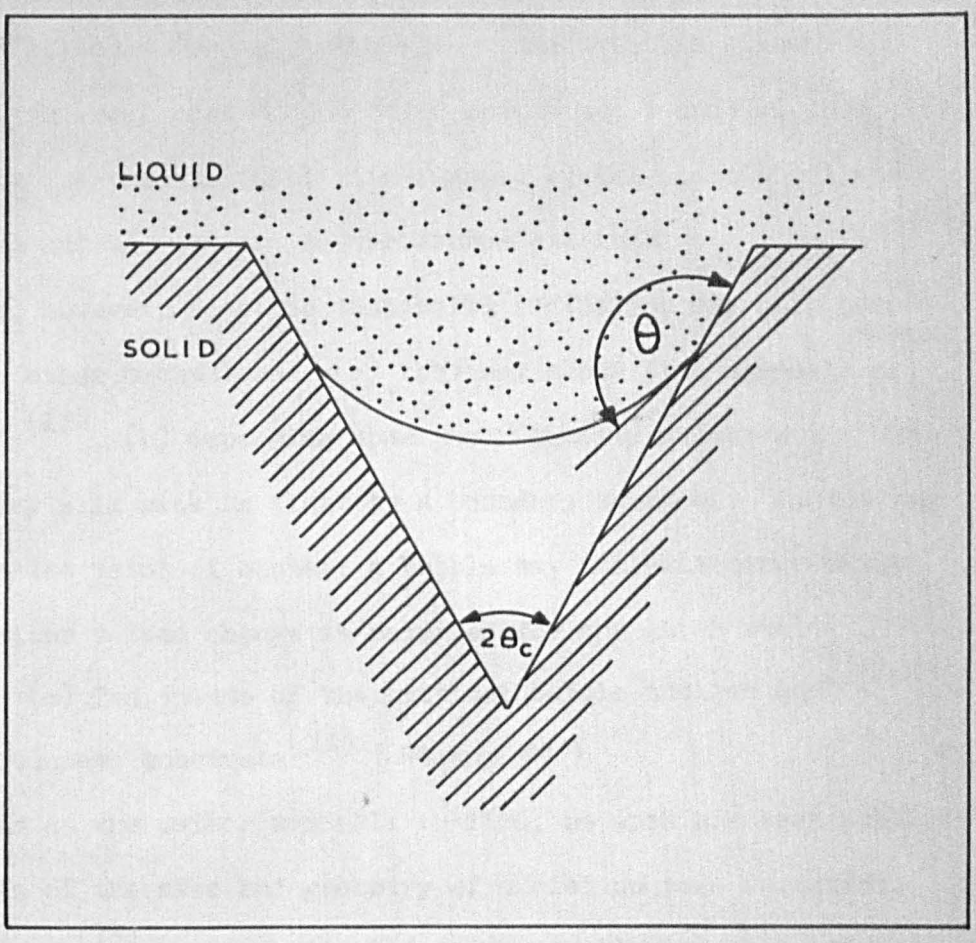

Figure 8(E).

Air trapped in a crack.

It is evident that solid inclusions do not raise the nucleation threshold sufficiently for nucleation to become possible since conditions in the real casting can never exceed the bounds of the rectangle which represents the limits imposed by the plastic collapse of the casting and the maximum gas pressures attainable.

It is, however, feasible that solid inclusions may help pore nucleation by other mechanisms: (a) they may block fine channels of feeding liquid[12], (b) depending upon their density relative to that of the liquid they will sink or float to a boundary surface. In the region very close to the point of contact a bubble may nucleate more easily because a smaller volume change is required for any given radius (Figure 8B); (c) The volume of the critical bubble nucleus may be reduced by a concave substrate[11] (Figure 8C).

As far as the author was able to find, no work has been published on the effects of the size and geometry of nuclei on pore formation, although Fletcher[13] has investigated theoretically the nucleation of the solid phase from the liquid on to particles of various shapes, and some theoretical work on the nucleation of solid from the vapour demonstrates that macroscopic steps on the solid surface greatly aid nucleation for certain contact angles[14]. Steps of atomic height corresponding to the emergence of screw dislocations are known to occur on the solidification front of pure tin[15]. It is reasonable to suppose that such steps are present at the solid-liquid interface of other metals, and that these steps may influence the nucleation of pores.

Nevertheless, it is encouraging that the experimentally determined contact angles of liquid nickel on sapphire and polycrystalline alumina are not very different (see appendix) and moreover, experiments by Turpin and Elliott[10] on the homogeneous nucleation of oxide inclusions from iron melts yielded values for interfacial energies very close to those measured by macroscopic methods on very imperfect surfaces. These experimental facts lend confidence to the application of bulk concepts, such as surface tension and contact angle, to the investigation of atomistic phenomena such as nucleation.

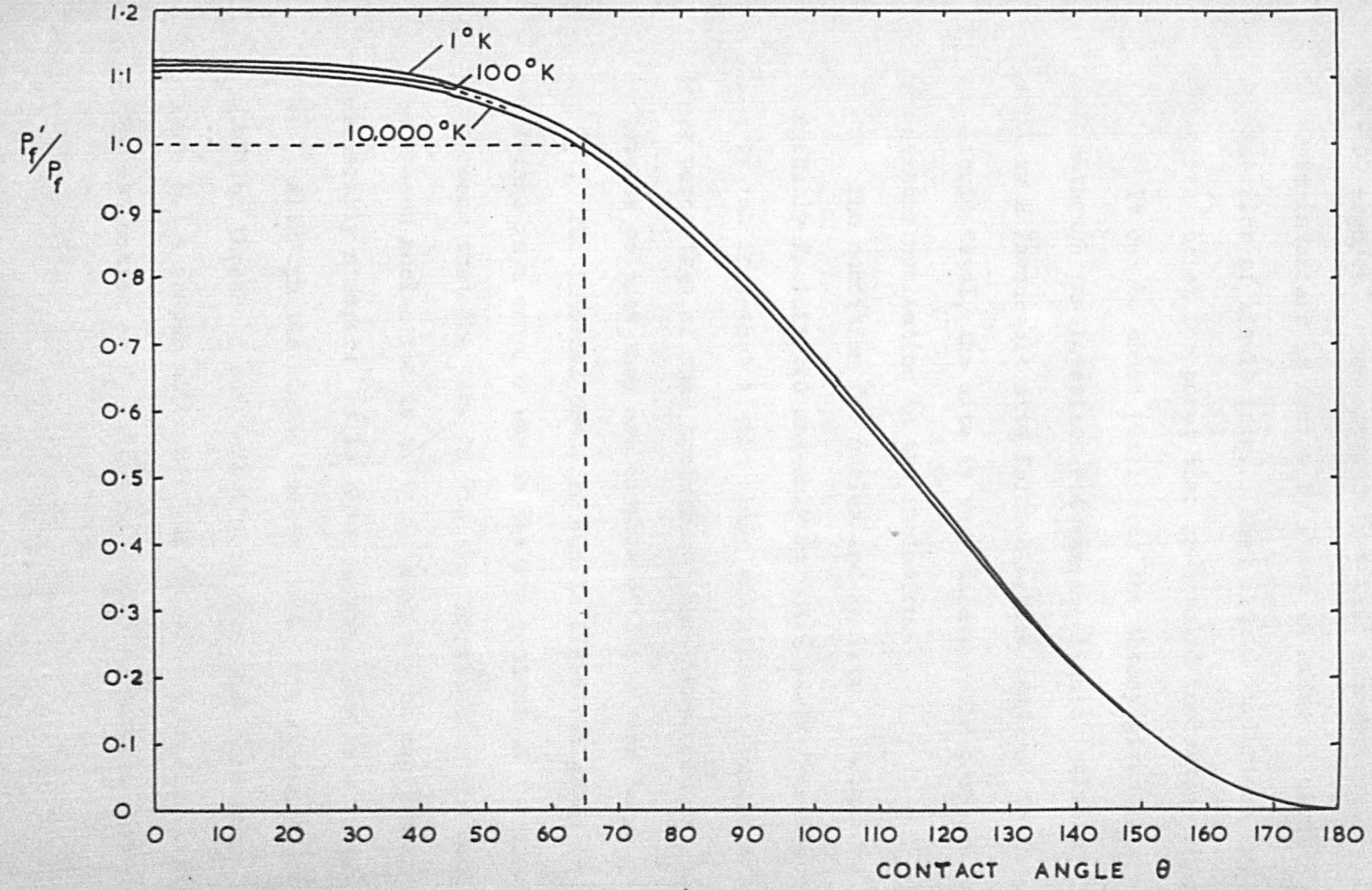

Fig. 9.

Ease of bubble formation by heterogeneous nucleation on a plane solid surface as a function of contact angle, θ . Calculated from equation 17.

2.3.2. Liquid Inclusions.

Many non-metallic inclusions in castings are liquid until well below the solidus temperature of the casting alloy. Almost invariably they have comparatively low surface tensions (in the region of 250-600 ergs/cm^2; see appendix) so that homogeneous nucleation of pores in their interiors is easier by about an order of magnitude compared with the interior of liquid iron. Most liquid inclusions are therby more effective nuclei for pores than most solid inclusions (Figures 6 and 7).

It can be shown (utilising the theory given in the appendix) that although the interface between the liquid inclusion and liquid metal is a favourable site for nucleation compared to the interior of the liquid metal, the site is very unfavourable compared to homogeneous nucleation in the inclusion.

The condition for nucleation in liquid inclusions (equation 19) is probably facilitated not only by their small fracture pressures but also by the fact that liquid slags and glasses (which constitute a large percentage of such inclusions) have very open crystallographic structures so that they are capable of dissolving large quantities of gas[14]. The internal pressure due to dissolved gases in the inclusion may depend in a complex way on the gas content of the liquid metal, which means that the line in Fig. 6. representing the condition for homogeneous nucleation in a liquid slag may be non-linear and considerably steeper: it is shown accordingly as a tentative dotted line. Although the liquid inclusions do not appear to raise the nucleation threshold sufficiently to make pore formation feasible, (Figure 6.) a proper allowance for the effect of dissolved gas, and a better estimation of P_f values is likely to reverse this conclusion.

2.3.2 Complex Inclusions.

Complex inclusions are common in castings of nearly every type: In iron and steel, solid alumina-type particles are often contained in a liquid sulphide or silicate matrix (although the small contact angles of the latter make decohesion unfavourable at this boundary). In cast iron, graphite (which appears to make high contact angles with most inorganic liquids) is often adjacent to low melting point sulphides and phosphides.

Employing equation (10a) to determine the fracture pressure of the liquid phase of the inclusion, and then reducing this value by applying equation (17) then it is possible to obtain very low fracture pressures. Assuming a surface energy for the liquid of 250 dynes/cm^2, and very poor wetting of the solid phase ($\theta \simeq 160^\circ$),* then decohesion at the solid-liquid interface occurs at about -200 atmospheres. This is more than an order of magnitude lower than fracture pressures obtainable with single phase inclusions, and may be relatively easily attained by either gas or shrinkage in relative isolation or in combination.

Immiscible liquids are quite common in complex inclusions and the author has extended Fisher's analysis to determine fracture pressures for the liquid-liquid boundary (see appendix). It is to be regretted however that very little data is currently available on interfacial energies between non-metallic liquids at such high temperatures,[134, 135] although measurements of contact angles and interfacial energies between liquid iron and various slags are reasonably plentiful.[166-175]

*Reference 181 gives some evidence that 160° may be a maximum possible contact angle for any liquid on a solid.

2.3.4 Gaseous Nuclei.

2.3.4.1 Gas bubbles in suspension.

Rapid, turbulent pouring of castings may cause air bubbles to enter the liquid metal[20]. If the bubbles are sufficiently small they may rise in a time great enough to allow the formation of a solid skin on the casting, and so be trapped. A bubble which is too small however may require for its stability an internal pressure of gas higher than the equilibrium gas pressure which the bulk of the melt can provide, thus the bubble will dissolve.

Considering the first part of this problem: From Stoke's Law the time of rise of bubbles through a distance of 10 cm. is taken as a rough guide to the bubble's lifetime in suspension (Table 5.). A solid skin will form on such a casting within a time of the order of a minute, or somewhat less. Such bubbles require internal excess pressuresin excess of 2.8 atmospheres. Initially the high internal pressures in these bubbles are possibly met by compression of the included air since it is likely that these small bubbles are the result of the collapse of larger bubbles, and possibly by the thermal expansion of the air. Finally however the bubble must dissolve for a reasonable equilibrium gas pressure in properly deoxidised steel containing normal amounts of hydrogen and nitrogen is only about 1-2 atmospheres at the most.

Although their solutions cannot easily be applied to liquid steel because of its complexity, various authors have solved the diffusion equations for various simple gas-liquid systems[187-191] to find the time of dissolution of a gas bubble. If its rate of dissolution is sufficiently slow to allow the bubble to survive long enough to impinge on a well established solidification front, then it will almost certainly grow because of the local high build up of gas in solution together with a probable reduction in surface tension.

The presence of such a gas nucleus means that high negative pressures can never be reached in parts of the casting in hydrostatic communication with the bubble. For instance if an exterior negative pressure is reached which nearly equals in magnitude the internal

TABLE V.

Data on bubbles in suspension in liquid iron.

Bubble Radius (cm)	Time to rise 10 cm. (sec)	Excess Pressure in bubble (atm)
4.0×10^{-4}	10^{3}	8.9
1.3×10^{-3}	10^{2}	2.8
4.0×10^{-3}	10	0.89
1.3×10^{-2}	1	0.28

gas pressure (3 atm. for a bubble 1 μ radius) then the bubble will expand to macroscopic size, relieving the external pressure (equation 1.). Thus, as Blake points out[8], the tensile strength of a liquid body is in practice determined by the size of the largest gas bubble present.

In conclusion, although the possibility of such nuclei cannot be ruled out, the required and possible lifetimes are shown to be nearly mutually exclusive, so they constitute an unlikely source of porosity. It may be noted that such nuclei may be avoided by the use of suitably careful casting techniques or by casting in vacuum.

2.3.4.2 Gas-filled Crevices in Solids.

The vapour bubbles produced by boiling water in a glass container can be seen to be nucleating from distinct points which could be pockets of gas contained within small crevices in the wall of the container. Nuclei of a similar nature are thought to be responsible for the 'boil' in an open hearth furnace[21-23].

In a casting, however, the boundary of the liquid metal at some stage during solidification is not analogous to the inner surface of the glass container, nor to the bath of the open hearth, which were both previously in contact with the air before receiving the liquid cover. The boundary of the liquid surface in a solidifying casting is formed by a phase transformation, and because of this, perfect atomic contact would be expected at every point. The same applies for indigenous inclusions (i.e. formed in the melt). Gernez[24] demonstrates that crystalline solids formed in the liquid and which had never been in contact with a gas were incapable of inducing effervescence in the liquid which was supersaturated with gas (to a pressure however of probably only about an atmosphere).

Thus in a casting, porous inclusions containing gas can only have an exogenous origin (i.e. were washed in from the tip of the ladle, or from the mould wall etc.).

Harvey[25] describes a stabilising mechanism which relies on the fact that a bubble which has a lower internal pressure than that of the surrounding liquid can be in equilibrium with the liquid providing it has a concave surface (Fig. 8E). Their theory leads to a value of the fracture pressure

$$P_f' = A_1 P_m - A_2 P_g$$

where P_m is the maximum pressure to which the melt has been subjected, P_g is the equilibrium gas pressure in the bubble, and A_1 and A_2 are constants depending upon the angle of the crack and the advancing and receding contact angles, θ_a and θ_r. If θ_a and θ_r are approximately equal, then A_1 becomes unity, A_2 becomes zero, and since P_m is usually one atmosphere an unstable expansion of the nucleus

occurs when a shrinkage pressure of about -1 atm. is reached (i.e. about zero absolute pressure).

It is clearly not helpful to discuss such gas-filled crevices in any more detail since any number of geometries can be envisaged: Blake[8] suggests a type which becomes narrower towards its mouth, as a narrow-necked bottle, and thus enclosing gas irrespective of contact angle criteria.

The growth and emergence of gas bubbles from crevices is described theoretically in some detail by Vallet[21] in relation to the carbon 'boil' during steelmaking, and investigated experimentally with water and other organic liquids by many investigators[182-187] - particularly with a view to understanding heat transfer in boilers.

2.4 NUCLEATION BY ATOMIC COLLISIONS.

In their various theoretical models of liquids, the investigators of fracture pressures failed to include the presence of occasional fast moving, high energy particles from space (Cosmic Rays) and the relatively high density of energetic alpha particles due to the decay of traces of radioactive matter which are prevalent everywhere. Although no direct evidence exists to determine whether such phenomena do in fact influence pore formation in liquid metals, the purpose of this section is to assess this possibility as far as possible by inference from other data.

In 1953 Glaser first demonstrated that fast moving atomic particles can cause the nucleation of bubbles in metastable liquids[27]. This observation has been put to widespread practical use in the construction of bubble chambers which illustrate the track of a particle through the liquid by corresponding trail of bubbles. Most chambers utilise superheated liquids, although some[28] employ a liquid super-saturated with gas under pressure, which is closely analogous to the conditions in a solidifying casting. More recently, several investigators have measured the effect of various radiations on the fracture pressures of liquids[29-31] which are shown in some cases to be very much reduced. These studies have been so far only directed at water, organic liquids, and a few heavy liquids such as Xe and UF_6[35].

Early theories[29] assumed that in a collision of the energetic particle with an atom in the liquid, the charge associated with the particle would be redistributed over the surface of an embryonic bubble. The effect of the mutual repulsion of the charge would act in opposition to the surface tension and thus aid nucleation. If this were true then the possibility of bubble formation by this mechanism in liquid metals would appear to be remote because of their high conductivity. However, more recent theories[33,34] which have had a fair measure of experimental success, indicate that nucleation occurs by the deposition of very localised quantities of energy by a direct knock-on of the incident particle with an atom in the liquid, causing a small region to become vapourised.

Thus a close analogy can be drawn with the production of radiation damage in solid metals, where it is now well established[37] that an incident particle of sufficient energy will produce intense vibration in the region surrounding its encounter with a lattice atom. The region finally cools to contain a high density of vacancies.

It seems reasonable to conclude therefore that a similar event in a metallic liquid will produce a vapour bubble exceeding the size of the critical bubble required by classical nucleation theory, so that P_f will be lowered.

We now turn to a consideration of the possible sources of suitable radiation.

2.4.1 Cosmic Rays.

Sette and Wanderlingh[32] have shown that the cavitation threshold for water subjected to ultrasonic vibration is affected in a complex but reproducible way by the thickness of a lead box which encloses the apparatus. The results are explained in terms of cosmic rays intercepting the lead shield and giving rise to secondary particles which may also cause nucleation events in the metastable liquid.

Nevertheless, as a prolific source of bubble initiation, which seems to be required to explain porosity in real castings, cosmic rays may be rather unlikely for several reasons:

(i) The frequency of arrival of cosmic rays[36] is only about one particle/minute/cm^2, so that relatively few particles will enter a normal sized casting during the critical final stages of solidification, when gas and shrinkage pressures are rising more rapidly.

(ii) At ground level only approximately 30 per cent of the total incident radiation ~~at ground level~~ consists of the strongly interacting 'soft' variety, thus most particles will pass harmlessly straight through a casting.

(iii) At a late stage in solidification (i.e. when the fraction of liquid present is small) it is unlikely that a primary (or secondary) collision within the casting will be within the highly strained residual liquid.

(iv) In order for nucleation by cosmic rays to be favourable, P_f must be lowered by at least one or two orders of magnitude since the collision site will not in general be adjacent to a solidification front where conditions of high gas content and lower surface tension prevail, nor at interfaces within complex inclusions, where decohesion is relatively easy.

The possibility of bubble nucleation by cosmic rays is by no means ruled out in large castings, since slower freezing means that more time is available for a favourable collision to occur, and the area and depth of the casting also increase this possibility. Furthermore, of course, only one such event is necessary to initiate porosity which may branch and spread throughout a casting.

2.4.2. RADIOACTIVE DECAY.

Small amounts of radioactive elements are present in most metals. Investigators of radioactive phenomena (who may have to construct apparatus and research rooms with a low radiation background) have difficulty in obtaining materials with sufficiently small amounts of such impurities and often utilise steel from dismantled battleships since this is known to be low in active contaminants. Modern steels are relatively highly contaminated as a result of the fall-out from atomic explosions, and perhaps occasionally from the increasing amounts of radioactive waste from industrial, medical and nuclear power sources.

The decay of an atomic nucleus may result in the release of one or more alpha or beta particles. The latter are electrons which are too small in mass to cause any important damage from the viewpoint of the nucleation of pores. Electron bombardment of solid metals is known to produce only occasional single atomic displacements in the lattice[37].

In contrast, alpha particles are heavy and have high energy, resulting in severe local damage to the lattice of solid metals[37], and thus probably resulting in vapour bubbles in liquid metals. Table 6. gives a list of naturally occurring radioactive isotopes which produce alpha particles on decay. The number of decays per minute varies directly as the fraction of the isotope present in the element, and inversely as the length of the half-life. Only Th and U are seen to produce a significant number of decays per minute, although it is quite feasible that some artificially produced isotope may have found its way into the metal; for instance 1 p.p.m. of Ra 226 or Pa 231 in 1 cc. of metal will produce 10^8 and 10^7 decays/minute respectively. There are several dozen artificial isotopes which are alpha-emitters.

Bubble nucleation by fission fragments from the spontaneous disintegration of an unstable nucleus such as U may ordinarily be discounted (except for the casting of pure uranium or similar fissionable material) because such events are many orders of magnitude more rare than alpha-decays.

TABLE VI.

Naturally occurring radioactive isotopes which produce alpha particles on decay.

Isotope	Abundance in pure element (%)	Half Life (years)	Energy of alpha particle(s) (MeV)	No. of decays per minute due to 1 ppm element in 1cc liquid metal	
Nd 144	23.9	2.4×10^{15}	1.83	10^{-5}	
Sm 147	14.97	1.2×10^{11}	2.23	10^{-1}	
Gd 152	0.200	1.1×10^{14}	2.14	10^{-6}	
Hf 174	0.18	2×10^{15}	2.50	10^{-7}	
Pt 190	0.0127	10^{12}	3.3	10^{-5}	10^{-5}
Pt 192	0.78	$\sim 10^{15}$	2.6	10^{-6}	
Th 232	100	1.39×10^{10}	4.0	10	
U 234	0.0056	2.5×10^{5}	4.75	20	41
U 235	0.7205	7.1×10^{8}	4.5	1	
U 238	99.2739	4.51×10^{9}	4.18	20	

Data from Chart of the Nuclides prepared at Institute Radiochemistry, Nuclear Research Centre, Karlsruhe, Germany. July 1961.

Several factors favour the creation of pores by the decay of radioactive contaminants rather than by cosmic radiation: 1) The radiation is 'in situ', and thus exactly where it is required to create pores - there is no problem of the radiation having to penetrate just the correct distance into the casting. 2) Alpha particles are strongly interacting and will in general not escape from the casting so that the process operates at maximum efficiency. 3) Given a favourable partition coefficient the contaminants will be concentrated, together with other impurities, into the centre of the casting where both gas and shrinkage will both aid nucleation to the greatest advantage. 4) The frequency of cosmic rays is very constant[36] although it is the experience of foundries that porosity 'comes and goes' for no apparent reason. The blame is sometimes traced to gases in solution and other causes, but an additional reason may well be the wide and erratic variation in radioactive contamination from one batch of metal to another.

2.5. RELATION BETWEEN SHRINKAGE AND GAS PRESSURES IN VARIOUS CASTINGS.

From elementary considerations, omitting several important factors discussed in Section 1., Flemings and co-workers[38] deduce an expression for the equilibrium pressure of a diatomic gas in solution in the residual liquid of a casting

$$P_g = \left(\frac{C_o}{f_L (K_L - K_s) + K_s} \right)^2 \qquad \ldots(20)$$

where C_o is the original gas concentration at the start of solidification, f_L is the fraction of liquid at some later instant, K_L and K_s are the solubility constants for the gas in the liquid and solid metal respectively. For a cylindrical casting of a mushy freezing alloy these authors derive from geometry

$$f_L = \pi \bar{a}^2 n \tau_o \qquad \ldots(21)$$

where n is the number of feeding channels per square centimetre of cross section, (a) is the mean radius of the channels, and τ_o is tortuosity factor associated with the non-linearity of the channels. Also

$$P_s = B/a^4 \qquad \ldots(22)$$

where B is a function of the size of the casting, the dendrite arm spacing, and the thermal properties of the metal and mould. Thus eliminating (a) from equations (20) and (22) we obtain the locus of the line AB (Fig. 2.):

$$P_g = Co^2 / \left[\pi n \tau (K_L - K_s)(B/P_s)^{\frac{1}{2}} - K_s \right]^2 \qquad \ldots(23)$$

Similar relations may be obtained from the work of these authors for the cases of unidirectional dendritic solidification, for cellular solidification, and for the case of a cylindrical casting in a skin freezing metal.

Considering now the situation in which a volume of liquid is isolated from supplies of feeding liquid, the pressure in this confined liquid volume is[39]

$$P_s = 2 \gamma_{LS}/a - 2Y \ln (b/a) \qquad \ldots(24)$$

assuming for simplicity that P_o and P_d are negligible and that the whole casting is in a plastic condition. γ_{LS} is the energy of the liquid-solid boundary, Y is the yield strength of the metal at that temperature and strain rate, a is now the radius of the liquid core b is the distance from the centre of the confined liquid to the nearest free surface of the casting. From geometry (assuming approximately spherical symmetry)

$$f_L = a^3/b^3 \qquad \ldots(25)$$

substituting (25) into (20) and eliminating (a) from the resulting equation and (24) will give the relation between P_s and P_g for a region of confined liquid in a casting.

2.6. Growth of Pores.

2.6.1. Kinetics.

Once nucleation of a pore has occurred at B (Fig. 2.) the strain energy in the liquid and surrounding solid is suddenly released by the expansion of the pore and the pressure in the liquid jumps to point C.

A cine-film of eutectic alloy solidification by Davis[210] shows that pores spring to equilibrium size in a time shorter than the shutter speed of the camera (about $^{1}/_{24}$th second) and thereafter grow only a little at a very slow rate until solidification is complete. Experiments involving ultrasonic cavitation in liquids indicate that this rapid growth period occupies less than 1 millisecond[213], and calculations involving inertial forces in the liquid suggest that the period is nearer 1 microsecond[211], although if heat transfer considerations are included in the calculation[212] then growth times again become of the order of milliseconds. An interesting rheological approach to this problem is outlined by Hoffman and Myers[217] in an investigation into cavitation dynamics in thin liquid films.

Some quite relevant experimental studies on the growth rates of bubbles in boiling liquids may be referred to[207-209].

Following the ideas of Whittenberger and Rhines[2], further nucleation in this body of liquid is impossible because hydrostatic tension cannot develop so long as shrinkage is being accommodated by growth of the existing pore. As freezing progresses however, the gas concentration in the residual liquid will increase, shifting its pressure-concentration state to the right of Fig. 4. Point D may never be reached, however, if the available gas has sufficient time to diffuse to the existing pore, or if

solidification overtakes the region first. Nevertheless, if parts of the liquid in hydrostatic communication with the pore are sufficiently distant so that their gas content is not drained by the growing pore, but allowed to increase, then D may be reached so that more pores will form.

After the first rapid stage of growth two extreme modes of growth may be distinguished: (a) when the pore is in perfect communication with feeding liquid its rate of growth is determined by the rate of gas deposition alone, and (b) when liquid feeding is cut off (and when pores have already been nucleated) then in the absence of gas the total volume of pores that will develop must equal the shrinkage of the body of isolated liquid.

Growth by gas precipitation may be limited either by the rate of diffusion of gas through the liquid phase, or by the rate of diffusion across the bubble interface, whichever may be the slower. Either process is complicated (a) by the increase in surface area of the cavity, which, because of the complexities of pore shape, need not be simply related to the quantity of gas released (b) by the irregularly changing ratio of gas-liquid to gas-solid surface; (c) by the flow and possible turbulence of the gas-solvent liquid as the pore grows; and (d) by the changes in solubility and diffusion coefficients with alterations in temperature and composition. Hence it is not to be expected that the rate of pore growth by gas rejection will follow any simple law.

Nevertheless several authors[187-192] have attempted to analyse the growth of gas bubbles in a liquid, making the great simplification of assuming a spherical bubble at rest in an infinite liquid.

Shrinkage-controlled cavity growth is probably more susceptible to analysis since it must proceed in direct

proportion to the quantity of heat extracted from the body of confined liquid. Ruddle[214] has provided an exhaustive critical analysis of such heat flow solutions for castings.

2.6.2. Final Size of Pore.

The single cavity formed at B (Fig. 2.) has a growth advantage over the cavities which start their growth later at D: the single pore is initially larger than the later pores because of the longer time and the stored elastic energy available for its growth, and thereby also grows at a faster rate because of its greater surface area available for gas transfer.

Growth is arrested by local completion of freezing. In principle it will never be stopped by completion of gas precipitation since an infinite time is required to bring a diffusion process to equilibrium. Accordingly, it is expected that pores will be larger the longer the time allowed for their growth.

Easy nucleation means that very little plastic collapse of the casting will occur since the hydrostatic tension will never reach high values. Thus the resulting porosity will be a maximum i.e. numerically equal to the solidification contraction - of the order of 3% - or possibly higher with the assistance of gas. In the case of difficult nucleation (high P_f' values) pore nucleation is delayed until the shrinkage pressure reaches the necessary high value to satisfy the nucleation condition. This means therefore that the final pore will be small because of the prior occurrence of a considerable amount of solid feeding.

The final size of a pore in the fully solidified casting may be influenced somewhat by viscous or plastic flow in the manner of sintering. A survey of sintering mechanisms is given by Ramqvist[215] although for such processes to

become properly effective (since sintering normally occurs under initially stress-free conditions) the high internal gas pressure or surrounding hydrostatic tension which in the first place both contributed to the creation and growth of the pore, and which now ipso facto oppose its collapse, must therefore first be dissipated before sintering can take place.

The shape of a pore will also be modified to some extent by diffusion in the solid state[216].

3. FEEDING MECHANISMS.

There appear to be at least 5 mechanisms by which the difference in volume between the liquid and solid states can be accommodated in a solidifying casting, however not all of the mechanisms need operate in any single case. Adequate feeding of any one of these means relieves the hydrostatic tension in the remaining liquid, and so reduces the possibility of the nucleation and the subsequent enlargement of a pore. The feeding processes are dealt with in the order in which they occur during freezing, and this order coincides with a progressive transition from what might usefully be termed 'open' to 'closed' feeding systems.

3.1. Liquid Feeding.

Liquid feeding is the most 'open' feeding mechanism and generally precedes other forms of feeding (Fig. 10.) although in skin freezing metals and eutectics it is normally the only method of feeding. It has been much investigated both theoretically and experimentally and for this reason is probably the best understood of all the types of feeding. Wallace[227] gives a comprehensive review up to 1959.

Inadequate liquid feeding leads to formation of porosity by the elementary non-nucleation process by the spread of the primary shrinkage pipe into more distant regions of the casting. (Section 2.1.).

3.2. Mass Feeding.

This is a term coined by Baker[228] to denote the consolidation of a fluid mass of solid crystals and residual liquid.) The movement of this slurry is arrested when the growing crystals impinge and interlock. Pellini[229] suggests that this occurs at a critical value of 60% solid for steels; Flemings et.al.[230] infer from their experiments

SCHEMATIC REPRESENTATION OF
FEEDING MECHANISMS
FIG. 10.

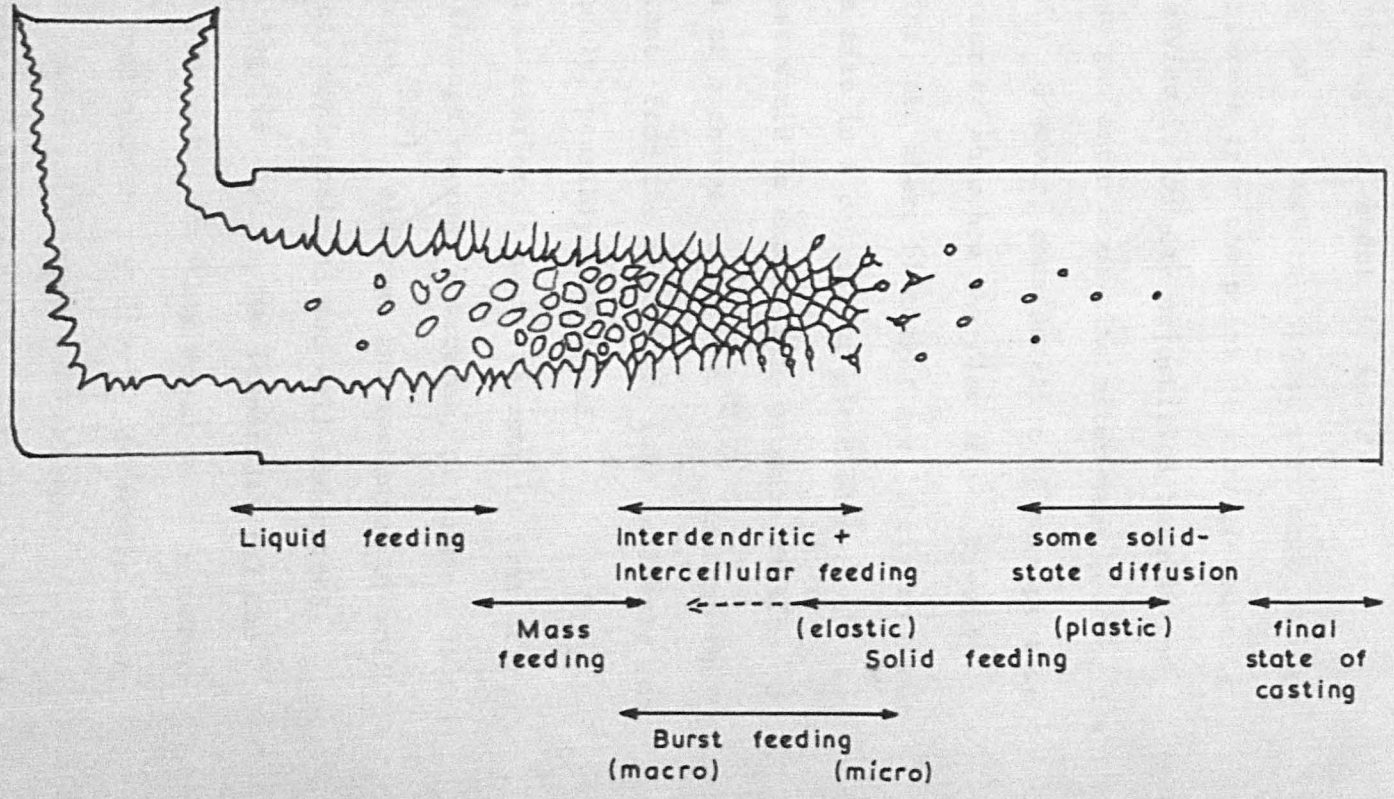

on, the flow of liquid through a dendrite mesh that 'flow channelling' through the mushy zone of Al-4.5%Cu alloys occurs at up to 68% solid, and the experiments by Singer and Cottrell[231] on the mechanical strengths of Al-Si alloys at temperatures above the solidus indicate that the mushy zone gains mechanical strength at about 60% solid.

Many of the earlier authors suggest that mass feeding is the important process from the point of view of reducing porosity. Such a view is largely unjustified because the critical feeding stages occur some time after mass feeding has practically ceased. However, consideration of this process is warranted in order to show how the flow of the liquid-solid mass could indicate where blockages are likely to occur with a given grain size in a casting of given geometry. For instance the process would be expected to produce choking of the liquid channel at a change in section[229], so that the sections more distant from the feeder are less perfectly fed, and therefore, finally, possibly less sound.

The problem is similar in some respects to that of the flow of soils through various apertures, of which a useful review exists by Brown[232], although the mechanics of soil flow is still largely empirical and not well understood. Furthermore the analogy is weak in two respects: (a) the dendritic shape of some metal crystals would cause premature interlocking (more analogous to the flow of dendritic metal powders familiar in powder metallurgy) and (b) the considerable plasticity of the dendrites at the solidification temperatures which would tend to act in opposition to a premature interlocking effect.

An improvement and possible extension of this feeding process by refining the grain size might, however, impair the subsequent interdendritic feeding, although equation (28) suggests otherwise. Nevertheless, this illustrates the

important point that a change in any particular casting variable may affect various types of feeding in opposing ways.

3.3. Interdendritic Feeding.

Allen[1] in 1932 coined the term "interdendritic feeding" to describe the flow of residual liquid (which was compensating for the volumetric contraction, α, on solidification) through the mushy zone of a casting and made the first serious attempt at a theoretical analysis: if P_a is the pressure applied to the feeder head, and P_e the pressure at the tip of an interdendritic channel, then the rate of flow along the channel is $(P_a-P_e)/\mu L'$ where μ is the viscosity of the liquid metal and L' a function of the length and diameter of the channel (L' tends to increase as the channel narrows - which could easily be demonstrated quantitatively if Allen had used the well-known Poiseuille's equation at this point). Now if dm/dt is the rate of solidification the rate of contraction will be $\alpha dm/dt$ so long as no pores form, so that

$$(P_a - P_e)/\mu L' = \alpha dm/dt$$

or

$$P_e = P_a - \mu\alpha L' \, dm/dt \qquad \ldots(26)$$

As solidification proceeds the paths for the feed metal become progressively constricted until the pressure P_e falls below a critical value at which pores will nucleate. Allen assumes that this critical value is the effective internal gas pressure while Flemings[230] considers that the value is zero. Section 2. has shown that both these assumptions are incorrect in general, although Flemings assumption will probably be justified if exogeneous inclusions are present in the melt.

More detailed analyses by Walter, Adams and Taylor[233] and later by Piwonka and Flemings[230] consider the pressure drop along a horizontal cylindrical sand casting of a pure metal. Their results have a similar form to that of Allen:

$$P_e = P_a - 32\,\mu\alpha\lambda^2 L^2/a^4\,(1-\alpha) \qquad \ldots(27)$$

where a is the radius of the liquid core; λ a heat flow constant (see list of symbols) and L is the length of the channel. The values of 'a' calculated to give zero pressure at the end of the channel are found to be in excellent agreement with pore radii found by experiment (as the liquid thread pulls apart the resulting cylindrical pore is assumed to have the same radius as that of the liquid core when nucleation occurred) which are of the order of 0.05 cm.

The problem of the solidification of a long freezing range alloy in a horizontal cylindrical sand mould can be approached in a similar manner, except that flow is assumed to take place in n channels per unit area (where n may be taken as the reciprocal of the square of the dendrite arm spacing) rather than in a single channel, and the channel length is the casting length multiplied by a tortuosity factor τ_o (numerical value close to 2). The result is

$$P_e = P_a - \frac{32\mu\alpha\lambda^2 L^2}{(1-\alpha)a^4} \cdot \frac{\tau_o^2}{\pi b^2 n} \qquad \ldots(28)$$

Normally $\tau_o^2/\pi b^2 n$ is smaller than 1 by several orders of magnitude, hence by comparison with equation (27), pores in a mushy freezing alloy will be much finer than pores at the centreline of a pure metal. While this equation applies strictly only to the extreme of mushy freezing where the solid is uniformly distributed throughout the casting, the equation can also be used to describe pore formation in the cases intermediate between entirely mushy and skin freezing conditions i.e. in cases where some centreline

shrinkage occurs but where dendrite growth also results in more or less evenly distributed microporosity.

The same authors also derive analogous equations for a plate casting in a pure metal, for conditions of cellular solidification, and for conditions of unidirectional dendritic solidification under steep temperature gradients.

In addition it may be noted that much interesting related research has been carried out on the flow of various liquids through compacted beds of particles of various geometries[220-226].

All this theoretical work, however, presupposes conditions of laminar flow of the liquid, which leads to the further presupposition that the pressure drop across the mushy zone is the maximum pressure drop in the system. It is conceivable that localised reductions in pressure could occur at random points within the zone for at least three reasons, which are now examined in turn:

(i) The liquid flow channels would be expected to contain many narrow constrictions. From an elementary application of Bernoulli's theorem one would expect that an increase in velocity of a liquid stream at a constriction in a channel would produce a reduction in pressure of

$$\Delta P = \frac{\rho V_o^2}{2}\left[1 - \left(\frac{A_o}{A}\right)^2\right] \qquad \ldots(29)$$

where ρ is the density of the liquid, V_o its original velocity, and A_o and A are respectively the original and contricted cross-sectional areas of the channel. Reynolds in 1901 demonstrates this phenomenon in a classical experiment:[234] Water was caused to flow through a glass tube which had a narrow constriction. As the water velocity was increased, a critical velocity was observed at which the water at the narrowest part of the constriction became opaque with minute bubbles which

extend some distance down-stream. At the same instant a loud hissing noise occurred which was assumed to be associated with the collapse of the bubbles.

Equation (29) predicts rather larger falls in pressure than are to be expected in practice because of the neglect of viscous drag from the walls of the channel which would tend to favour the direction of liquid through easier neighbouring channels.

(ii) Liddiard[235] suggested that the rapid accelaration of residual liquid through the dendrite mesh as solidification nears completion might create turbulent conditions. This seems unlikely however in view of the wide applicability of formulae, such as Poiseuille's, which are based on laminar flow to the problem of liquid penetration through porous media[225-6].

(iii) Various authors[202,235] have supposed that vortices may occur during interdendritic feeding, and that a bubble may nucleate at the centre of a vortex if the fall in pressure at this point is sufficient. However the predicted fall in pressure depends upon the particular mathematical model chosen. Liddiard[235] and Dean[202] both quote

$$\Delta P = - \Gamma^2 \rho / 8\pi^2 r^2 \qquad \ldots(30)$$

where Γ= the circulation (a measure of the intensity of the vortex) ρ = density of the liquid; r = radius vector. At the centre, therefore, the pressure difference falls to minus infinity. This is only true for a 'free' vortex, whose rotation is zero at the liquid boundary and increases towards its centre.

A 'forced' vortex corresponds to a region of liquid of radius R circulating with constant angular velocity w (as a rigid disc). The pressure differential between

the boundary of the vortex and its centre is finite, and is given by

$$\Delta P = - w^2 R^2 \rho/2 \qquad \ldots(31)$$

Prandtl and Teitjens[236] attempt to describe a mathematical model corresponding more closely to a real vortex: it consists of a free vortex containing a core of radius r_v of forced vortex. The pressure reduction is again finite

$$\Delta P = - \Gamma^2 \rho /4\pi r_v^2 \qquad \ldots(32)$$

Despite this progressive refinement, all these models are inadequate to explain the pressure drop at the centre of a real vortex for two reasons: (a) the models are two dimensional, so that in a real liquid considerable relaxation of a hydrostatic tensile stress would occur along the third dimension, i.e. parallel to the axis of the vortex; and (b) the models neglect the stages of the growth and decay of a vortex, so that the pressure differential would be expected to exhibit a maximum at some stage in its life[237].

A closer theoretical and experimental examination of the hydrodynamics of liquid flow in the mushy zone of a casting may reveal that vortices, or at least certain types of vortex, are not permissible and that the laminar flow theories require no revision.

3.4. Burst Feeding.

Observations of the late stages of solidification of many aluminium alloys, and of commercially pure aluminium (in the form of a drop of liquid alloy on a levelled sand surface, or of the feeder heads of castings) show clearly that the level of the last portion of inter-dendritic liquid sinks into the dendrite mesh not smoothly,

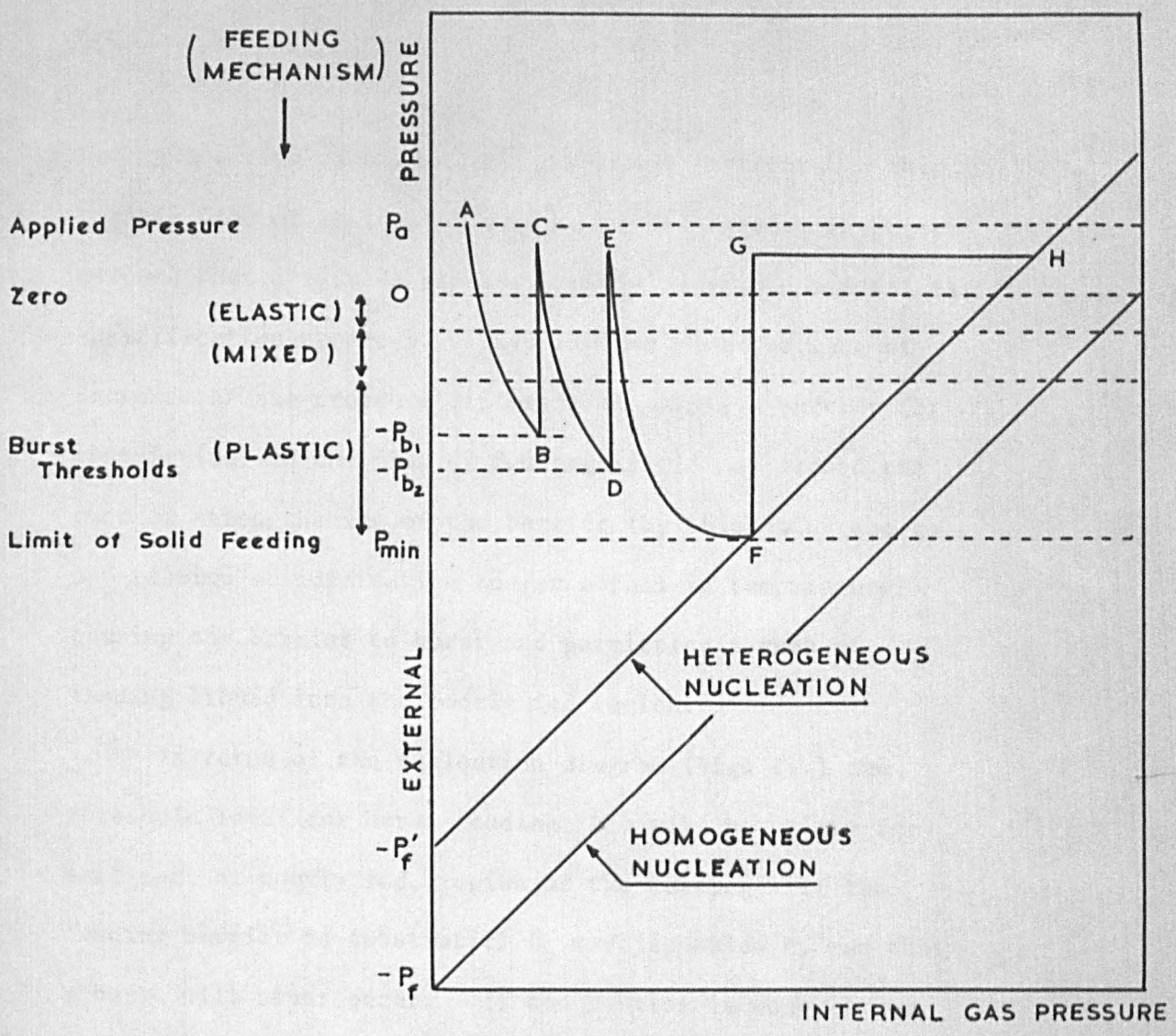

Figure 11. Schematic Representation of Solid Feeding Mechanisms and Burst Feeding effectively delaying the occurrence of pore nucleation.

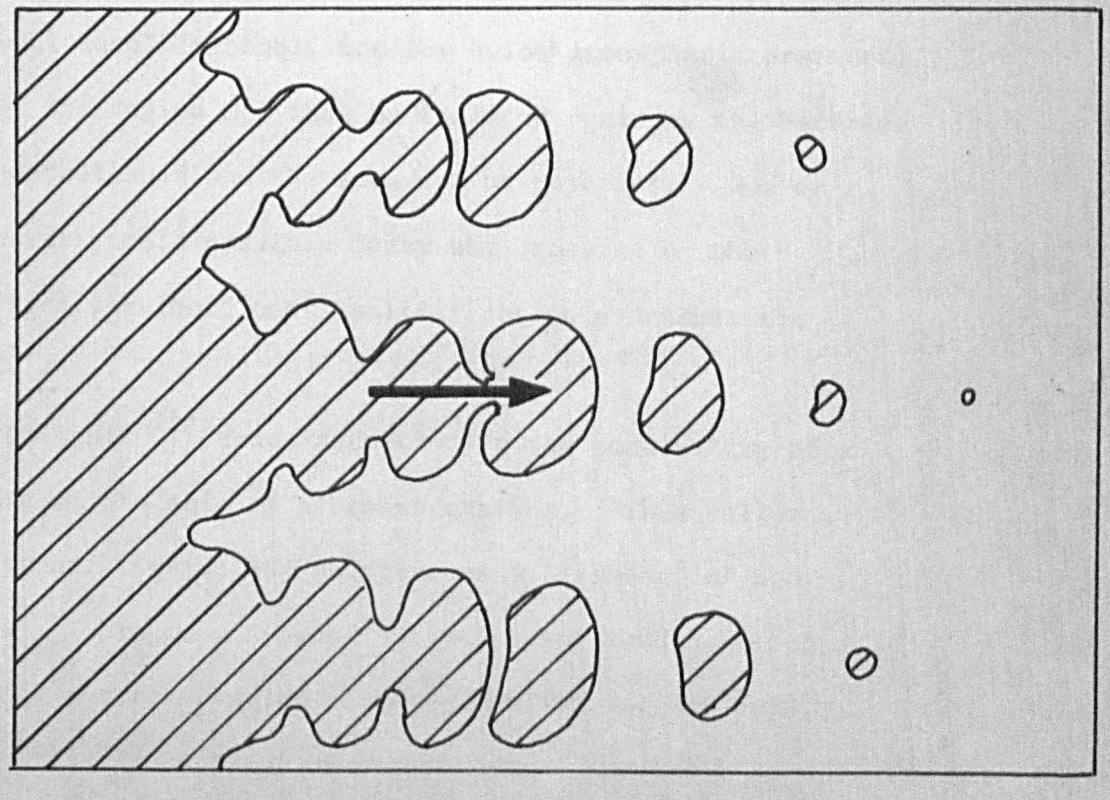

Figure 12. Schematic Representation of Burst Feeding into an Isolated Volume of Interdendritic Liquid.

but in a series of abrupt, discontinuous movements. This erratic flow of residual liquid is to be expected if it is allowed that a reduced pressure builds up within a metal as solidification proceeds. This implies that the rate of increase of the pressure differential across a barrier (or restriction) to the flow of feeding liquid may exceed the rate of strengthening of the barrier (by thickening due to progressive solidification and/or a fall in temperature) causing the barrier to burst and permitting a rush of feeding liquid into the poorly fed region.

In terms of the nucleation diagram (Fig. 11.) the threshold level for burst feeding, P_b, will be unique for each fed, or poorly fed, region of the casting: If the feeding barrier is substantial P_b may lie below P_f' so that a burst will never occur. If the barrier is weak, P_b may lie only just below the level of elastic-plastic deformation. If the burst threshold is crossed at B then the rush of feeding liquid into the region will raise the pressure to the local level (probably not far below atmospheric pressure) at C. The region may then be isolated again as the barrier is re-established and the sequence be repeated. One or more bursts could possibly delay the crossing of the nucleation threshold until solidification overtakes the region.

Pellini[229] draws attention to the possibility of a puncture of the skin of a bronze casting. This relieves the internal tension and so prevents a 'dishing' of the surface. This is a type of surface burst feeding - but which, of course, results in more porosity and not less.

Similarly, successive burst feeding may occur in a casting until the supply of feeding liquid becomes exhausted. At this stage subsequent bursts will consist of inrushes of air into progressively more distant regions of

the casting, resulting in a system of completely interconnected porosity which could probably have been avoided by providing a larger feeder, or by keeping the feeder hot with the application of exothermic compounds etc.

Neglecting these cases of gaseous bursts (which correspond to the growth of cavities and not feeding processes) two extremes of burst feeding may be envisaged: a macroscopic and a microscopic variety.

A macroscopic barrier may arise across the width of a casting due to the choking of the dendrite 'sieve'. This practically impervious mesh will bow into the region of reduced pressure (this will be accentuated by atmospheric pressure, but can occur without it) and eventually may break.

Microscopic regions of trapped liquid may occur between dendrite arms (Fig. 12.). The dendrite arms are rather stubby (i.e. high width/length ratio) and so will be relatively stronger than the macroscopic barriers. Nevertheless, the probability of bursts into such regions is still high since these liquid regions are sufficiently small to have a high probability that they will contain no nucleation sites, so that hydrostatic tension may attain much higher values than may occur in practice in macroscopic volumes. The observed erratic falls in liquid level in Al-alloys correspond to volumes of feeding liquid of the order of 2×10^{-3}cc, which indicates trapped liquid regions of about 3×10^{-2} cc, although more careful measurements are required before firm conclusions can be drawn.

Although a complete theoretical analysis of burst feeding is not practical because of the indefinite number of possible geometrical arrangements of barriers within a simple casting, some simple geometries could be analysed by the method of Svensson[233] who investigates the bursting

of thick spherical shells using an elastic-plastic model. This may be a means of providing some interesting insights into this problem, particularly with a view to investigating the relative rates of the strengthening of barriers and the rate of increase of the pressure differential. Such an investigation might lead to a denial of the existence of confined liquid regions below a certain size threshold - this would have an important influence on some theories of the origin of microporosity.

3.5. Solid Feeding.

This concept is introduced to denote the inward movement of the solidified outer shell of the casting to compensate for the shrinkage on solidification, the driving force being the pressure differential between the inner and outer surfaces of the solid shell (and therefore, in vacuum, only the internal hydrostatic tension).

All types of feeding require a pressure differential otherwise no liquid flow could occur. Hence solid feeding (even if it amounts to no more than an elastic, and therefore reversible, deformation) must occur to some extent even during simple liquid feeding. The more severe pressure differentials produced during mass- and interdendritic-feeding may start to produce a permanent plastic collapse of the casting.

Experimental evidence for solid feeding is so widespread that it is surprising that its importance in relation to porosity has not been appreciated before.

Baker[228] and Ruddle[239] discuss the surface collapsing of the flat surfaces of castings, and Chamberlain and Sulzer[240] find that the phenomenon is only observed in castings which are both poorly fed and of low gas content (the latter resulting in low porosity) and is

eliminated by reversing these two factors; thus solid feeding can operate in the same way as liquid feeding to reduce porosity. Jackson[241] provides some quantitative data on the overall shrinkage of castings. Always, however, the surface sinks have been attributed solely to atmospheric pressure, whereas if part of the driving force results from the hydrostatic tension in the residual liquid because of the solidification contraction, then sinks nearly as severe could have been produced in vacuum.

Recent German work[249,250] does draw attention to this phenomenon in relation to the overall feeding of the contraction on solidification, and refers to it as the "einfallvolumen".

Some early theories of the origin of microporosity assumed that if a small interdendritic volume of liquid metal were isolated from supplies of feeding liquid then a pore must necessarily occur to make up the volume deficit on freezing[251-255]. This can now be seen to be an oversimplification. Both Allen[1] and Whittenberger and Rhines[2] appreciated that a negative pressure would arise in such a confined liquid and the latter authors qualitatively discuss nucleation of pores under such conditions.

In view of the pore nucleation conditions outlined in Section 2., it is of interest to determine exactly what shrinkage pressures can be developed in a solidifying casting. For the following quantitative attempts at this problem spherical symmetry has been universally adopted (inner and outer radii of the solidified shell are respectively a and b): by virtue of its geometry the sphere is the most difficult shape to collapse, and therefore results in the highest possible values for the shrinkage pressure. Similar analyses could be developed for other geometries but in any case small liquid regions which are entirely enclosed

by a large solidified volume of a casting approximate reasonably well to spherical geometry.

In many of these models a distinction must be drawn between the solidification rate $\dot{a}$ and the rate of deformation of the solidified shell at the solid-liquid interface, which is $\alpha\dot{a}$ if the very small elastic expansion of the liquid may be neglected (this is justifiable since $P << G$ where G is the bulk modulus of the liquid). Thus assuming that the strain at the inner surface of the shell is[238]

$$\varepsilon = (2/3) \ln (a/a_o)^3 = 2 \ln (a/a_o) \quad ...(33)$$

then the strain rate $\dot{\varepsilon}$ at the solidification front may be taken to be $2\alpha\dot{a}/a$.

Rigid Shell Model.

On the assumption that only the liquid expands elastically to make up for the volume deficit as the solid shell thickens (the solid is assumed to be perfectly rigid) Nussey[224] finds theoretically

$$(G + P_a) b^{3\alpha} = (G + P_s) a^{3\alpha} \quad ...(34)$$

where P_a is the externally applied pressure and P_s the shrinkage pressure. The expression yields values for P_s, however, which are extremely high. Liddiard[235] in a previous qualitative discussion of this problem suggests that the elastic pulling-in of the solid shell may greatly relieve the internal stress. The following models take up this suggestion in several ways.

Elastic-Plastic Model.

From elementary elastic-plastic theory it can be shown[39] that as the shell increases in thickness, the internal tension progressively builds up so that the yield point of the solid is exceeded when the internal pressure reaches about $-2Y/3$ where Y is the yield stress. After

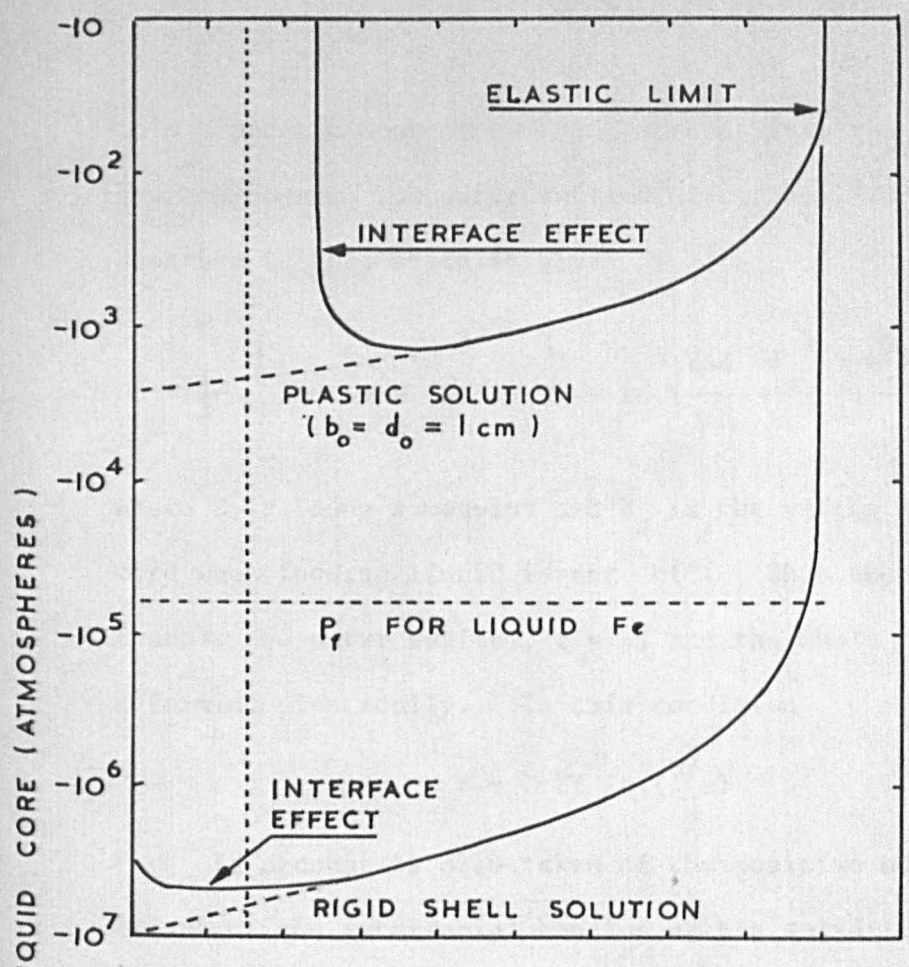

Figure 13A.

A comparison of the pressure in the residual liquid of a solidifying sphere of Fe, 1 cm. radius, calculated from the rigid shell and elastic-plastic models.

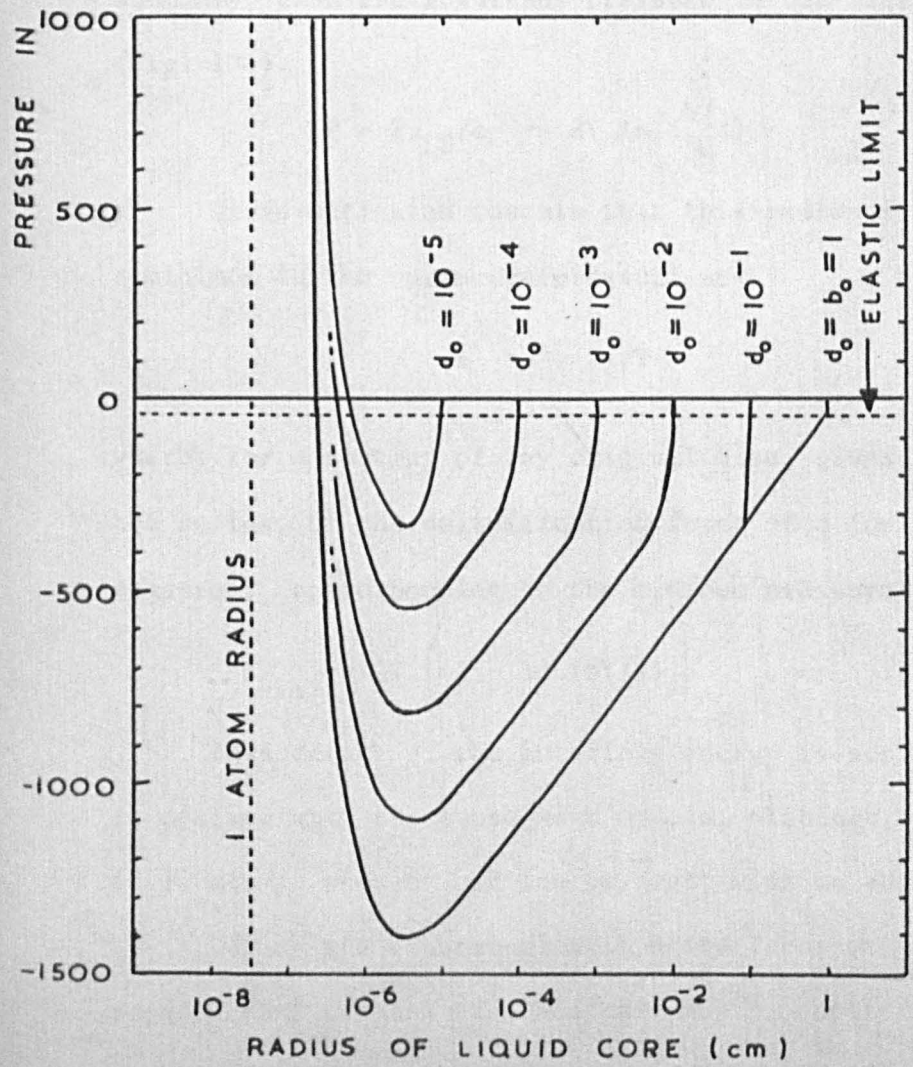

Figure 13B.

Solutions of the elastic-plastic analysis calculated for various initial radii (d_o) of trapped liquid regions at the centre of a solidifying sphere of iron, 1 cm. radius.

this a plastic zone of radius C spreads from the inner surface towards the outer surface of the shell. The pressure in this state is given by

$$P = \frac{-2Y}{3}\left[1 - \frac{2\alpha E\ (d_o^{\,3} - a^3)}{3Y\ b^3} + \ln\left\{\frac{2\alpha E\ (d_o^{\,3} - a^3)}{3Y\ a^3}\right\}\right] \quad ...(35)$$

where E is Young's modulus and d_o is the radius of the liquid core when feeding liquid is cut off. When the plastic zone reaches the outer surface, c = b, and the whole casting is deforming plastically. In this condition

$$P = -2Y \ln (b/a) \quad ...(36)$$

If account is also taken of the positive compressive effect of the interfacial tension at the solid-liquid boundary, then the resultant pressure in the liquid becomes (Fig. 13.).

$$P = 2\gamma_{LS}/a - 2Y \ln (b/a) \quad ...(37)$$

Differentiation reveals that this expression predicts a minimum in the shrinkage pressure at

$$a = \gamma_{LS}/Y \quad ...(38)$$

which, for a casting of any original size, gives a value for the radius of the solidification front of a few hundred Angstroms, corresponding to the minimum pressure

$$P_{min} = 2Y\left[1 - \ln (bY/\gamma)\right] \quad ...(39)$$

This effect of the interface energy is not mentioned in dealing with the subsequent models, although, naturally, it is always present and can be dealt with as above.

During the elastic-plastic state Tabor et.al.[242] suggest that a relaxation analysis may be applied to the problem of the progress of the plastic boundary, which they find to be diffusion controlled. In this way the effect of the rate of freezing may be evaluated. Such an approach

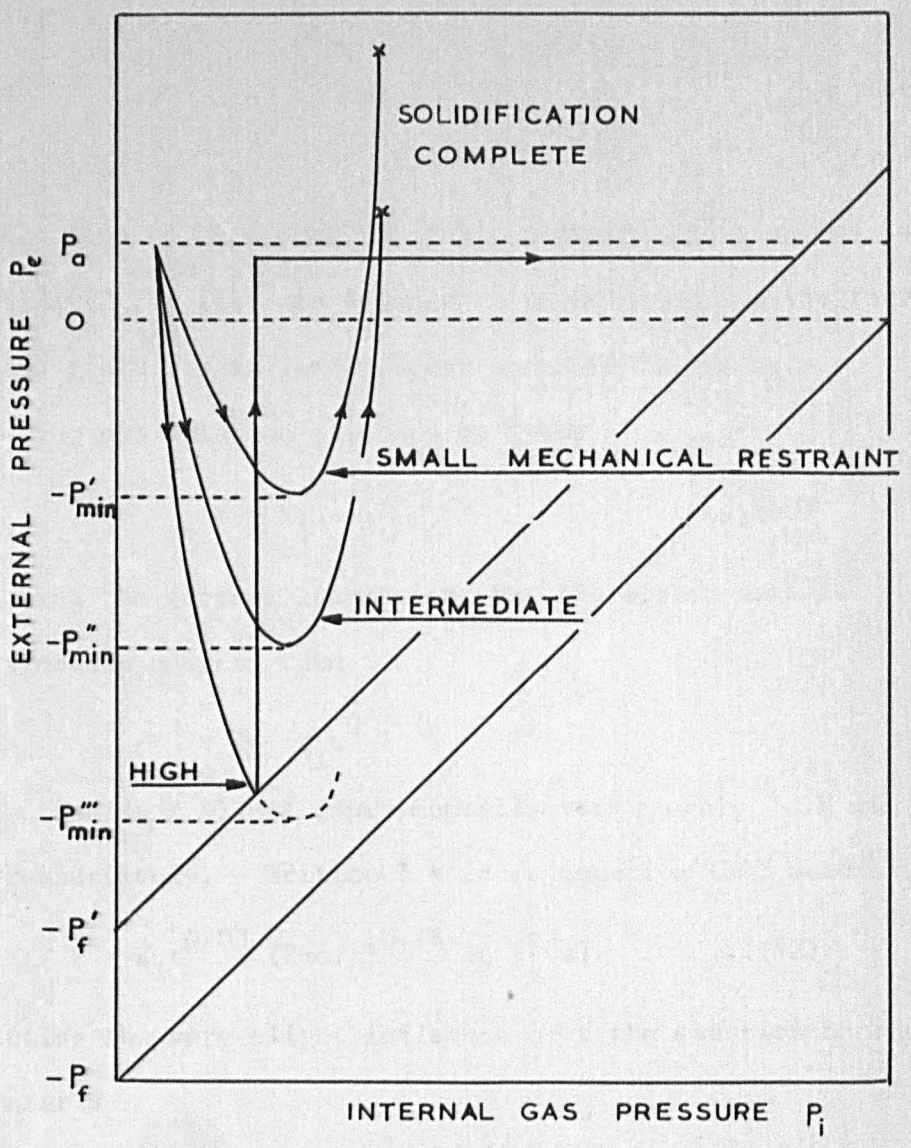

ACTION OF SOLID FEEDING IN PREVENTING PORE NUCLEATION

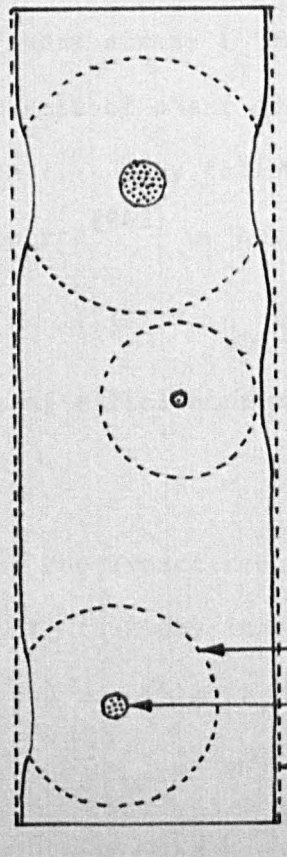

Trapped Liquid Regions giving rise to plastic zones which impinge on the surface of a casting, causing localised elastic and plastic deformation of the surface.

FIG. 14

is not attempted here, but the fully plastic condition may be investigated for its rate dependence if we allow for the fact that the yield stress is dependent upon strain and strain rate using the relation proposed by Tabor

$$Y = K_1 \varepsilon^{\mu} \dot{\varepsilon}^{\nu} \qquad \ldots(40)$$

and making the further assumption that the strain rate is approximately uniform then

$$Y = K_1 t^{\mu} \dot{\varepsilon}^{(\mu + \nu)}$$

where μ and $(\mu + \nu)$ are experimentally very roughly 0.03 and 0.18 respectively. Writing $\dot{\varepsilon} = 2\alpha\dot{a}/a$ equation (36) becomes

$$P = -K_1 t^{0.03} (2\alpha\dot{a}/a)^{0.18} \ln (b/a) \qquad \ldots(42)$$

Neglecting the very slight influence of t the equation becomes very nearly

$$P = -K_2 (\alpha\dot{a}/a)^{0.2} \ln (b/a) \qquad \ldots(43)$$

Bingham Flow Model.

A Bingham solid is one which is perfectly rigid up to a critical shear stress τ_c and subsequently deforms viscously so that the rate of shear strain $\dot{s}$ is proportional to the shear stress τ. Thus following the analysis by Mackensie and Shuttleworth[243] we have

$$\tau = \eta_{\infty} \dot{s} + \tau_c \qquad \ldots(44)$$

If the rate of radial strain is $\dot{\varepsilon}$ then

$$\dot{s} = \sqrt{2}\, \dot{\varepsilon} \qquad \ldots(45)$$

Substituting the Tresca result that the uniaxial yield stress $Y = 2\tau_c$ then the instantaneous viscosity from equations (44) and (45) is

$$\eta = \eta_{\infty} + Y/2\sqrt{2}\, \dot{\varepsilon} \qquad \ldots(46)$$

The rate of dissipation of energy per unit volume of the solid is

$$\dot{E} = 3\dot{\varepsilon}^2 \eta \qquad \ldots(47)$$

so that the rate of dissipation of energy throughout the whole shell is

$$3 \int_a^b \dot{\varepsilon}^2 \eta \, dv = 12\pi \int_a^b \dot{\varepsilon}^2 r^2 \eta \, dr \qquad \ldots(48)$$

We may now deduce that if the rate of radial displacement is $\alpha\dot{a}$ then the effective force generated at the inner surface of the shell is $\dot{E}/\alpha\dot{a}$, so that the corresponding pressure due to the restraint of the shell is $\dot{E}/4\pi a^2 \alpha\dot{a}$. Therefore

$$P = \frac{3}{a^2 \dot{a} \alpha} \int_a^b \eta \dot{\varepsilon}^2 r^2 \, dr$$

$$= -4\eta_\infty a^2 \dot{a} \alpha \left(\frac{1}{a^3} - \frac{1}{b^3}\right) - \frac{3Y}{\sqrt{2}} \ln \left(\frac{b}{a}\right) \qquad \ldots(49)$$

When the viscosity is zero the expression reduces to

$$P = -\frac{3Y}{\sqrt{2}} \ln \left(\frac{b}{a}\right) \qquad \ldots(50)$$

which compares favourably (to within 6%) with that deduced from the elastic-plastic analysis (equation 36).

When the yield stress is zero the Bingham solid behaves as a classical viscous material. When $b >> a$ equation (49) simplifies to

$$P = -4 \eta_\infty \alpha\dot{a}/a \qquad \ldots(51)$$

or if we may describe viscosity as a process characterised by an activation energy Q, then the shrinkage pressure for a purely viscous material becomes

$$P = -K_3(\alpha\dot{a}/a) \exp (Q/KT) \qquad \ldots(52)$$

Creep Models.

For an incompressible material the radial velocity of an element at radius r is given by $\dot{u} = (a^2/r^2)\dot{a}$ where u is the radial displacement of the element. Consequently the radial strain rate is

$$\dot{\varepsilon} = -\frac{2a^2}{r^3} \cdot \dot{a} \qquad \ldots(53)$$

Assuming now that the deformation is best described by a Sinh flow relation proposed by Sellars and Tegart[245] from theoretical analyses of creep and verified very convincingly by the rationalisation of a wide variety of data on high temperature mechanical properties, then

$$\dot{\varepsilon} = K_4 (\sinh \beta\sigma)^{m'} \exp(-Q/KT) \quad \ldots(54)$$

equating (53) and (54) and substituting the boundary conditions that when $r = a$, $\sigma = P$, and when $r = b$, $\sigma = o$, we have

$$2\alpha \dot{a} a^2 \left(\frac{1}{a^3} - \frac{1}{b^3}\right) = K_4 (\mathrm{Sinh}\ \beta P)^{m'} \exp(-Q/KT)$$

hence

$$P = -\frac{1}{\beta} \mathrm{Sinh}^{-1}\left[\left(\frac{2\alpha\dot{a}}{K_4 a}\right)^{1/m'} \exp\left(\frac{Q}{mKT}\right)\right] \quad \ldots(55)$$

if $b >> a$. Sellars and Tegart find n to be roughly 5 for most metals. Making the further simplification when P is less than about ~10 atmospheres (since $\mathrm{Sinh}\ x \simeq x$ when x is small)

$$P = -\left(\frac{2}{K_4 \beta^5}\right)^{0.2} \left(\frac{\alpha \dot{a}}{a}\right)^{0.2} \exp\left(\frac{Q}{5KT}\right) \quad \ldots(56)$$

In a somewhat similar analysis Tabor and colleagues[242] use a transient creep equation instead of equation (54), since they believe that it describes rather more accurately the situation where a plastic zone is continuously spreading. For the case of the whole body being in a plastic condition however, there can be no objection to the use of some of the more common creep relations applicable to a steady strain rate. Using a viscous creep equation $\dot{\varepsilon} = K_5 \sigma^5 \exp(-Q/KT)$ we obtain a result identical in form to equation (56).

Bearing in mind the differences in theoretical approach the qualitative similarities between the various results (equations 43, 52, 56) is reasonable, and the shrinkage stress is seen to increase with increase in (a) solidification contraction, (b) freezing rate, and (c) decrease

in radius of the liquid core. Quantitative results are not easy to obtain from equations (52) and (56) since there is a great lack of data, but equation (37) is worked out in detail. The results are given in Fig. 13. and show a maximum shrinkage pressure of the order of -1500 atmospheres. This figure falls to -900 atmospheres if other yield point data is used[39]. In either case the maximum hydrostatic tensile stress is several orders of magnitude lower than that required to homogeneously nucleate a pore, so that in the absence of suitable nuclei, a volume of trapped liquid will freeze sound due to the inward collapse of the surrounding casting. We may also conclude that if there are n nuclei (including inclusions, bubbles or alpha decays) present per unit volume of casting during freezing, and if there are 10n volumes of liquid trapped between dendrite arms, then approximately 90% of these regions will freeze sound.

4. FACTORS AFFECTING MICROPOROSITY.

A survey of experiments dealing with factors affecting porosity reveals that the earlier experimenters were largely unaware of the complexity of the phenomena involved, and as a consequence often exercised too little control of important variables. Many of their results, therefore, must be viewed with caution. Nevertheless, some attempt at rationalisation has been made in this review, with due regard to the uncertain nature of the evidence.

4.1. Gas Content.

Very little work has been carried out on the relation between gas content and porosity in steels and high temperature alloys. The practical difficulties of such investigations are very great, and the interpretation often open to doubt because of the several gasses in solution, and the many possible combinations of these gases in a bubble.

Some comparative work by Parsons[218] has demonstrated that, for a 0.3% C steel, poured in air and in vacuum, but solidified under atmospheric pressure, pouring in vacuum reduces microporosity. More quantitative considerations by Heide[219] throws light upon the contribution of the various gases present under various conditions to bubble formation.

Chamberlain and Sulzer[240] used aluminium alloys of "high" (0.35 ml H_2/100 g), "intermediate (0.25) and 'low" (0.15) gas contents cast in sand moulds, and found that high gas contents were associated with considerable porosity, while low gas contents practically eliminated porosity, but led to severe surface collapsing in poorly fed sections.

Experiments with an Mg-alloy degassed as thoroughly as possible and cast into moulds previously baked out at 900°C and filled with So_2 led Baker[228] to believe that he

had conclusively proved the existence of shrinkage porosity. However, realising the inadequacy of conventional degassing techniques, Whittenberger and Rhines[2] boiled Mg-alloys in a carbon crucible in an atmosphere of pure dry Argon, until a major proportion of the alloy had boiled away. The metal was cooled while remaining under its protective atmosphere and subsequently examined for porosity. None was revealed by metallographic examination, or by radiography, although density results seemed to indicate a porosity level of 0.02 to 0.10% which cannot be far outside their experimental error. Exposure of the melt to various gases, particularly H_2 and H_2S, vastly increased the porosity to almost 40%. After this demonstration of zero (or nearly so) porosity in the absence of gas, they also show that porosity can be found in gas-containing alloys which expand on freezing. They conclude that porosity cannot be nucleated by shrinkage alone, but can be nucleated by gas in the entire absence of shrinkage. However, once nucleated, the growth and the final size of the pore can, in certain cases, be practically entirely governed by shrinkage.

It is interesting that the above experiments are confirmed by Mrs. Beeton[256] who recommends the use of pre-boiled water (which, it must be remembered, expands on freezing) if clear ice-cubes are required.

Flemings and co-workers[304] deduce theoretically that the applied pressure, P_a, during casting reduces the percentage volume porosity by (a) increasing the solubility of the gas in the solid and (b) compressing existing pores.

$$\% \text{ Porosity} = (C_o - K_s P_a^{\frac{1}{2}}) \cdot \rho_s T_f / 273 P_a \quad \ldots(60)$$

C_o is the original concentration of gas (in ml/100 g), K_s Sievert's constant for the solid, ρ_s density of sound solid, T_f freezing point (^oK). The derivation assumes that the

pressure in the bubbles is equal to P_a which explains why this formula yields values for porosity which are at least a factor of 3 too large. Later work[230] by the same school shows that the equilibrium partial pressure P_g, of a dissolved gas is given by equation (20). Considering only gas as the source of pores, a critical amount of gas C_c must be present for pores to form at all. This follows directly by setting $P_g = P_a$, $C_o = C_c$ and $f_L = 0$

$$C_c = K_S P_a^{\frac{1}{2}} \qquad \ldots(61)$$

The formulae (20, 60, 61) neglect surface tension and the mode of solidification, so these authors proceed to show that surface tension increases the amount of gas which can be present initially without forming a pore, particularly when $n\tau$ is large. Correcting some minor errors in the original paper, the equations are

$$P_a = \gamma\left[\left(\frac{\pi n\tau(K_L - K_S)\, r_c^{\,2} + K_S}{2\pi n\tau\,(K_L - K_S)\, r_c^{\,3}}\right) - \frac{2}{r_c}\right] \qquad \ldots(62)$$

$$C_c = \left[\frac{\pi n\tau(K_L - K_S)\, r_c^{\,2} + K_S}{2\, n\,\,(K_L - K_S)\, r_c^{\,3}}\right]^3 \qquad \ldots(63)$$

To determine C_c, equations (62) and (63) are solved simultaneously to eliminate the critical bubble size, r_c. Provided C_c is greater than that given by equation (61) the final solid is supersaturated. This effect can be very great if the mode of solidification yields a high value of $n\tau$, so that little gas is available for the production of porosity.

Although predictions must be made with caution when using the above equations since they neglect the effects of shrinkage, there is a fair volume of experimental work to justify the view that a critical gas content must be

exceeded before porosity can occur for a given cooling rate during solidification, and that above this value, porosity increases with increasing gas content. This is found for aluminium alloys[41,257-9] and estimates of C_c for hydrogen in steels are given by Heide[219] and Smialowski[260].

From experiments concerned with cavitation induced by ultrasonics in water, Blake[213], in agreement with Briggs[261], found a cavitation threshold for water saturated with air at about -1.3 atmospheres (i.e. -0.3 atm. absolute), and for degassed water about -6.0 atmospheres (-5 atm. absolute).

4.2. Inclusions.

The nucleation of bubbles by certain inclusions is expected to be rather easier than nucleation in the interior of the liquid metal (Section 2.). The experimental evidence for this is reviewed.

Ransley and Talbot[259] compared the porosity found in Duralumin, 99.2% Al, 99.8% Al and 99.99% Al. For the same hydrogen contents they observed that the least pure material produced about 10 times the volume of porosity found in the purest material. Also, the points on the graph of gas concentration versus % porosity were very closely grouped about the mean line for the 99.2% Al, but were widely scattered for 99.99% Al. This suggests that where inclusions are plentiful little supersaturation occurs since pore formation is easy in all parts of all castings produced in this material, but when inclusions are sparse, there is a statistical probability that some specimens will contain significantly more inclusions than others, and regions of some castings may contain none, causing nucleation to be difficult or impossible. This interpretation is corroborated by a further observation which was obtained in this work: equation (60) predicts a linear increase in % porosity versus gas concentration and was derived assuming

easy nucleation (i.e. neglecting surface tension) whereas if nucleation is hindered by surface energy considerations the relations become more complex (eqtns. 20, 62, 63) and non-linear. The experimental results show a good straight line for the 99.2% Al and a curve for 99.99% Al. All other results on relatively impure Al show linear relations[54,55,57].

The Straube-Pfeiffer test for the gas content of Al-alloys was carefully investigated by Brondyke and Hess[262]. They concluded that the test was insensitive to hydrogen contents below 0.3 ml/100 g. because of the influence of inclusions. By filtration of the liquid metal to remove a large percentage of the inclusions a specimen which appeared "gassey" in the test (i.e. formed a large number of bubbles during solidification) could be made to appear perfectly degassed, although the gas content was unchanged. They point out that although the test does not provide an indication of gas content at these low levels of concentration, it does provide an estimate of pore-forming potential of the liquid, which is perhaps, of greater interest to the foundryman.

The theoretical considerations in Section 2. on the action of solid surfaces in aiding pore formation are given weight by the experiments of Abramov and Teumin[263] who induce cavitation in liquid Bi by the immersion of a solid surface vibrating at ultrasonic frequency. The threshold power imput to produce cavitation at the solid surface was found to be a function of ϕ, which was varied by plating the surface with various metals.

It is therefore feasible that liquid metal history may affect the amount of porosity, since a sufficient time at high temperature may cause certain harmful inclusions to be taken into solution, and so 'deactivating' the liquid metal (i.e. reducing its pore forming potential)[264].

4.3. Freezing Distance L, and Temperature Gradient dT/dx.

Considering an element of distance dx in the mushy zone of a solidifying alloy, across which there exists a temperature difference dT, if the temperature gradient is linear then integrating across the width L of the mushy zone gives

$$L = \frac{\Delta T_f}{(dT/dx)} \qquad \ldots(64)$$

where ΔT_f is the freezing range (under equilibrium conditions this is the liquidus temperature T_L minus the solidus temperature T_s). This relation is necessarily rather rough since real temperature gradients are far from linear, and ΔT_f may be effectively increased by several hundred percent during rapid freezing (for an alloy of a eutectic system ΔT_f becomes $(T_L - T_e)$ where T_e is the freezing point of the eutectic). L may of course be obtained directly by appropriately placed thermocouples in the solidifying casting.

Most investigations into the causes of porosity have used either the temperature gradient (usually measured at the solidus) or the freezing range as critical parameter, and have neglected L which would be expected to be a parameter rather more closely related to the incidence of porosity than either ΔT_f or dT/dx separately, and more particularly since L appears in all the pressure drop formulae (equations 26-28).

Several authors have claimed the existence of a minimum temperature gradient for the elimination of porosity in a particular alloy. Some results are listed in Table 7. together with a minimum value of L calculated from eqtn. (64). Two interesting observations may be made: (a) most of the minimum estimates of L exceed normal casting dimensions (it follows that in general, therefore, the mushy zone fills the casting), and (b) the values are remarkably scattered.

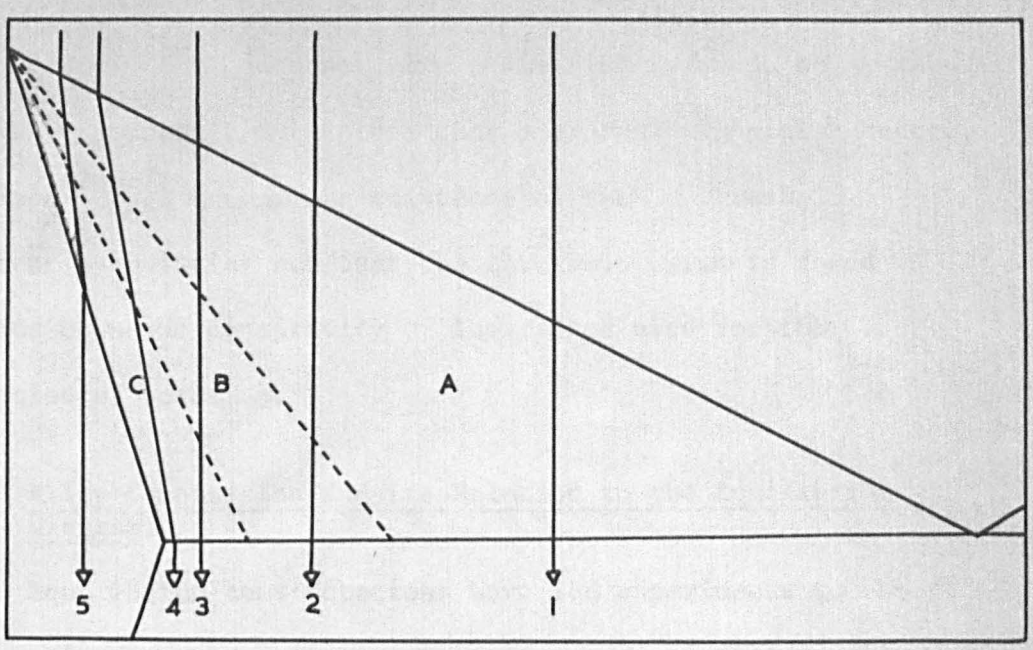

FIGURE 15

SCHEMATIC EQUILIBRIUM DIAGRAM SHOWING REGIONS OF (A) FREE CRYSTALS (B) IMPINGING CRYSTALS (C) "IMPRISIONED" LIQUID REGIONS

ADAPTED FROM BARDOT[276]

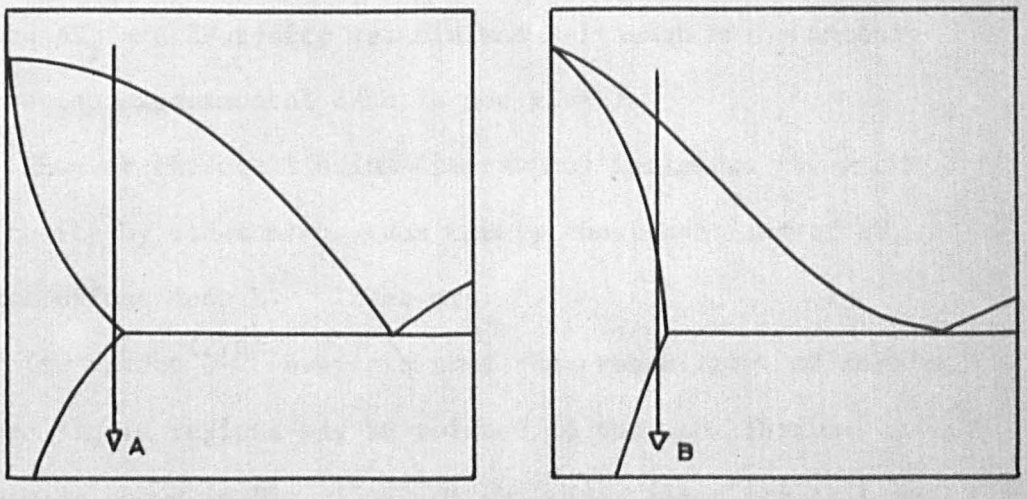

FIGURE 16

ALLOY 'B' WOULD BE EXPECTED TO BE MORE SUSCEPTIBLE TO POROSITY THAN ALLOY 'A'

ADAPTED FROM EASTWOOD AND DAVIS[277]

Bracale[265] does not give a limiting gradient to eliminate porosity, but infers that a gradual transition occurs. Flemings[266-7] denies the existence of such a threshold gradient by pointing out that the threshold which is found depends upon the sensitivity of the method used for the detection of porosity.

4.4. Alloy Composition and its Relation to the Equilibrium Diagram.

Equilibrium considerations have led experiments to expect that an increase of solute content of a eutectic alloy will increase ΔT_f, thereby increasing L and the resulting porosity. Czikel[275] reports some subjective assessments of the amount of microporosity, varying from "none" to "very pronounced", in steels of 0.2 to 0.46% C. For all 14 alloy systems studied by Whittenberger and Rhines[2] an approximately linear relation between ΔT_f and %Porosity was claimed (although unfortunately the precise experimental data is not given).

However the equilibrium diagram may influence the amount of porosity by other means than merely considerations of ΔT_f and its effect upon L. These are

(a) Bardot[276] suggests that the probability of forming trapped liquid regions may be related to the equilibrium diagram as shown in Fig. 15. Of the three alloy compositions shown, he would predict microporosity only in (3) since "imprisioned" liquid regions would be absent in (1) and (2). The writer has added alloys 4 - 5 in which trapped liquid would be expected under the non-equilibrium conditions in a real casting. This is dealt with in greater detail later.

(b) Eastwood and Davies[227] point out that if the contours of the liquidus and solidus surfaces are such as to permit a relatively large proportion of liquid to remain at the lower part of the solidification range, then the alloy

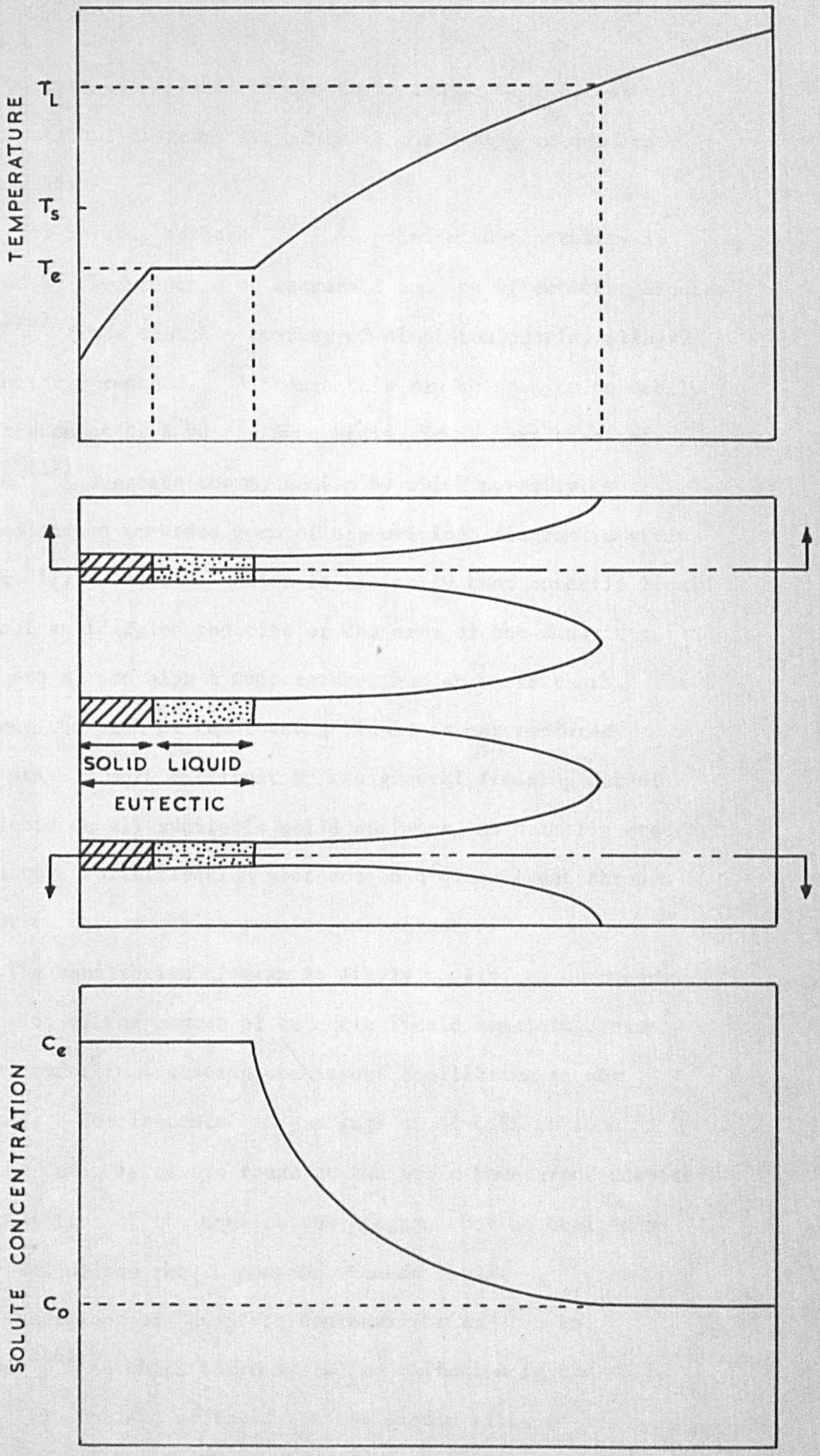

FIGURE 17

SCHEMATIC REPRESENTATION OF NON-EQUILIBRIUM EUTECTIC LIQUID IN A DENDRITE MESH.

ADAPTED FROM SCHEUER[12]

will be less susceptible to the formation of microporosity. Their original diagrams are given in a slightly amended form in Fig. 16.

(c) Several authors[269,273] propose that porosity is reduced by the presence of increased amounts of eutectic liquid. Lees[279] finds that hot tearing of aluminium casting alloys is similarly reduced. Although this can be seen to be nearly a re-statement of Bardot's hypothesis, it is more than this; Schener[12] suggests the mechanism by which porosity is reduced and an ammended form of his original diagram is given in Fig. 17. The explanation is basically that eutectic liquid does not solidify on the tips or the arms of the dendrites, which are at too high a temperature, but at their roots. In this way the path of the feeding liquid is not rendered progressively more difficult by the general freezing out of the liquid on all available solid surfaces, as normally occurs, but rather, solidification proceeds on a plane front through a dendrite network which remains unobstructed.

The equilibrium diagram is likely to give an erroneous indication of the amount of eutectic liquid remaining, simply because under real casting conditions equilibrium is not attained. For instance, in castings of Al-4.5% Cu some eutectic $CuAl_2$ is always found at the grain boundaries despite the prediction of the equilibrium diagram that no $CuAl_2$ can be present unless the Cu content exceeds 5.65%.

Conditions of "complete non-equilibrium" can be defined[246] in which there is (a) no diffusion in the solid state, (b) complete diffusion in the liquid state on a microscale, and (c) no macrosegregation. This leads to a maximum of coring by the dendrites, and a volume of residual liquid given by[279-282]

$$f_L = \left(\frac{C_o}{C}\right)^{1/(1-k)} \qquad \ldots(65)$$

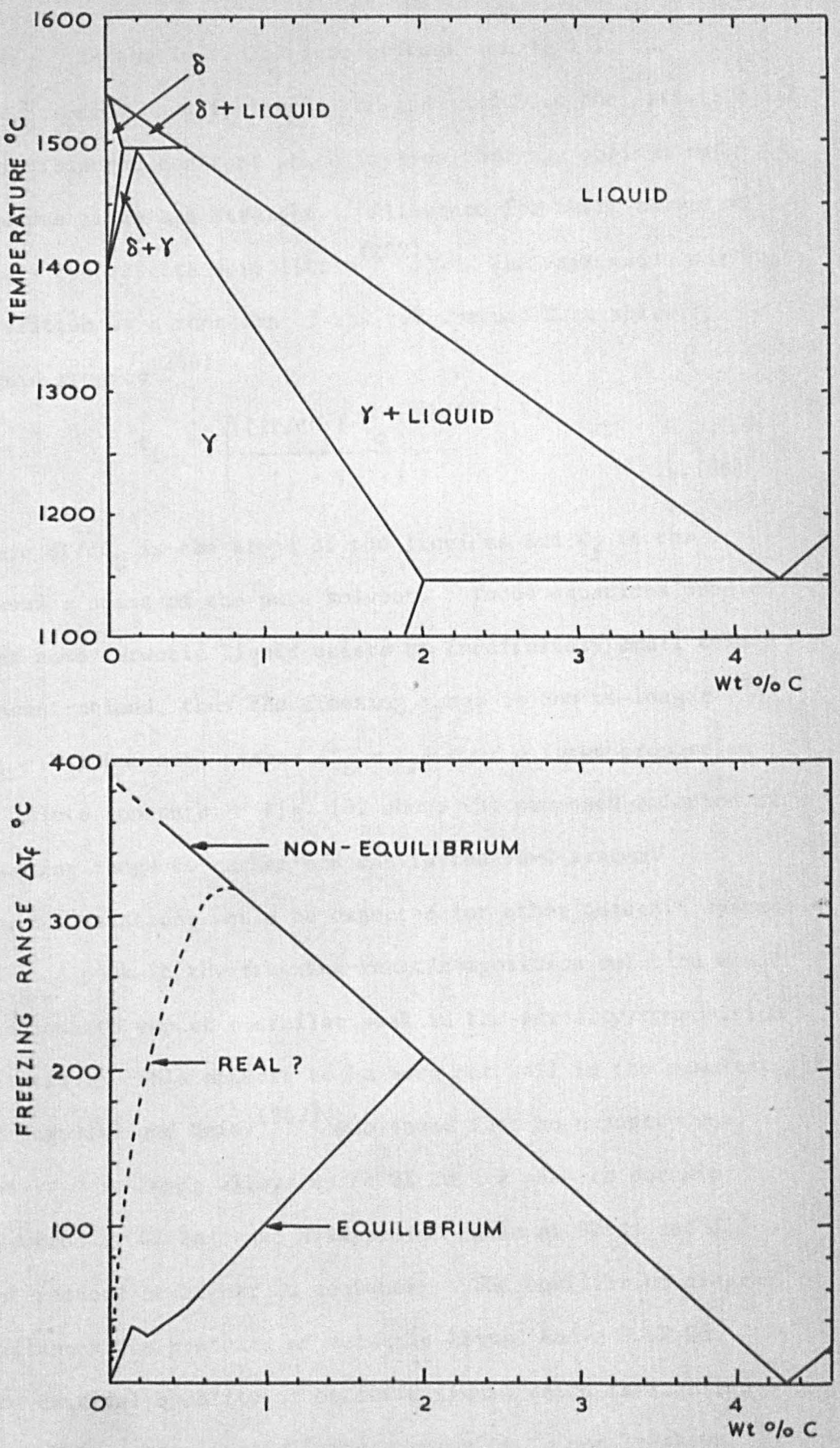

EQUILIBRIUM DIAGRAM AND FREEZING RANGE — COMPOSITION CURVES FOR IRON-CARBON ALLOYS.

FIGURE 18

where C_o is the initial solute concentration, C is the concentration when f_L liquid remains, and K is the partition ratio (assumed constant which implies that the solidus and liquidus lines are straight. Allowance for their curvature alters the results very little[232]). The expression may be re-written as a function of the temperature T at which f_L liquid remains[246]

$$f_L = \left[\frac{(dT/dC_L)\ C_o}{T_f - T} \right]^{1/(1 - K)} \qquad \ldots(66)$$

where dT/dC_L is the slope of the liquidus and T_f is the freezing point of the pure solvent. These equations predict that some eutectic liquid exists at indefinitely small solute concentrations, thus the freezing range is now no longer $(T_L - T_s)$ but more nearly $(T_L - T_e)$ over a large proportion of solute contents. Fig. 18. shows the proposed relation of freezing range to carbon content in the Fe-C system. Similar relations would be expected for other eutectic systems.

A peak in the freezing-range/composition relation would lead one to expect a similar peak in the porosity/composition relation. This appears to be born out well in the results of Lagowski and Meier[283] who found that no porosity was observed in Zn-Mg alloys up to 3% Zn; a peak in porosity occurred at 6% Zn; and disappeared again at 9% Zn and did not reoccur at higher Zn contents. The equilibrium diagram indicates the presence of eutectic liquid above 8.4% Zn. The critical quantity of eutectic liquid which is required to be present to just eliminate porosity is easily shown from the above formulae to be 11.7%.

Other information[278,284] on the Al-Mg system, where solid solubility exists to 17.4% Mg, indicates that porosity is present up to about 10% Mg and above this suddenly decreases. The critical fraction of eutectic liquid can be shown to be 8.2%.

TABLE 7.

Reported values of the minimum temperature gradient to reduce porosity in various alloys.

Material	Minimum Gradient (^{o}C/cm)	Non-equilibrium ΔT_f (assumed) (^{o}C)	Calculated minimum value of L (cm)	Ref.
Cu85-Sn5-Pb-5Zn5 (2"x2" bars)	8	>130	16	268-9
(length 12")	9"	13		11	
	6"	33		4	
88Cu-8Sn-4Zn	1 - 3	>130	43 - 130	271
88Cu-10Sn-2Zn	25	>160	6.4	229
Mg-6Al-3Zn (A Z 63 A)	1	25(?)	25(?)	272
Al-4.5Cu	5 - 13	100	7 - 20	270
Al-7Mg	1	70	70	273
0.3 C steel (plates)	1 - 2	> 40	>18 - 36	229.
(bars)	6 - 12	> 40	> 3 - 6	274

4.5. Rate of Solidification, dm/dt.

Budgen[285] reports that slower cooling produced greater porosity in Al-alloys. He explains this on the assumption that the greater time interval, Δt, between the liquidus and solidus fronts allows more gas to be precipitated. Furthermore, the greater width of the pasty zone facilitates the entrapping of gas bubbles which would otherwise escape by floating out to the surface. For similar materials, Ransley and Talbot[259] also found that the amount of porosity was a direct function of the time interval Δt. By casting an Al-alloy, saturated with hydrogen, into steel moulds at various temperatures, Whittenberger and Phines[2] showed that porosity was inversely proportional to the rate of freezing, although a fall in porosity at very slow rates was attributed to loss of gas from the surface of the ingot during solidification. Also, using Al-6% Cu and Al-5% Si with hydrogen contents of 0.2 and 0.4 ml/100 g. Bhattacharjya[286] showed that for Δt between about 20 and 200 seconds, the relation between porosity and Δt was closely linear with a slope of 1% porosity per 100 seconds solidification interval. However for low gas contents (0.16 ml/100 g.) and shorter solidification intervals (10 to 50 seconds) this linear relation broke down, and, despite some scatter, a reverse trend is perceptible in the results.

It is feasible that at low gas contents and high solidification rates, viscous flow between dendrites becomes important. Allen's formula (eqtn. 26.) predicts that the pressure drop along an interdendritic channel is directly proportional to the rate of solidification. The same implication is present in subsequent formulae (equations 27-28) because of the heat flow term λ.

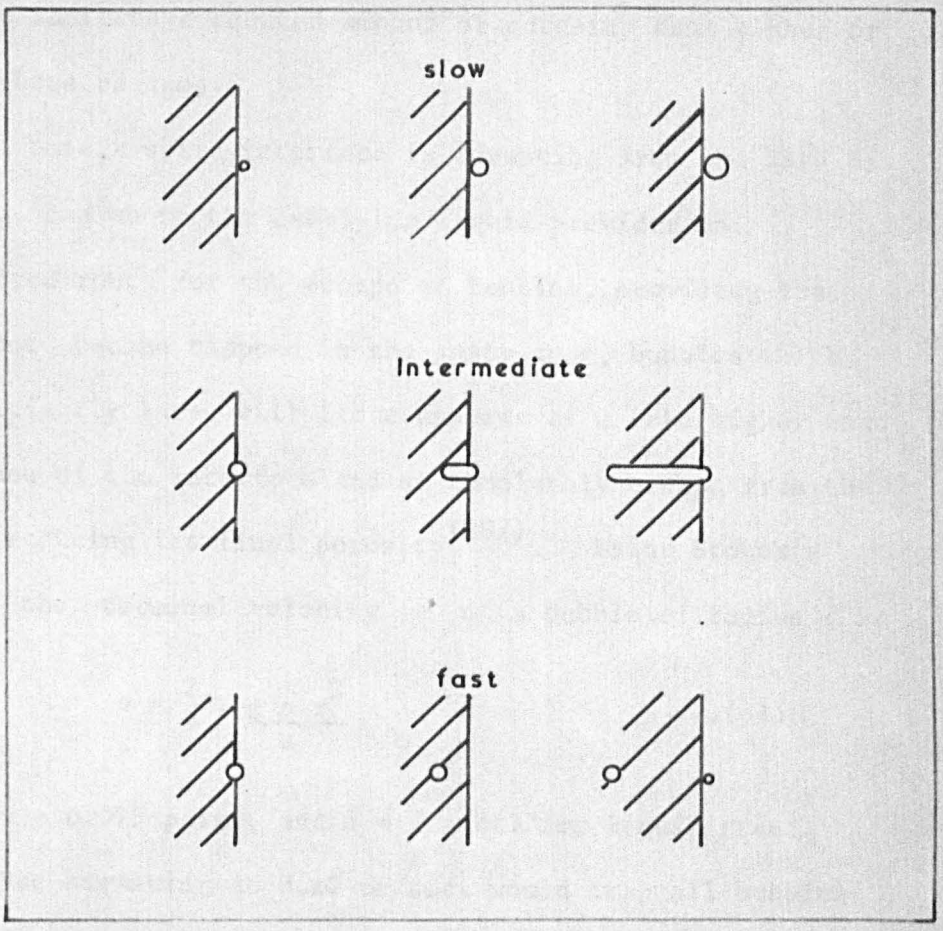

Effect of interface velocity on pore morphology.
Chalmers[11]

FIGURE 19

The grain size and dendrite arm spacing are both reduced by more rapid solidification. Formula (28) would therefore indicate a reduced amount of porosity from either or both of these changes.

Where a solid interface is advancing from the base of a casting, and where the overlying liquid provides an unobstructed route for the escape of bubbles, providing that they do not become trapped in the pasty zone, bubbles which are sufficiently large will float upwards at a rate higher than the advance of the interface and so completely escape from the casting, reducing its final porosity[287]. Using Stokes's equation, the terminal velocity v of a bubble of radius r is

$$v = \frac{2}{9} \cdot \frac{g \rho r^2}{\mu} \qquad \ldots(67)$$

Assuming μ = 0.025 poise, and ρ = 7 g/cc. for liquid steel, an interface advancing at 0.10 cm/sec. would trap all bubbles smaller than about 10 micron radius, but would allow bubbles larger than this, and which were not already enmeshed, to float out. A narrow mushy zone would enhance this effect by permitting a greater proportion of the larger bubbles to escape.

The work of Chalmers and Newkirk[288] on solidifying water indicates that the rate of advance of the solid interface, in skin freezing systems at least, affects both pore size and morphology. At the slower freezing rates, the larger bubbles which are pushed ahead of the interface may detach and float out of the casting, again reducing the final level of porosity. This study makes an interesting comparison with that of Uhlman et.al.[289] who find that there exists a critical interface velocity for each type of inclusion, below which particles are rejected, i.e. pushed along by the interface, and above which they are entrapped. By this means, slowly frozen castings will have a higher density of inclusions

segregated in the residual liquid, and therefore easier pore nucleation, while, conversely, fast frozen castings will be cleaner in the interdendritic regions, tending to suppress pore nucleation. This effect is not likely to be very important in commercially pure alloys since even if very fast cooling produced no segregation of inclusions, there would still be a sufficient density of inclusions in the residual liquid for effective pore nucleation.

Solidification rate will also affect microsegregation of solutes, and the volume fraction of residual liquid, f_L. This is dealt with more fully under Section 4.4. from which it is evident that most generally encountered solidification rates result in perfectly non-equilibrium structures and therefore constant amounts of f_L.

Finally, solidification rate, in conjunction with certain other parameters[126], will determine the mode of freezing; whether the interface will be planar, cellular, dendritic or whether general equiaxial nucleation of the solid throughout the melt will occur. The planar interface will produce no microporosity (unless it be centreline porosity) and the other varieties of solidification are described analytically in Section 3.3. Cellular and dendritic solidification may result in higher concentrations of segregates than a planar interface[290].

Summarising, a high solidification rate will produce lower porosity because of (a) smaller grain size; (b) smaller dendrite arm spacing; (c) shorter solidification interval, Δt; (d) shorter freezing distance, L; (e) an increase in residual liquid, f_L; (f) few segregated inclusions. Other factors which will operate in opposition to the above, tending to produce higher amounts of porosity are (a) pressure drop due to viscous flow is higher; (b) bubbles are unable to float

out because of their limited rate of rise; or become entrapped by Chalmer's mechanism; (c) nucleation will be easier because of decreased surface tension of the residual liquid. A careful consideration of the last three factors reveals that although they may tend to increase porosity a little, their major influence may be rather to produce finer and more numerous pores. Thus, in general, for a given mode of solidification, faster freezing rates will reduce the amount of porosity and produce finer pores.

The effect of various factors on the solidification rate may be estimated from Ruddle's formula[214] for the solidification time, t_s, of a casting (although it is strictly only applicable to castings in moulds of semi-infinite wall thickness, and the derivation neglects corner and surface curvature effects)

$$t_s = \left[\frac{W\ (H + S\ (T_c - T_f)\ )}{1.123\ Aq\ (T_i - T_m)} \right]^2 \qquad \ldots(63)$$

where W is the weight of the casting; H is the latent heat of fusion; s is the specific heat; T_c, T_f, T_m, T_i are the temperatures of casting, freezing, the mould, the mould-metal interface; A is the area of the casting; q is the thermal diffusivity of the mould. Writing superheat $\Delta T_s = T_c - T_f$, and approximately $T_i = T_f$, and introducing a constant z

$$t_s = z \left[\frac{H + S\ \Delta T_s}{T_f - T_m} \right]^2 \qquad \ldots(69)$$

Thus solidification time is seen to increase with both mould and metal temperatures, and becoming infinite when T_m is maintained constant at T_f. However, both superheat and mould temperature have several effects upon porosity in addition to their effect upon the freezing rate; these are dealt with separately.

4.6. Superheat, ΔT_s.

Superheat is defined as the difference between the casting temperature, T_c, and the liquidus temperature, T_L (or freezing point, T_f).

If a region of volume Vo of a casting becomes entirely surrounded by perfectly rigid solid, then, according to Simonik[291], the volume V, of a resulting pore would be (correcting a small omission)

$$V = V_o (\alpha + \alpha_L (T_{av} - T_f)) \qquad ...(70)$$

where T_{av} is the average temperature of the confined liquid, α_L is the coefficient of thermal expansion of the liquid. The equation (70) predicts a greater volume of porosity for higher values of T_{av}, and it is argued that T_{av} may be raised by increasing the superheat. Jackson[292] also proposes this idea. However the additional porosity produced by higher superheats by this mechanism can be safely neglected as the following considerations show: the difference $(T_{av} - T_f)$ is not likely to exceed about 1^oC[93], and α_L is very small, of the order of 0.02% per ^oC for carbon steels[293], compared with α, which may vary between about 3 and 12% depending upon carbon content[294].

A high superheat may also provide the mould with considerable extra heat, resulting in an effectively higher mould temperature (considering particularly investment moulds) and will therefore be expected to make some change in the temperature gradients and the solidification interval, Δt. This point is taken up in detail in Section 8.

The effect of superheat is further complicated by its effect upon liquid metal history. Bogdanov[264] suggests that at high temperatures nuclei for bubble formation are taken into solution in the liquid metal so that the liquid becomes "deactivated". On the other hand, if melting is

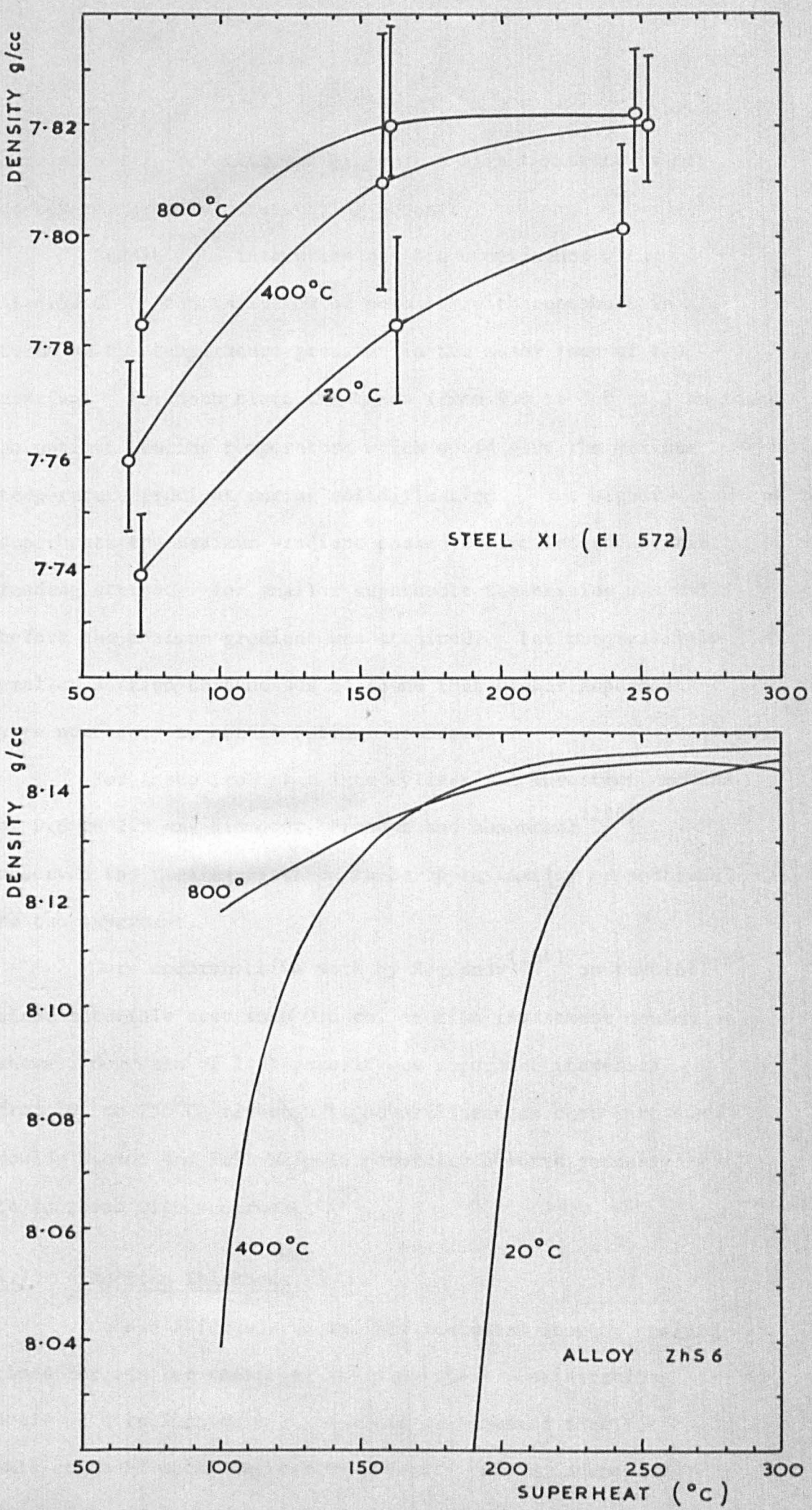

The effect of mould temperature and superheat on air-poured turbine blade alloys XI (Creep-resisting austenitic Cr-Ni steel) and ZhS6 (creep-resisting Ni-base alloy) by Bogdanov(264).

FIGURE 19A

carried out in air then gas pick-up at high temperatures may be severe, greatly accentuating porosity.

Ruddle[295] interprets all his experiments with Al-4.5% Cu on the variation of porosity with superheat in terms of the temperature gradient in the mushy zone of the casting. For each plate thickness (from 0.6 to 3.8 cm.) he found an optimum pouring temperature which would give the maximum temperature gradient during solidification. For higher superheats the maximum gradient passed before interdendritic feeding started; for smaller superheats the casting was solid before the maximum gradient was attained. For progressively smaller section thicknesses he found that higher superheats were necessary to obtain optimum soundness.

For Armco iron cast into cylindrical investment moulds of 0.6 to 2.5 cm. diameter, Present and Rosenthal[296] observed the feeding distance to be approximatley proportional to the superheat.

More comprehensive work by Bogdanov[264] on turbine blade materials cast into 0.6 cm. section investment moulds shows a decrease of 1.3% porosity as superheat increases from 70° to 250°C, although in several bronzes cast into s and moulds Hanson and Pell-Walpole generally observe porosity to increase with superheat[203].

4.7. Section Thickness.

Ruddle's formula (eqtn. 69) indicates shorter cooling times for smaller castings. Applying those considerations dealt with in Section 4.5. it would be expected that for well degassed metal increasing porosity should accompany decreasing section thickness, and vice versa for metal containing rather more gas in solution.

Ruddle's experiments[295] on plates varying in thickness from 0.6 to 3.8 cm. cast in Al-4.5% Cu at 700°C into sand moulds demonstrated that the minimum porosity occurred in the plates of intermediate thickness, and that above and below this thickness the porosity increased because of inadequate temperature gradients during the period of interdendritic feeding. Similarly, early authors[254] were of the opinion that in very thin sections (approximately less than 1 cm.) increasing porosity was due to simultaneous solidification over the whole cross section because of the small temperature gradients present.

4.8. Mould Temperature, T_m.

Mould temperature is only of real interest in ceramic moulds, and is, incidentally, a useful variable for investigations into porosity. Although it might be expected that a reduction in mould temperature might reduce the amount of porosity by increasing the temperature gradient, practically every experimenter has negated this prediction.

Present and Rosenthal[296], in agreement with Adams[297], observed that feeding distance was increased in a 0.2% C steel by increasing the mould temperature.

From foundry experience of casting turbine blades, Tedds[298] records that increasing the mould temperature from 1000 to 1150°C greatly reduces centreline porosity in long blades. In more controlled experiments on similar alloys, Bogdanov[264] observed an increase in density (corresponding to an elimination of 1.4% porosity) as the mould temperature was increased from 20 to 800°C.

The reasons for these surprising results are discussed in Section 8.

4.9. Applied Pressure, P_a.

A pressure applied to a solidifying casting would ~~require~~ reduce porosity by three possible means: (a) increasing the solubility of gas in the solid; (b) preventing nucleation of bubbles; (c) compressing existing voids. Equation 60. is derived assuming (a) and (c) but neglects nucleation difficulties.

Three main methods are available for casting under pressure: (a) The pressure is applied to the feeder head of the casting after pouring, either by the introduction of gas from a cylinder[299,300] or by the introduction of gas producing pellets[301-2]. The exact time of application of the pressure is very critical, making the process unreliable in practice[300], and the pressures which can be used are severely limited by the penetration of the liquid metal into the walls of the sand mould, and by the occurrence of swells on flat surfaces of the casting. All these disadvantages are removed by casting (b) in an autoclave, and (c) against a counter-pressure[303].

The application of pressure to a variety of alloys confirm that porosity is reduced and mechanical properties are improved by casting under pressure[1,304-6].

However, for very high pressures, Babington and Kleppinger[307] found that the quality of Al die-castings did not improve significantly when the pressure exceeded 1350 atmospheres (the yield point of a strong Al alloy at room temperature is about 300 atmospheres). Russian workers[303] found that porosity was not further reduced by pressures above 1900 atmospheres in steel solidified under the pressure produced by a piston.

Comparisons of steel cast in air and in vacuum[309] showed that the vacuum cast material was the more porous. This increase in porosity was attributed to the lower pressure. As far as the author is aware, no thorough work has been

published on the effect of lower pressures on porosity. This is surprising since if porosity is governed mainly by the expansion of gas bubbles then the important parameter is the number of times the gas pressure may be increased. For instance above atmospheric pressure a factor of about 10^3 increases in pressure is attainable with good equipment, whereas from 1 micron to 1 atmosphere is an increase in pressure by a factor of 10^6, which represents a useful and easily accessible range of pressures as a research tool. If however porosity is limited by nucleation criteria, then absolute pressures are important, so that 1 micron may be effectively regarded as zero pressure, and negative shrinkage pressures are possible. In view of the results of this experiment on steel it seems likely that porosity is not limited by nucleation difficulties, but is limited only by growth considerations.

4.10. Surface Tension, γ.

Bhattacharjya[286] compared the numbers and sizes of pores found in unidirectionally solidified 99.99% Al and Al-3% Bi. The freezing characteristics of both were very similar (ΔT_f is only 4^oC for the Bi alloy) but the residual liquid in the Al-Bi alloy was rich in Bi and therefore low in surface energy (the surface energies of Al and Bi are 860 and 380 ergs/cm^2 approximately). Pores were observed in the Bi-rich interdendritic regions and were reduced in average diameter by a factor 10, and correspondingly increased in number per unit volume by a factor 10^3, for melts of similar gas content. The results were interpreted in terms of easier nucleation in liquids of low surface energy, and also illustrate the elementary fact that from the point of view of nucleation the surface energy of the bulk liquid is relatively unimportant, but the surface energy of the highly impure residual liquid is the critical parameter.

A further interesting point is that up to about 1958 Bi was thought to be naturally slightly radioactive, emitting alpha particles on decay. This was because even the purest forms of Bi commonly available contained a small amount of highly radioactive impurity. This may be a contributing factor to these results because of the enhanced number of nucleation opportunities corresponding to the higher density of energetic alpha particles in the residual liquid.

4.11. Grain Size.

Liddiard and Baker[310] suggest that a fine grain size should improve mass feeding. The theoretical work by the school at M.I.T. on the pressure reduction due to viscous flow (equations 27, 28) suggest that easier interdendritic feeding should also accompany decreasing grain size.

Cibula[311,312] found that porosity tended to increase linearly with grain size for Al alloys and bronzes, but found a large scatter in his results. Calvert[313] confirms this linear relation. Lagowski and Meier[283] greatly reduced porosity in Mg-Zn alloys with the use of grain refiners.

However, the picture is not so clear cut, since recent work on Al-alloys in this Department[314] has shown a definite increase in porosity with decreasing grain size. These conflicting results could be due to an effect upon the width of the mushy zone, which is not an independent variable, and in differences in gas content from one cast to another.

A comparison of Al- and Mg-alloys solidified under similar conditions revealed that Mg-alloys contained the least porosity. Liddiard and Baker[310] attribute the difference not merely to grain size (their Mg-alloys were rather finer-grained than the Al-alloys) but to dendrite morphology also. Dendrites in Mg-alloys (with hexagonal crystal symmetry) form small rosettes with six main branches in one plane, and little

or no growth at right angles. In Al-alloys (with cubic symmetry) the dendrite arms extend in six mutually perpendicular directions, and by this means interlocking more and so hindering mass feeding, providing greater resistance to liquid feeding and trapping more liquid. Furthermore, it is likely that plate-like dendrites would pack more densely than three dimensional dendrites.

4.12. Taper.

It has been pointed out[315] that the fundamental reason for tapering an originally parallel casting is to achieve taper in the liquid flow path. Brinson and Duma[316] pioneered a systematic investigation into the effect of tapers varying from 4.8 to 18° on the density of cast steel plates. In spite of some scatter, their results show that a large taper did not further increase the density above that obtained with the minimum taper. They also proved that a non-linear taper could be made more efficient than a straight taper. Using earlier experimental data, Wlodawer[317] deduces an ideal curve for the tapering of casting. Sullivan[315] proposes a parabolic taper from theoretical considerations. Earlier calculations and confirmatory experiments by this school[233] show that a linear taper of 1.7° is sufficient to feed a round, sand-cast bar of a pure metal to complete soundness.

Experiments on wedges cast in bronze[318] show that step-wedges are more difficult to feed than otherwise identical linear wedges. This observation might be simply explained by Pellini's suggestion[229] that at a change of section the feed metal which is sucked into the smaller section may carry with it solid material which may plug the entrance. Later work[319] however casts doubt on the general validity of this mechanism.

4.13. Vibration during Solidification.

In this largely unexplored field Jagaciak and Jones[320] and Dmitrovich and Butsel[321] have found that the application of vibration to solidifying castings improves their soundness. Although the full explanation of this result may be complex, part of the cause may be attributed to the finer microstructures produced.

4.14. Pouring Rate.

In extensive experiments on various bronzes, Hanson and Pell-Walpole[203] found that porosity decreased with slower pouring speeds. The effect is most probably the result of the high temperature gradients which maintain an artificially small width of the mushy zone.

5. THE QUANTITATIVE MEASUREMENT OF POROSITY

Investigations into the phenomenon of microporosity have been severely hampered by the lack of a convenient and precise method for its assessment. Certain unusual techniques have been suggested for the quantitative measurement of porosity, for instance the use of indentation hardness[323-4] and measurements of thermal and electrical conductivity[328]. However, six main techniques which are used more generally are examined below.

5.1. Feeding Distance.

Feeding distance is defined as the length of casting which can be fed to perfect apparent soundness. This widely used parameter can only be used for comparative purposes, and can in no way be related to the quantity of porosity. In this respect the results may be actually misleading, as the work of Weins[325] suggests, since conventional X-ray techniques on thick sections are not sensitive to regions of fine, dispersed microporosity, which may therefore appear sound and increase the apparent feeding distance.

5.2. Pressure Tightness.

Alternative methods of measuring pressure tightness are described by Johnson[271], and Trojan and Flinn[326-7]. Although the pressure tightness of a complete casting may be tested, detailed investigation requires a thin slice of the casting, between 0.08 and 0.64 cm. thick, normally taken from the thermal centre of the section. Although the method is rapid and easy it has large disadvantages: it is subject to a sampling error, and of necessity, only the interconnected pores are assessed, which may bear little relation to the total porosity present.

5.3. Ultrasonics.

Abrahams and Lavender[329] have demonstrated that microporosity can be detected as a fine, "grass-type" of oscilloscope indication. Furthermore, Smolen and Rosenthal[330] claim that ultrasonic attenuation appears to be more sensitive than radiography in the detection of microporosity. They found a linear relation between density and the number of echoes, so that there is some hope of developing a method of assessing porosity in a quantitative and non-destructive manner by this means.

5.4. Metallography.

An evaluation of procedures in quantitative metallography for volume-fraction analysis is given by Hilliard and Cahn[331] and Gladman and Woodhead[332]. However, generally the method is arduous and the scatter in the results is high. The unreliable element in the results derives not only from the expected standard deviation due to the point counting method (this can be reduced as far as desired by increasing the number of points), but from the severe sampling error involved in attempting to estimate bulk quantities from a single plane section. Nevertheless, the technique provides additional information on the distribution and morphology of the pores.

The rapidity and ease of obtaining results with the quantitative television microscope could reduce the sampling error since it would be feasible to examine many more sections. This technique would then be a powerful tool for the quantitative investigation of porosity.

5.5. Radiography.

In general, X-rays are not sensitive to porosity of linear dimensions smaller than about 2% of the thickness of the section. This is largely due to the blurring of the image because of increasing average distance from the film as the

section increases. Definition is further reduced by the mottling of the image due to diffraction effects associated with large grain size of the specimen[333], and in unmachined castings by surface roughness. Trillat[334] and Sharpe[335] have reviewed the technique.

For the study of microporosity it is clear that thinner sections having a smooth surface finish must be used. Many workers have used 0.002 cm. thick sections[10] for the study of microporosity, and Flemings[11] has observed pores of only 3.5μ in diameter by using a thickness of 0.005 cm. Investigators at British Steel Castings Research Association[12] recommend 0.05 cm. thickness. However, in a casting of about 1.0 cm. section there is a real possibility that such thin sections might entirely miss the important regions of porosity. To reduce this sampling error somewhat, the author has used specimens 0.125 cm. thick and found that pores of 10μ diameter could still be distinguished; the loss of detail represented no loss of useful information from the point of view of a quantitative assessment.

An early attempt at quantitative evaluation of the resulting radiographs was made by Busk[336]. A later method employing point counting is described by Flemings[287], and subsequently further improved to give a direct value for the percentage of porosity[337].

5.6. Density.

Several important disadvantages attend the use of density as a measure of porosity. In complex alloys the proportions of the phases present may change because of differences in cooling rate, heat treatment, or working, so that the density of the sound material is never known with certainty. The results are also affected by the presence of inclusions and macropores. Finally, the method is

rather insensitive for dense alloys such as steels, so that many previous investigations using this method have failed because experimental scatter has obscured real changes in density due to the presence of porosity. A noteworthy exception is described by Ruddle[333].

Some of these disadvantages may be overcome as follows: In multiphase alloys a constant proportional relation between the phases present may be attained between castings made from the same melt (although other casting conditions have been varied) by appropriate annealing treatments. Duplicate specimens reduce the chance of error due to occasional large inclusions or macropores. The insensitivity of the method can be overcome by careful technique and accurate weighing, although for light alloys the sensitivity is in any case considerably better than that for steels.

In order to determine the density of the perfectly sound alloy investigators often attempt to remove the porosity by rolling followed by annealing. However this method introduces porosity due to the breaking up of inclusions. A more accurate and reliable method is to estimate the percentage porosity from a seminicroradiograph of the most sound casting of a particular melt, and relate this to the densities of the remaining castings.

The density technique has the powerful advantages of (i) being a non-destructive method, (ii) eliminating sampling error for a given specimen, and (iii) yielding directly a quantitative value for the volume fraction of porosity.

6. EXPERIMENTAL PROCEDURE.

6.1. The Mould.

6.1.1. Design.

The test pieces were closely modelled on actual cast turbine blades and consisted of a blade 10 cm. long by 3 cm. wide and of thickness varying from 0.125 cm. to 1.00 cm. Tapers of 2°, 4°, 6° and 8° could also be superimposed on any thickness of blade.

Preliminary measurements on thin sections indicated that the castings solidified within about 3 seconds. Since this is of the same order as the time required to pour the casting it was felt necessary, at least for the first part of this investigation, to top pour castings so that the coldest metal would be at the bottom of the mould and vice versa, thus aiding directional solidification and keeping porosity within reasonable limits.

Spherical feeders of 3.5 cm. diameter were chosen as being the most efficient whilst providing a minimum of interference with thermal gradients in the test casting. Vents 3 mm. diameter were added to the tops of the feeders to allow the wax to escape during burning out.

The gating system was kept deliberately rather narrow (1.6 cm. diameter) to facilitate a constant rate of filling of the mould despite fluctuations in the rate of pouring.

6.1.2. Construction of the wax pattern assembly.

The test pieces and gating system were made by injecting a special low shrinkage wax (filled Fascim Wax) at 70°C into Duralumin dies at a pressure of 50 lb/in^2. The complete pattern was assembled with a hot knife, ensuring that all joints were carefully smoothed to avoid sharp projections and edges of refractory being washed into the metal stream. A finished assembly is shown in Plate 1.

Plate 1.

Wax Pattern.

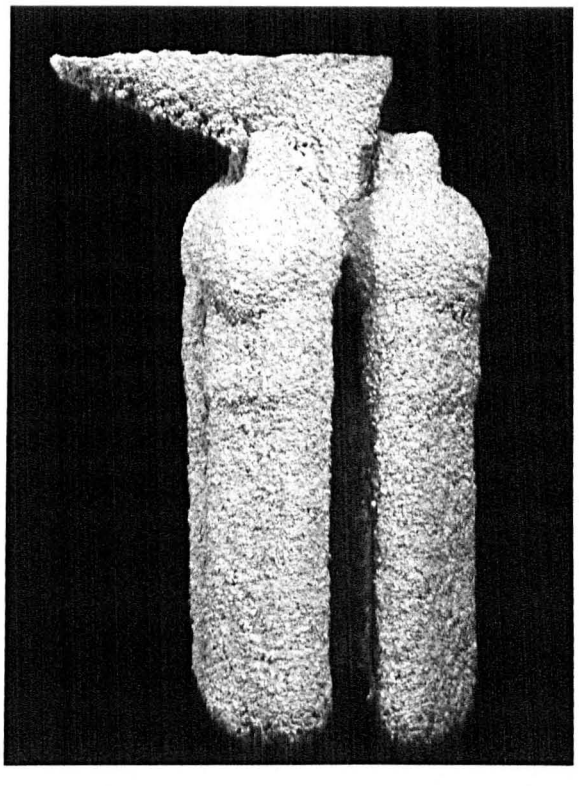

Plate 2.

Complete Mould.

6.1.3. Formation of shell moulds.

The wax pattern was dipped into a primary solution consisting of a colloidal silica base containing a suspension of 200 mesh zircon (zirconium silicate). The wet pattern was then suspended in a fluidised bed of 30-30 grade sillimanite (aluminium silicate) and allowed to dry. A secondary coating of refractory was applied by dipping the pattern into a solution of ethyl silicate containing a suspension of 200 mesh sillimanite and then immersing it in a fluidised bed of 16-30 grade molochite (a heavily calcined aluminium silicate). The pattern was then hung in an atmosphere of ammonia for about two minutes which caused gelling of the ethyl silicate, and finally left to dry in air for five minutes to allow excess ammonia to evaporate. A further five secondary coats were applied, producing a shell approximately 0.6 cm. thick, and left to dry for twelve hours.

Care was taken to maintain the acidity of the secondary dip solution between 2 and 3 pH to prevent premature gelling of the solution.

6.1.4. Dewaxing and Firing.

The moulds were dewaxed by placing them in a furnace at 1000°C. This shock heating technique allowed the wax to burn out without expanding throughout its bulk resulting in cracking of the shell, as happens in slow heating. The shell was finally fired in air at 1100°C in an electrically heated furnace for at least five minutes to remove all traces of carbon.

6.2. Mould Preheating before Pouring.

When casting in air, the mould was heated to 1100°C in an electrically heated furnace for 5 minutes to remove as much moisture as possible. The mould was then cooled in the same furnace to a temperature a little above (about 20°C)

that required for pouring. The mould was then rapidly removed from the furnace and the metal poured. The temperature loss involved in this operation was measured and found not to exceed 20°C even for the highest mould temperatures.

The same heating cycle was used in vacuum, but the mould remained inside the heating furnace during pouring thus the temperature control was rather better than that for the air casting, and was estimated to be ± 5°C.

6.3. Melting and Casting.

Air melting of steels was performed in a 40 lb. induction tilting type furnace with lip pouring. A rammed basic lining was used. The melt was deoxidised with 0.1% of aluminium immediately before pouring. Six moulds could be poured direct from the lip of the furnace in rapid succession thus ensuring similar pouring temperatures, composition and gas content. Finished castings were shot-blasted to remove adhering refractory and oxide and vacuum annealed at 950°C for 1 hour prior to taking density measurements.

Aluminium was melted in a 20 lb. Salamander crucible, coated with an alumina wash, in a Morgan gas-fired furnace and the temperature checked by means of dipping alumina-coated chromel-alumel thermocouples. A temperature of 800°C was never exceeded in order to keep down the gas content. The melt was degassed with proprietory degassing tablets and poured at 750°C into moulds held at 200°C. The pouring ladle was preheated by previously stirring the melt: this procedure also reduced the temperature loss during pouring to less than 2°C. In the first series of casts, oxygen-free high-conductivity copper was added in increments of a length of a long rod which was also used to stir the melt. A series of castings was produced of various Cu contents up to 17% Cu. Two repeat series were

made up to lower Cu contents using the remainder of the high copper alloy from the first melt as a temper addition.

The procedure for the vacuum melting of high temperature alloys was to pump the chamber down to below 10μ pressure. Melting was then carried out in a 20 lb. induction tilting unit in an alumina crucible. The metal temperature was brought to the required pouring temperature (± 5°C) by means of dipping silica sheathed Pt-PtRh thermocouples into the melt. The charge was then poured into moulds held in separate heating furnaces on a rotating platform. Different pressures of argon could be introduced within about 10 seconds before the pouring of each mould. Any excess metal was poured off into an ingot mould. The finished castings were shot blasted prior to testing.

6.4. Measurement of Density.

The well known Archimedean formula for apparent density was used

$$\rho = \frac{W_A \rho_L}{W_A - W_L}$$

where W_A = weight in air

W_L = weight in liquid

ρ_L = density of liquid (from tables)

Weighings were performed on an automatic balance and were accurate to ± 0.2 mg. Specimens were weighed and the zero re-checked repeatedly (not usually more than three times) until both the weight reading and the zero were constant. The water temperature was read to 0.05°C which was on the threshold of affecting the accuracy of the final result. A small drift in temperature of the water of the order of 1°C per day was obtained by using a very large quantity of water - about ten litres - in a thick-walled glass vessel.

Kodak wetting agent was added to the water in concentration 3 ml/l which was found not to affect the density of water within the accuracy of other measurements. This minimised the adherence of bubbles to the surface of specimens (which were always closely inspected for bubbles on all sides before weighing) and gave a constant meniscus angle at the liquid surface at the point of entry of the wire. Occasional bubbles on the surface of the water which attached themselves to this meniscus could change the weight reading by 3 mg. or more.

The support wire was 0.008 cm. diameter molybdenum, carefully chosen from the batch so as to be quite smooth to the touch (for example it was found that tungsten wire when rough, affected the meniscus shape in an erratic manner causing inconsistent readings).

The weighings in air were perfectly unambiguous, but those in liquid were observed to change with time. A specimen weighing say 100 g. might increase in weight by 2-3 mg. in about five minutes. Part of this weight change was due to the adjustment of the temperature of the specimen to that of the liquid but this could be minimised by allowing the specimens to approximately equalise their temperature with that of the water by placing in the balance case adjacent to the water container for about an hour before taking the weighings in water. Other occasional increases in weight could not be attributed to this cause and were thought to be the gradual seepage of water into internal pores. No increase in weight could be attributed to the slight discolouration (representing a very light rust film) of the steel specimens in the water.

The final accuracy achieved depended upon the weight of the specimen. For a specimen weighing 1 g. an accuracy of about 1 part in 400 can be expected; and for specimens weighing 10 and 100 g., 1 part in 4,000 and 40,000 respectively.

6.5. Determination of % Porosity.

In order to determine the percentage of pores from the density measurements it is necessary to evaluate the density of the perfectly sound material. For carbon steels this was attempted by cold rolling the specimen to about 75% reduction in thickness, annealing at 950°C for 1 hour in vacuum to regain the original quantitative relation between the phases present, and finally determining the density. This method however gave unsatisfactory results which were attributed to the opening of pores due to the breaking up of inclusions, and in any case the method was impossible to apply to high temperature alloys which cannot be hot rolled. Hence from a given cast the specimen which showed the highest density was intensively examined by metallographic and semi-microradiographic techniques in order to obtain a rough estimate of its % porosity (an accurate assessment was unnecessary - even if it were obtainable - since the quantity was very small). Once the density ρ_s of the sound material had been estimated, the % porosity of each of the other specimens of the same cast could be obtained

$$\% \text{ Porosity} = \frac{(\rho_s - \rho)}{\rho_s} 100$$

where ρ was the density of the casting of unknown porosity content.

For a steel specimen weighing 1 g. and containing 1% porosity the maximum limits of error are $\pm$ 1%; for specimens of 10 g. and 100 g. containing the same amount of porosity the corresponding maximum errors are respectively $\pm$ 0.1% and 0.01%. In practice the smallest specimens employed in these investigations weighted about 100 g. so that the accuracy was always better than $\pm$ 0.01%. These accuracies are improved by a factor of about 2.5 for Al and its alloys.

6.6. Radiographic Techniques.

The as-cast specimens of 0.2 cm. thickness were lightly surface ground to produce a good finish. Gevart double-coated D.2. film was used with a 0.015 cm. lead backing screen, and was placed in contact with the specimen. The anode-film distance was 100 cm. and the exposure about 20 minutes at 100 KV and 10 ma.

A longitudinal line count was carried out on the resulting radiographs to measure the total length of line which traversed porosity as a percentage of the total length of the specimen. The main disadvantage of this method of interpreting the radiographs was that a faint or dark image could occupy the same length of the scanning line, but obviously correspond to different porosity in depth. A rough allowance could be made for this by giving different weights to images of different intensity. It would clearly be a useful refinement to measure the area under a microdensitometer scan, so that from several scans an reasonable integration of the total porosity could be estimated. Nevertheless, the simple line count technique was extremely easy and quick to perform and has yielded good comparative results.

For semi-microradiography 0.125 cm. thick specimens were machined from the geometric centres of the cast specimens. The surface finish resulted from careful machining on a precision surface grinder.

The sample was placed in a light-tight envelope in contact with the emulsion of a fine grained X-ray film. A sheet of plastic foam placed behind the film ensured good contact between the film and sample.

Filtered Cobalt radiation is ideal for this work[337] since absorption coefficients for the inclusions expected to be present should be higher than the matrix, thus showing up

lighter than the background, and so clearly distinguishable from pores, which give dark images. However, to give reasonable exposure times, unfiltered cobalt radiation was used. The sample was placed 25 cm. from the target of 1 square mm. This geometry should give, at worst, a resolution of the order of 5μ. Exposures were 3 hours at 36 KV and 8 ma.

6.7. Solid Feeding Experiment.

A mould was prepared as described in Sections 6.1. and 6.2. consisting of spheres of sizes 2, 1.5, 1.0, 0.75, 0.5, 0.38, 0.25 inches run via very long narrow ingates of diameters 0.25, 0.19, 0.13, 0.094, 0.063, 0.063 and 0.063 inches respectively. The latter represented the smallest diameter of ingate with which it was feasible to use without constant breakages during the coating of the wax. Thus, as far as possible, a constant geometry obtained for all the spheres. They were mounted on a circular assembly as symmetrically as possible to balance metal flow and heat content within the mould. The wax assembly and the finished mould are shown in Plates 3. and 4.

P.K.24. alloy was induction heated to 1620°C in an alumina crucible in a vacuum of 1-5 microns. This temperature was held constant for 30 minutes in order to outgas the metal as far as possible. During this time the mould was heated to 1100°C for 5 minutes in the same vacuum chamber. This was designed to drive off as much water vapour from the mould as possible. The mould was then cooled to 1000°C at which temperature it was maintained until the metal was poured. The alloy was poured at 1620°C in vacuum and allowed to cool to near room temperature before air was admitted into the chamber and the casting removed.

The densities of the spheres were determined as described previously and semi-microradiographs were made of 0.125 cm. thick sections from the centres of the four smallest spheres, which were highest in density.

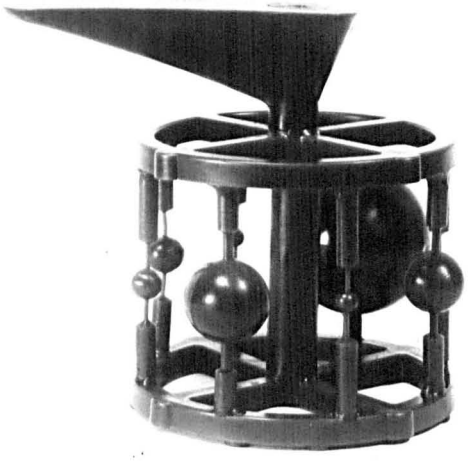

Plate 3.

Wax pattern for non-fed spheres.

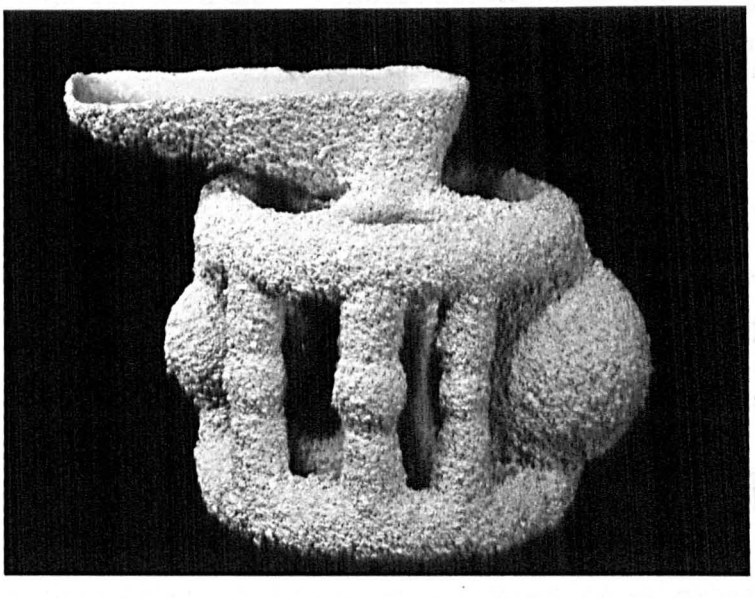

Plate 4.

Completed Mould.

7. RESULTS.

A general observation common to experiments on all alloys was that for similar casting conditions, smaller section thicknesses were invariably associated with higher porosity.

7.1. Effect of Superheat and Mould Temperature.

For the 3 carbon steels (Fig. 20.) increasing mould temperature is seen to reduce porosity, whereas superheat appears to have almost negligible effect.

The vacuum cast P.K.24 alloy behaved rather differently (Figs. 21. and 22.). At the lower pouring temperatures porosity showed a peak with increasing mould temperature, but tended to decrease at the higher pouring temperature.

7.2. Effect of Composition on Porosity.

Each composition of steel reported above corresponds to a single cast, so that comparisons between specimens of the same cast are not influenced by variations in composition, particularly gas content. An alternative presentation of these results to investigate the effect of carbon content necessarily involves comparisons of different casts, rendering any conclusions, at best, only tentative. This caution is given weight by a comparison of a 0.25% C steel cast into 0.75 cm. section mould at 300°C which gives porosities of 0.45% (Fig. 20.) and 0.13% (Fig. 25.). This second cast was deoxidised by about 5 times the normal addition of Al.

Fig. 23. was constructed, nevertheless, but without regard to the effect of superheat (assumed to be practically negligible) and includes data from a cast of electrolytic iron. It shows a prominent peak in porosity at about 0.7% C.

A rather different approach to the experimental data was used in interpreting the Al-Cu results:

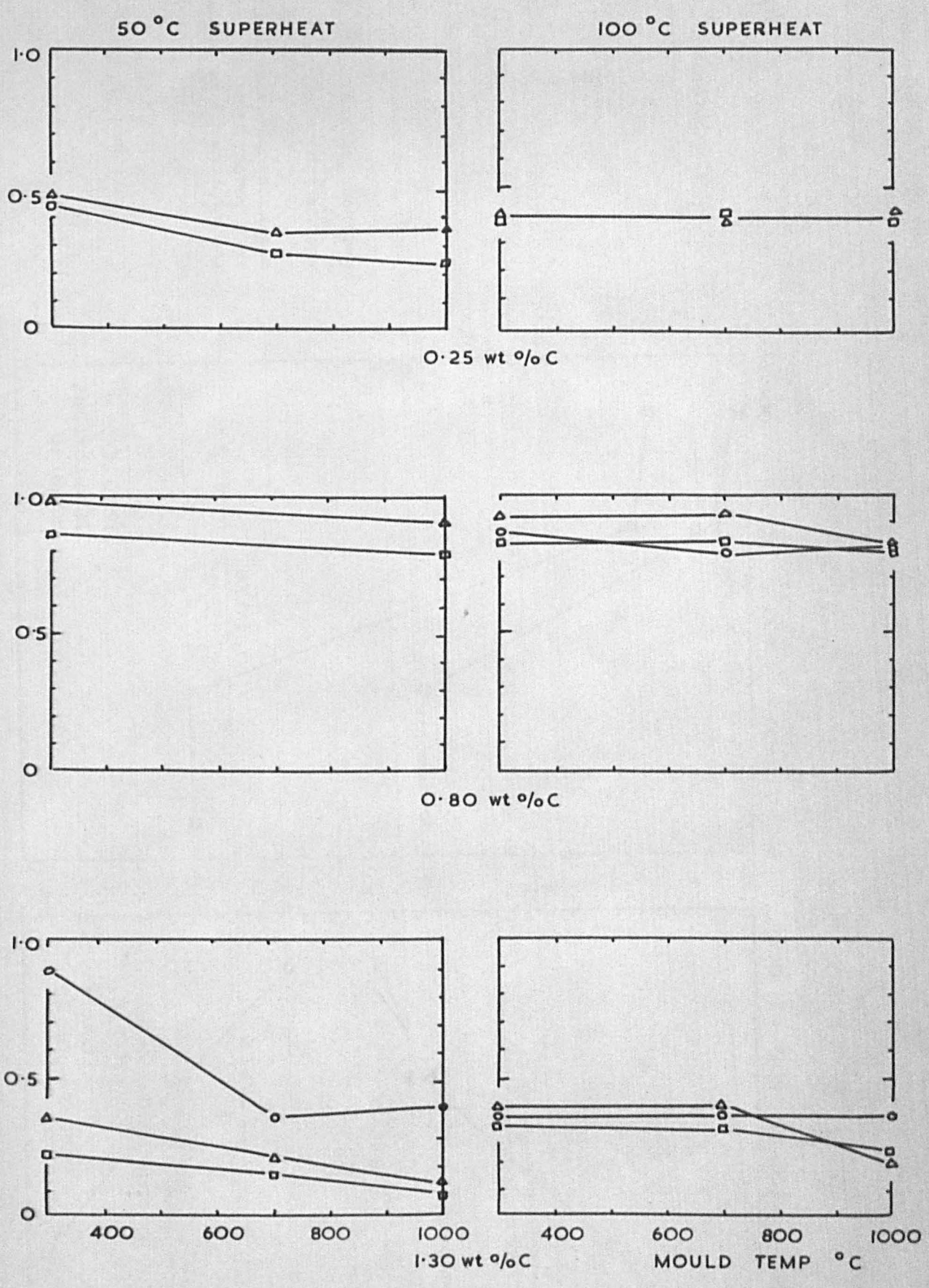

°/o MICROPOROSITY IN 3 CARBON STEELS : EFFECT OF MOULD TEMPERATURE, SUPERHEAT AND SECTION THICKNESS (○ 0·5, △ 0·75, □ 1·0 cm)

FIGURE 20

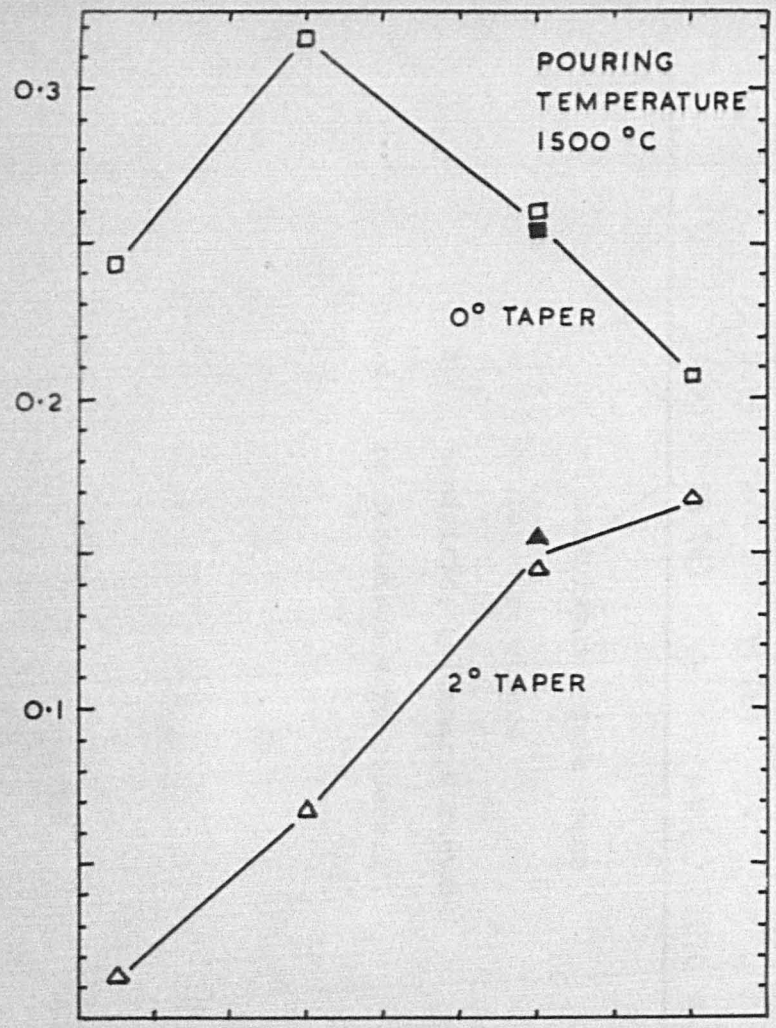

FIGURE 21.

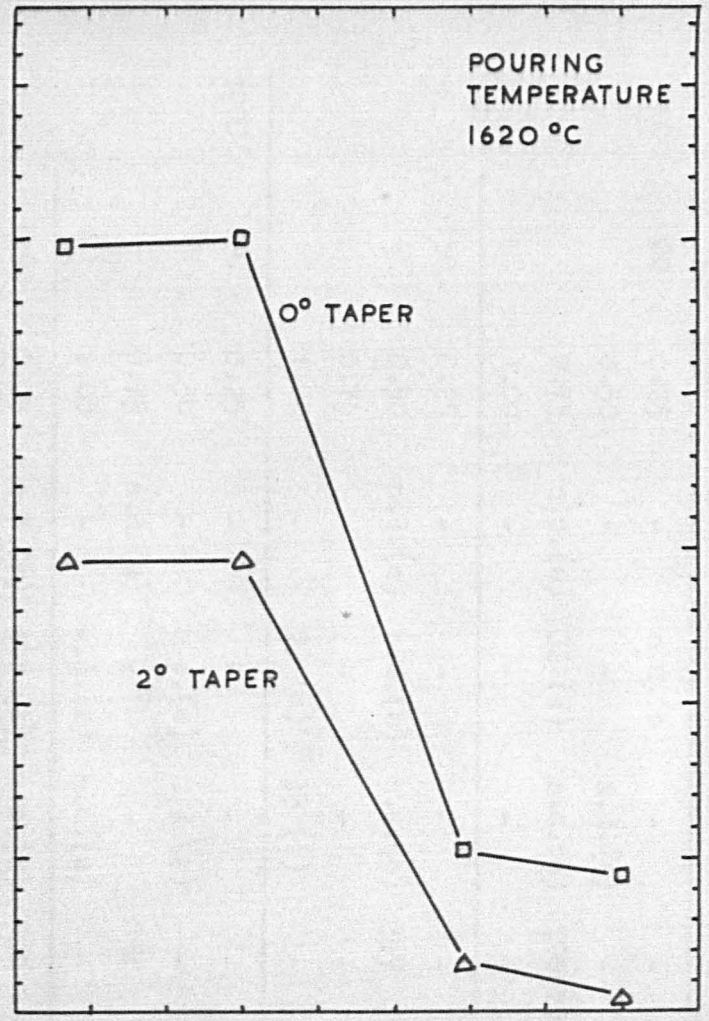

FIGURE 22.

Porosity in PK 24 Alloy as a function of mould and metal temperatures.

Vacuum 15μ.

Section Thickness 0.5 cm.

Table 8.

Some measurements of grain size and secondary dendrite arm spacing in the three carbon steels.

Mould Temp. (°C)	Superheat (°C)	Section Thickness (cm)	Dendrite Arm Spacing (microns) 0.25%C	0.80%C	1.30%C	Mean Grain Diameter (microns) 0.25%C	0.80%C	1.30%C
300	80	0.25	-	n.d.(e)	-	-	100(?)	-
		0.50	-	-	n.d.(e)	-	-	88
		0.75	n.d.(e)	32 (e)	n.d.(e)	500(?)	-	97
		1.00	-	-	-	-	-	-
	150	0.25	-	-	-	-	-	-
		0.50	n.d.(e)	n.d.(e)	n.d.(e)	357	111	80
		0.75	-	-	-	-	-	-
		1.00	-	29 (e)	35 (e)	-	244	162
1000	80	0.25	-	-	-	-	-	-
		0.50	-	n.d.(e)	n.d.(e)	-	158	82
		0.75	n.d.(e)	-	-	834	-	-
		1.00	-	n.d.(e)	n.d.(e)	-	170	118
	150	0.25	n.d.(e)	40? (e)	n.d.(e)	500	127	145
		0.50	-	-	-	-	-	-
		0.75	-	35 (e)	-	-	222	-
		1.00	75 (d)	-	64 (d)	870	-	625

- no measurements were taken

e equiaxed structure

d dendritic, columnar structure

n.d. no dendrites were observed

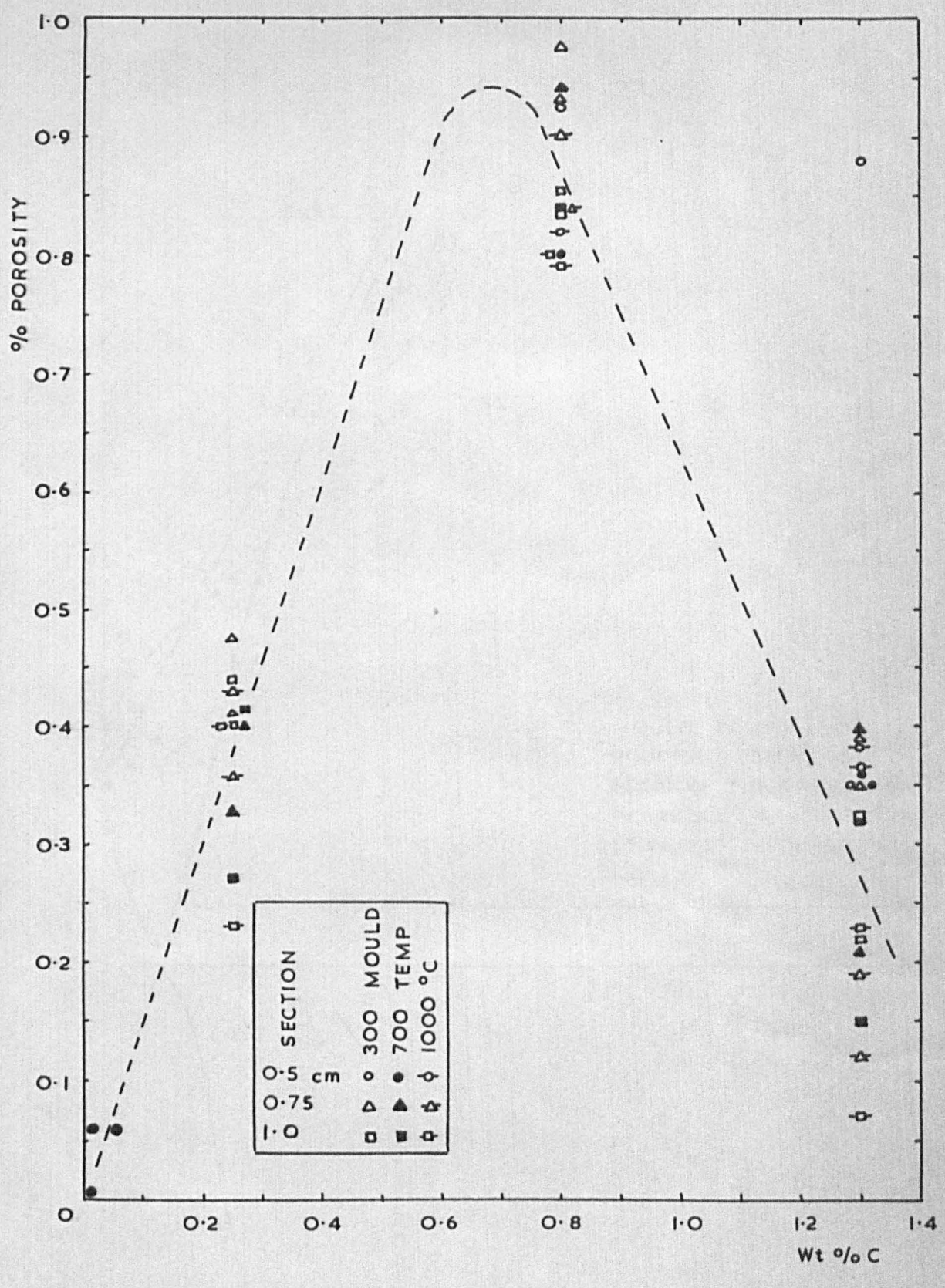

EFFECT OF COMPOSITION ON POROSITY IN IRON-CARBON ALLOYS

FIGURE 23

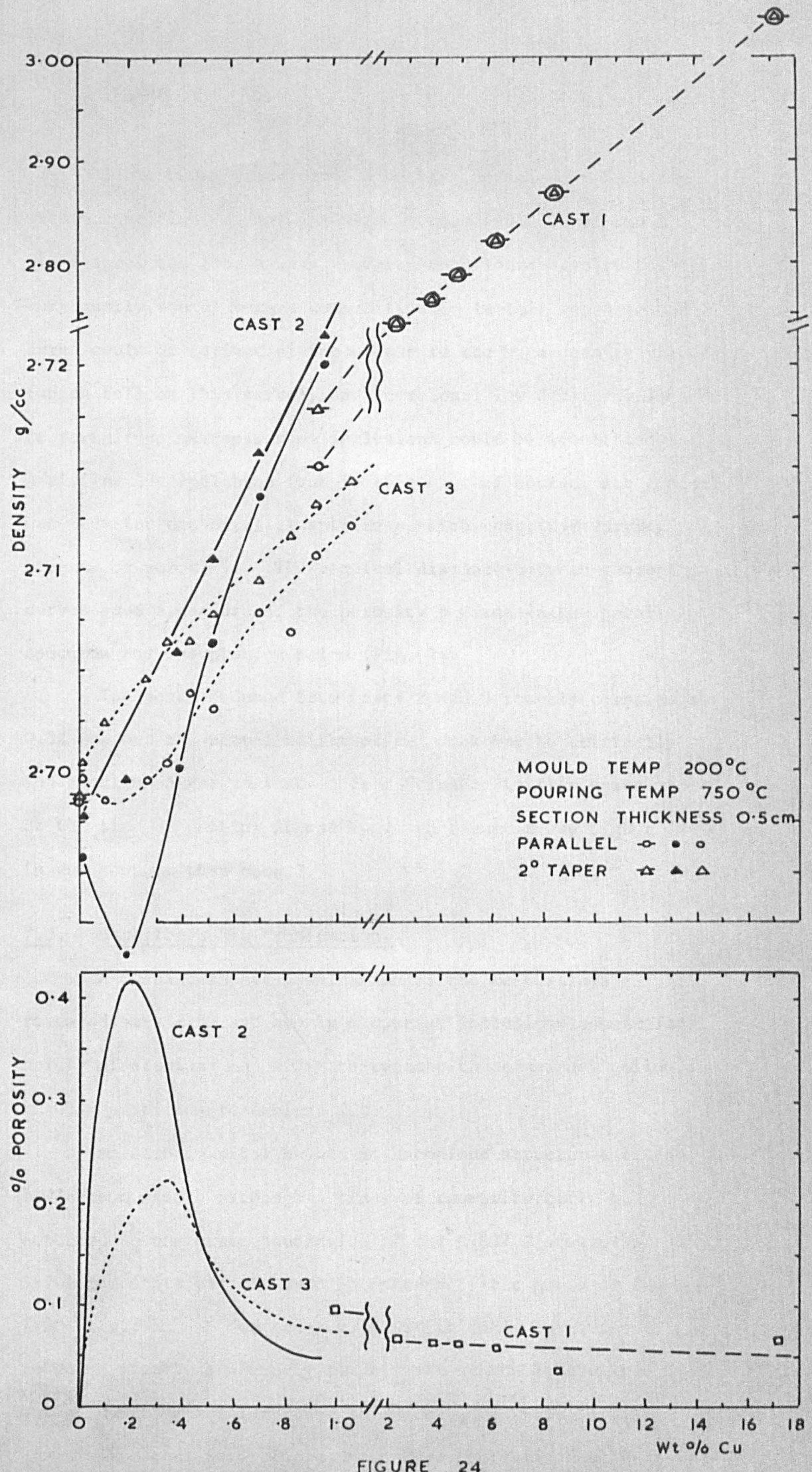

FIGURE 24

EFFECT OF COMPOSITION ON POROSITY IN Al-Cu ALLOYS

Since density increases smoothly, and closely linearly, with composition, a plot was made of the densities of the 2° taper specimens (which were verified metallographically to be very nearly sound) versus composition. In this way a smooth curve could be derived giving weight to the high density values (which fell on this curve), and occasional low density values due to fortuitous macropores or inclusions could be identified. A similar interpolation (but in this case of course, not linear) was made for the parallel specimens which contained varying amounts of porosity. The vertical distance between these curves gave a measure of the porosity present in the parallel specimen and was plotted below (Fig. 24).

The peaks deduced from casts 2 and 3 roughly coincide at 0.3% Cu, but the actual height of the peak may be critically dependent upon gas content. From Straube-Pfeiffer tests made at the time of casting it was known that cast 2 was higher in gas content than cast 3.

7.3. Metallographic Examination.

A metallographic examination of the Fe-C alloys revealed very fine and evenly dispersed inclusions consisting mainly of alumina- and silicate-types with occasional yellow, angular particles resembling TiC.

An etch in nital showed no anomalous structures in the low carbon steel, although a trace of cementite could be detected in the grain boundaries of the 0.80% C steel, and 5-10% cementite was observed in interdendritic areas of the 1.30% C steel. A few areas were sufficiently large to reveal a structure strongly reminiscent of the ledeburite eutectic, and was interpreted as evidence of strongly non-equilibrium cooling. These areas were quite distinct from the grain boundary and plate-like Widmanstatten cementite precipitated at lower temperatures in the solid state.

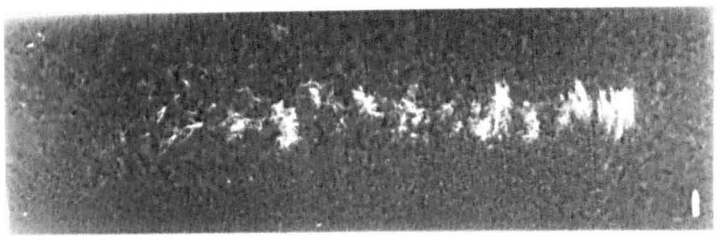

Plate 1. Mould Temperature 250°C.

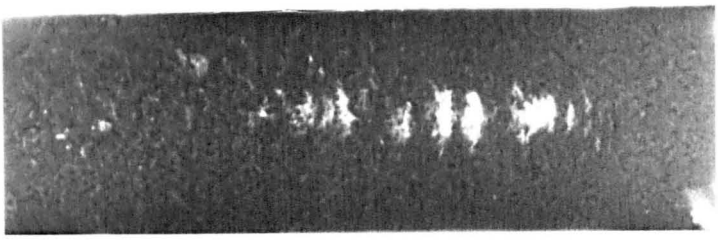

Plate 2. 500°C.

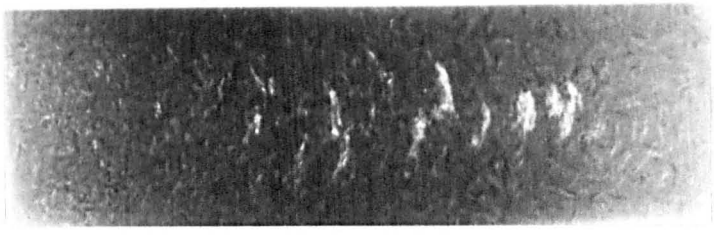

Plate 3. 800°C.

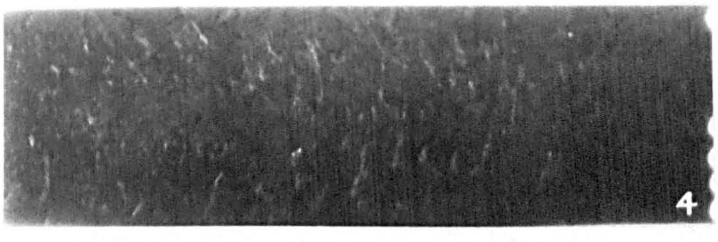

Plate 4. 1000°C.

Contact Prints of Radiographs of PK.24 alloy.

Pouring Temperature 1500°C. Section Thickness 0.5 cm.
Vacuum 15μ.

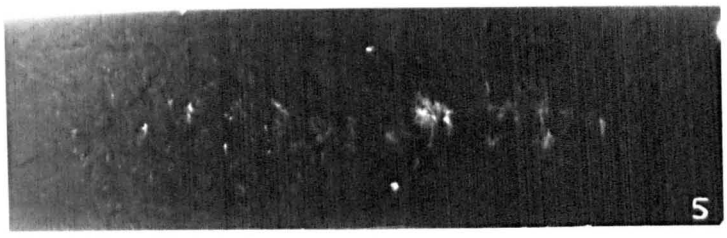

Plate 5. Mould Temperature 270°C.

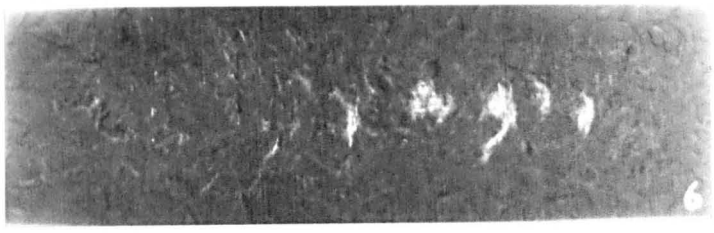

Plate 6. 500°C.

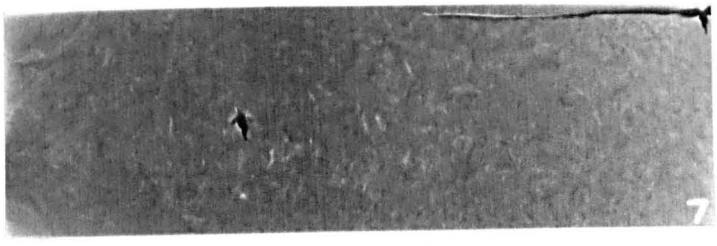

Plate 7. 800°C.
(Damaged Film)

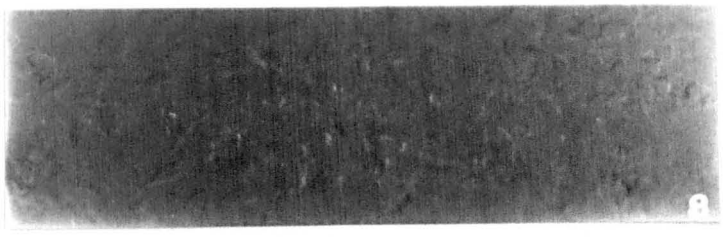

Plate 8. 1000°C.

Contact Prints of Radiographs of PK.24. Alloy.

Pouring Temperature 1620°C; Section Thickness 0.5 cm; Vacuum 15μ.

Measurements of grain size and dendrite spacing relating to the steels are given in Table 8. Each result represents a mean of at least 10 determinations on one polished section.

Metallographic examination of the Al-Cu alloys revealed a strongly cored structure in the dendrites even in the specimens of lowest copper content, and although from the equilibrium diagram eutectic would not be expected until 5.7% Cu, above 1% Cu eutectic appeared first in trace amounts, increasing to a practically continuous interdendritic film at 4.7% Cu.

7.4. Radiographic Examination.

Contact prints of radiographs of 0.5 cm. thick specimens of P.K.24 and X40 alloys are shown in Plates 3-5. It is evident that at lower mould temperatures porosity is concentrated in macroscopic form at the thermal centre of the casting, whereas at high mould temperatures it is widely dispersed and very fine. It is also just discernable that in this condition the actual amount of porosity along the centreline is very small compared to the region on either side. These observations are emphasised and made quantitative in the longitudinal line counts shown in Figs. 29. and 30.

The tendency for porosity to occur in layers is also clear in many of these plates.

7.5. Effect of Taper on Porosity.

The results for X40 alloy (melted in a 10 lb. indirect arc furnace, and poured directly from the furnace into moulds) are given in Fig. 26. A large increase in soundness was obtained by superimposing a 2° taper on the specimen, but little extra benefit is obtained by increasing the taper up to 8°.

Fig. 25. EFFECT OF TAPER AND SECTION THICKNESS ON POROSITY.

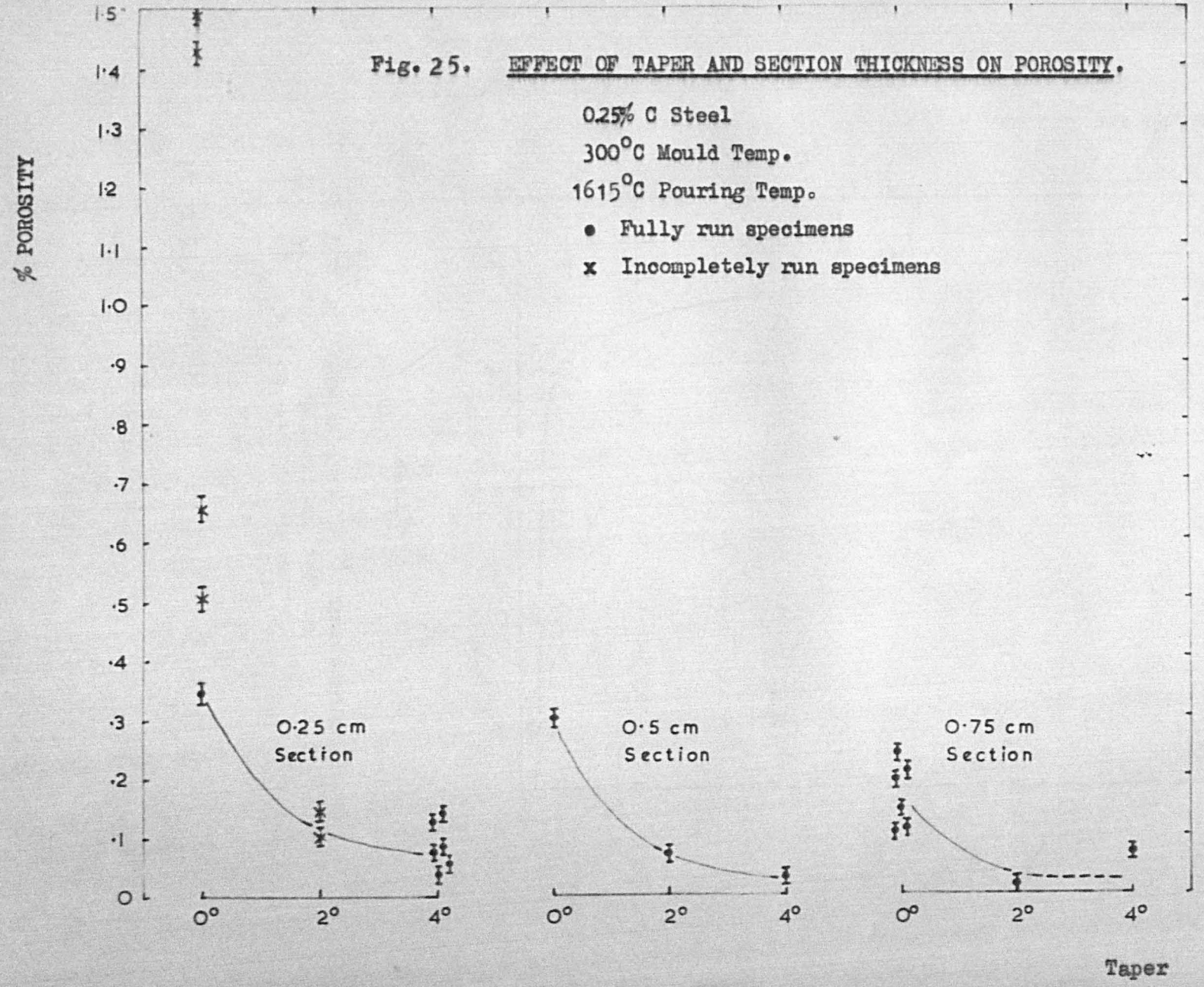

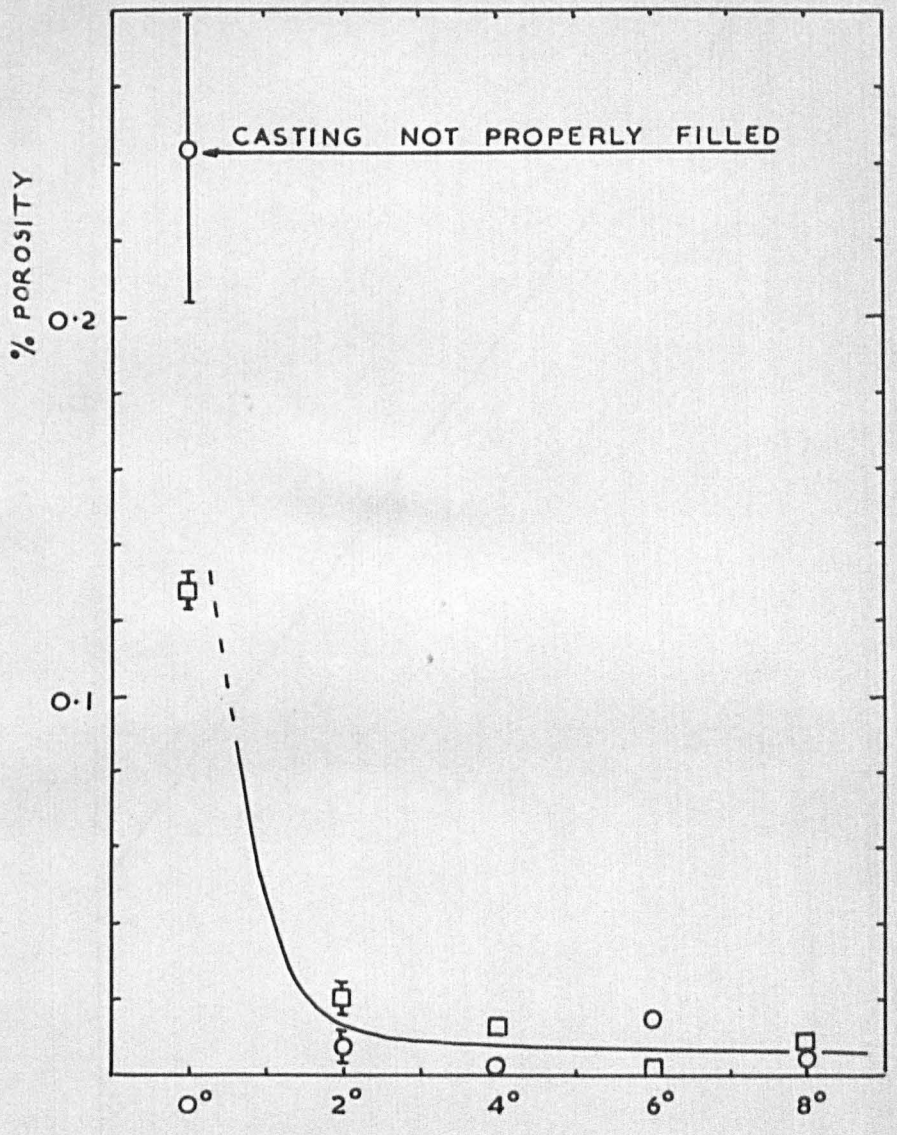

Fig. 26.

X40 alloy air cast at 1480°C into moulds at 900°C. (O) 0·12 cm. section
(□) 0.5 cm. section thickness.

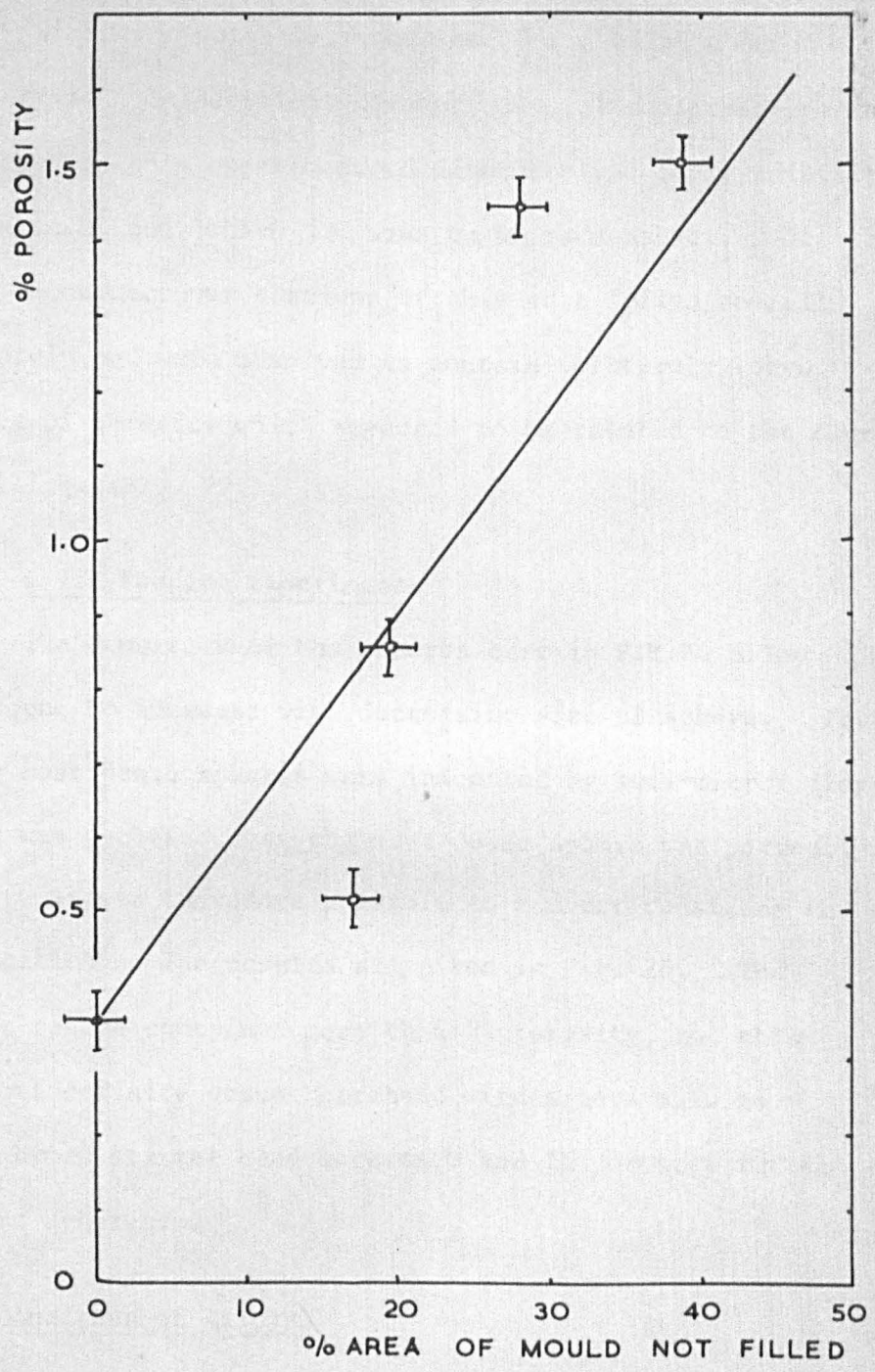

POROSITY IN MIS-RUN SPECIMENS OF 0.4cm SECTION, AIR-CAST IN 0.3%C STEEL AT 1610°C INTO MOULDS AT 300°C.

FIG. 27

Similar results were obtained for a 0.25% C steel (Fig. 25.). In addition, however, several duplicate specimens were cast in this experiment to determine the reproducibility of the technique, which is seen to be reasonable.

Some narrower sections of this cast failed to fill completely and were observed to contain relatively large amounts of porosity which appeared to be related to the degree of filling. (Fig. 27.).

7.6. Solid Feeding Experiment.

The densities of the spheres cast in P.K.24 alloy were found to increase with decreasing size of sphere. Four of the most dense spheres were inspected by semi-microradiography and it was verified that the most dense sphere was perfectly sound. It was therefore possible to convert densities to % porosities. The results are given in Fig. 28. The largest sphere contained more than 3% porosity, and this large but definite value decreased with sphere size to a rather broad scatter band between 0 and 1% porosity for the smallest spheres.

7.7. Analyses of Alloys.

Carbon Steels

Results Section	C	S	P	Mn	Si	Ni	Cu	Cr	Sn	Mo	Al	O
7.1 and 7.2	0.25	.04	.02	.52	.15	.08	.16	.07	.02	.03	.12	96.6
	0.80	.04	.01	1.29	.37	.07	.18	.07	.01	.02	.15	37.6
	1.30	.03	002	2.00	.14	.03	.12	.02	.01	.02	.01?	33.6
7.5	0.25	.03	.01	0.11	.04	.06	.13	.02	.02	.02	.11	216*

*This large value coincided with a high inclusion density.

FIG. 28

SPHERES OF PK24 ALLOY (CAST AT 1620°C INTO A MOULD AT 1000°C) DEMONSTRATING THE EXISTENCE OF SOLID FEEDING.

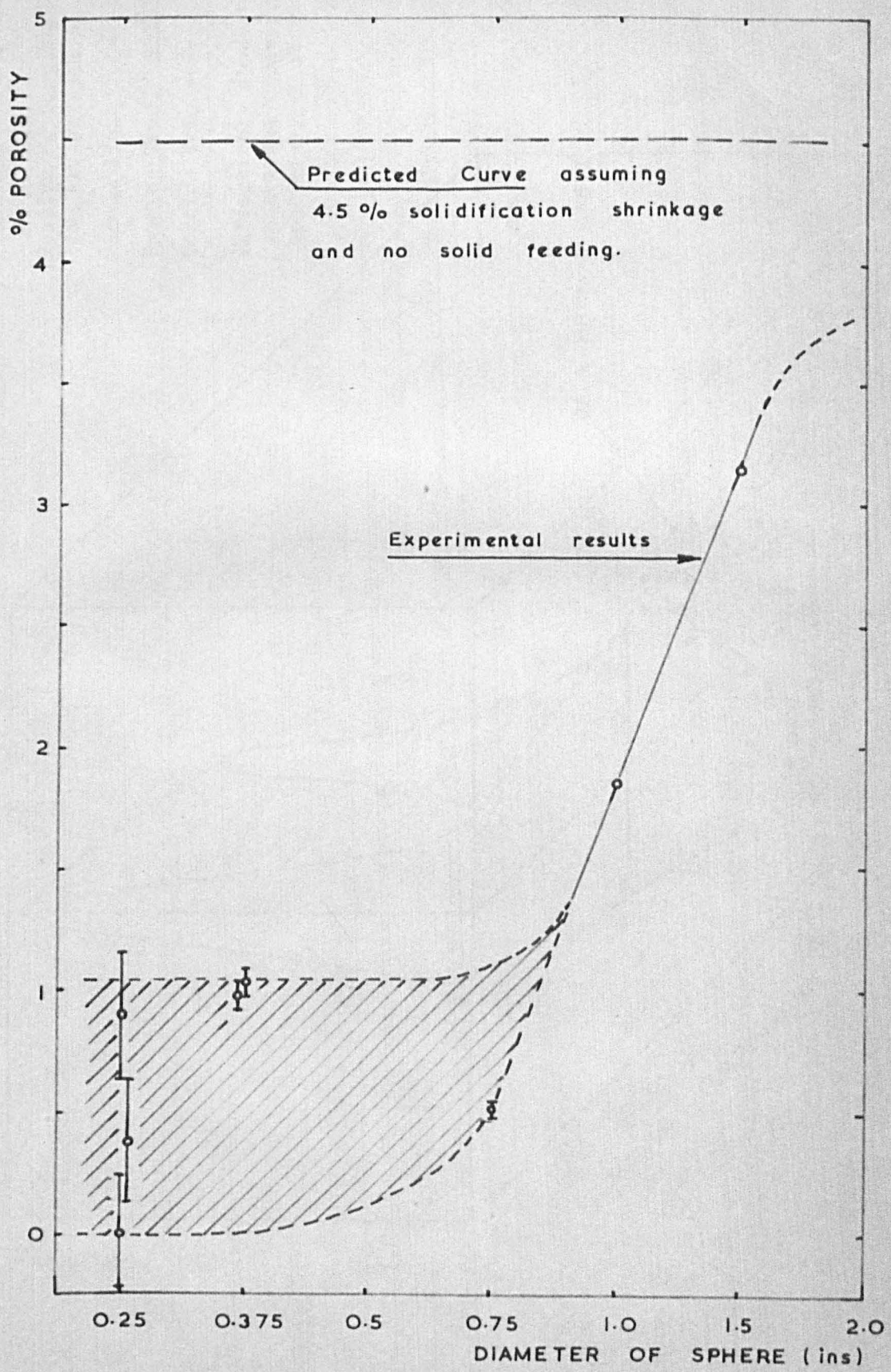

Figure 29.

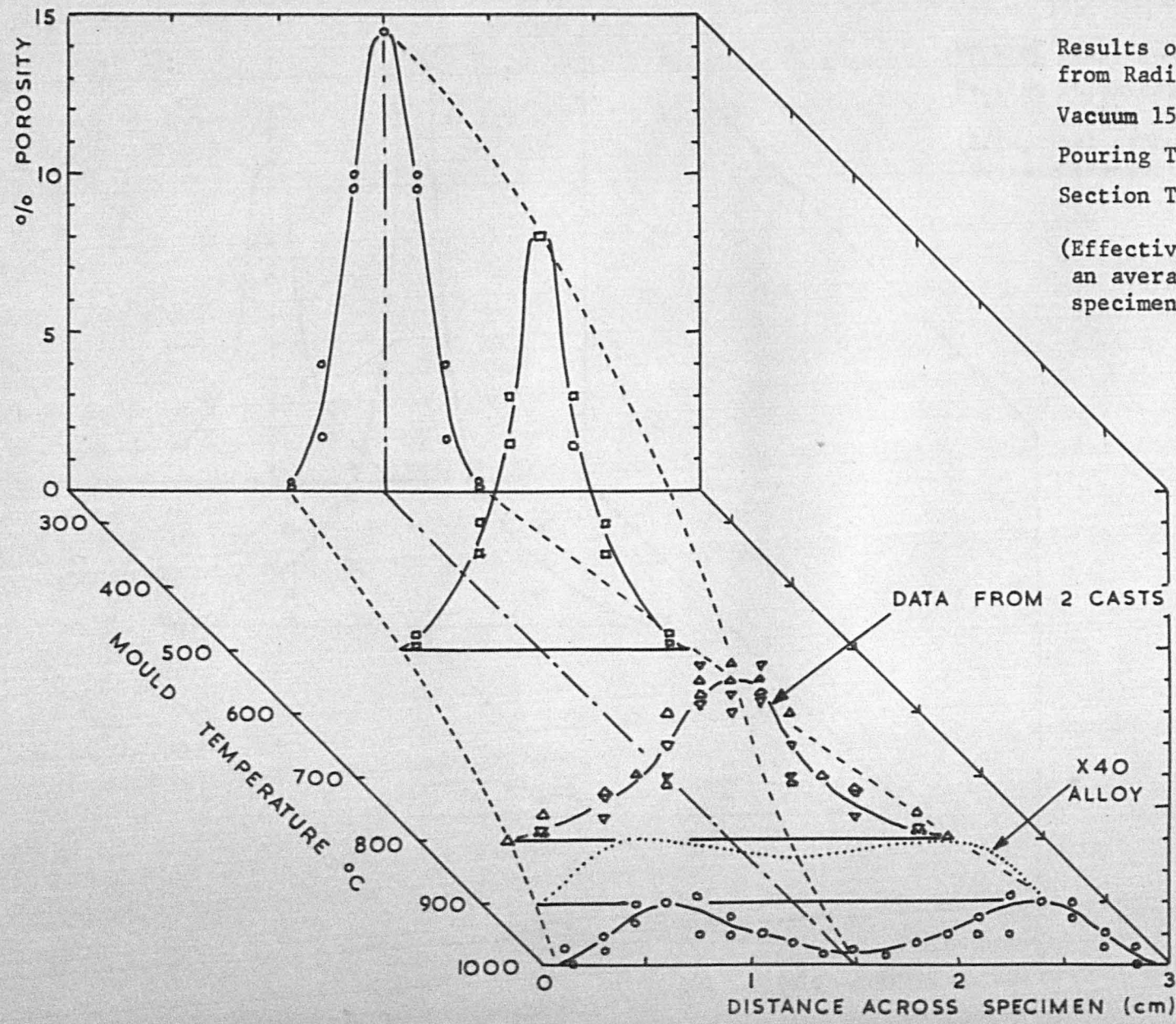

Results of Longitudinal Line Count from Radiographs of PK 24 Alloy.

Vacuum 15μ.

Pouring Temp. 1500°C.

Section Thickness 0.5 cm.

(Effectively shows Porosity across an average transverse section of specimen).

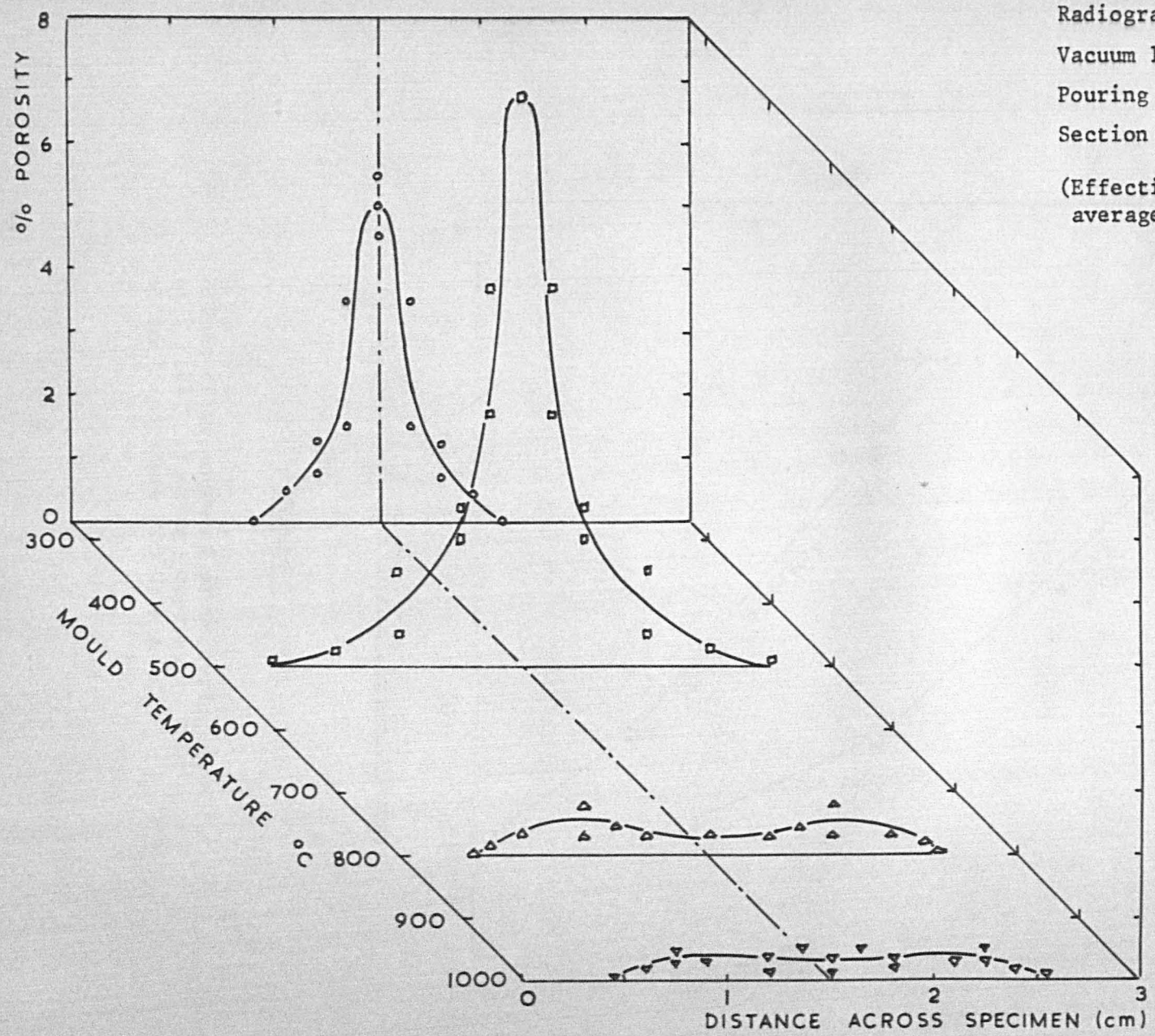

Results of a Longitudinal Line Plot from Radiographs of PK 24 Alloy.

Vacuum 15μ.

Pouring Temp 1620°C.

Section Thickness 0.5 cm.

(Effectively shows porosity across an average transverse section of specimen).

Figure 30.

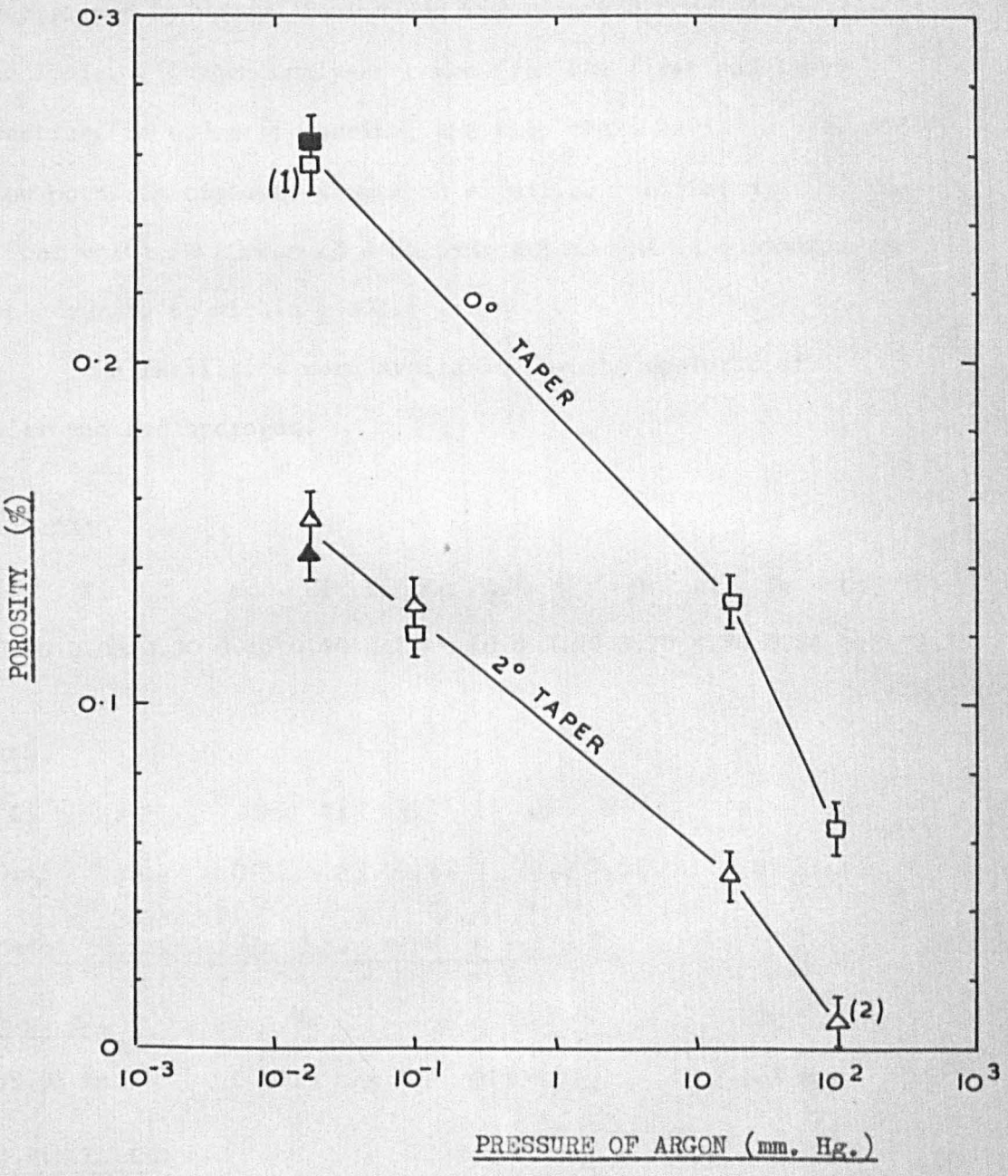

Figure 31.

Effect of pressure of argon during casting of P.K.24. (Pouring temperature 1500°C; mould temperature 800°C; ■ ▲ from Figure 21).

Values are given in wt.% of the element, with the exception of oxygen which is in p.p.m. The latter was determined by vacuum fusion and represents a total oxygen analysis. Oxygen analyses taken from the first and last castings in order of pouring, and from those having a high and low porosity content, showed no significant differences. The final value is a mean of 8 determinations and is estimated to be accurate to within ± 30%.

No facilities were available for the analysis of nitrogen and hydrogen.

P.K.24.

C	Ti	B	Mn	Si	Ni	Cu	Cr	W	Mo	Al	Fe	Co	Nb
0.10	0.06	0.30	0.16	0.44	Bal	-	10.8	3.90	3.20	5.70	0.84	0.34	2.25

X40.

C	S	Mn	Si	Ni	Cr	W	Fe	Co
0.45	0.030	0.62	0.63	10.9	26.0	7.57	1.23	Base

Major Impurities in Super Pure Al and O.F.H.C. Cu.

s.p. Al.	Si	Cu	Fe
99.9% min.	0.0015 max.	0.0075 max.	0.003 max.

O.F.H.C. Cu.	Bi	Pb
Cu + Ag, 99.95 min.	0.001 max.	0.005 max.

3. DISCUSSION OF RESULTS.

3.1. Solid Feeding.

The problem of solid feeding is considered first since the results and conclusions have bearing upon the interpretation of all the other experiments.

The spheres of all sizes were unfed to approximately the same extent because the whole casting geometry was kept as near alike as possible, so that the usual assumption would be that each would contain the same fraction of porosity, and this would be close to the value α, the solidification contraction, which is probably about 4.5 $\pm$ 1.0% for P.K.24 alloy (Fig. 28).

If, however, a negative pressure builds up in these confined volumes of liquid (Section 3.5.), then the exterior solid shell must be contracted by the reduced internal pressure (the exterior atmospheric pressure would normally assist this process; in the present work however vacuum conditions were used) at first elastically, and subsequently plastically as the deformation proceeds. The extent of this 'solid feeding' (i.e. the indrawing of solid material to compensate for the contraction due to solidification) depending upon two main factors (a) the mechanical strength of the solid, and (b) the value of the negative pressure. These factors require further discussion .

The exterior shell of the larger spheres will be relatively cool before solidification has far advanced towards its centre. Thus the solid will be relatively strong and better able to resist the internal suction effect. The negative pressure will therefore increase more rapidly, and soon exceed a certain critical level for nucleation, resulting in the creation of a pore. The pore will rapidly expand to equilibrium size, dispelling the internal stress

and arresting solid feeding, and thereafter grow slowly to compensate for shrinkage until solidification is complete. In a small sphere, the temperature of the exterior shell will have fallen very little by the time solidification is complete at its centre, so that plastic flow is facilitated for a longer time in relation to the solidification time of the sphere. By this means, the negative pressure is prevented from reaching high values even at a late stage in solidification, so that there is a possibility that in the absence of a sufficiently good nucleation site a pore will not occur. The casting will be sound despite almost perfectly non-fed conditions of solidification.

The problem of pore nucleation sites can be discussed statistically. If we arbitarily assume that there are about 10 nuclei/c.c. then statistically the small spheres of volume 0.1 c.c., will contain either a few nuclei, or none, whereas the larger spheres, of volume 50 c.c., will contain in the region of 500 nuclei. This means that the negative pressure which can be reached in the larger spheres will be limited by the presence of large numbers of nuclei which will promote nucleation at low hydrostatic tensions. As the sphere size decreases, the probability of the sphere containing no favourable nucleation sites increases, so that the negative pressure is allowed to reach the high values necessary for efficient solid feeding.

The results shown in Fig. 28. reveal the expected scatter in the quantity of porosity in the smaller spheres. Of the three smallest spheres only one was sound, indicating a nuclei density close to that assumed. The actual inclusion density of the alloy used is more nearly an order of magnitude greater than this, so that it seems probable that most inclusions are not favourable sites for pore nucleation, which is to be expected from considerations in Sections 2.3. and 2.4.

The results of this experiment cannot be accounted for by assuming any other feeding mechanism than that of solid feeding. This seems to be therefore a strong justification of the correctness and necessity for accepting this concept as an important feeding process.

The results are, however, amenable to an alternative interpretation in the sense that it is cooling rate rather than size of sphere which is important in affecting solid feeding in this particular experiment: if all the spheres cast were identical in size then a slow cooling rate, resulting in a higher temperature and consequently higher plasticity in the solid shell, would give a more dense casting. Therefore, in conditions where liquid regions are unfed, and yet are required to be perfectly sound, a slow cooling rate is required, in agreement with the quantitative predictions in Section 3.5.

8.2. Effect of Superheat ΔT_s, and Mould Temperature T_m.

In the experiments on P.K.24. alloy increasing superheat reduces porosity somewhat, but for the carbon steels superheat is remarkable for its complete inability to influence porosity except in the high carbon steel where its influence changes from increasing to decreasing porosity depending on the section thickness. The latter observations may be attributed to the rather small difference in superheats which was perhaps insufficient to clearly distinguish any tendencies.

Because of the small difference in superheats, the areas of the incompletely filled castings of another melt (Fig. 27.) are of considerable interest since it is probable that the areas of the castings are a measure of superheats close to zero, and since the porosity in these castings is very high, we may tentatively conclude that increasing superheat increases soundness in carbon steels.

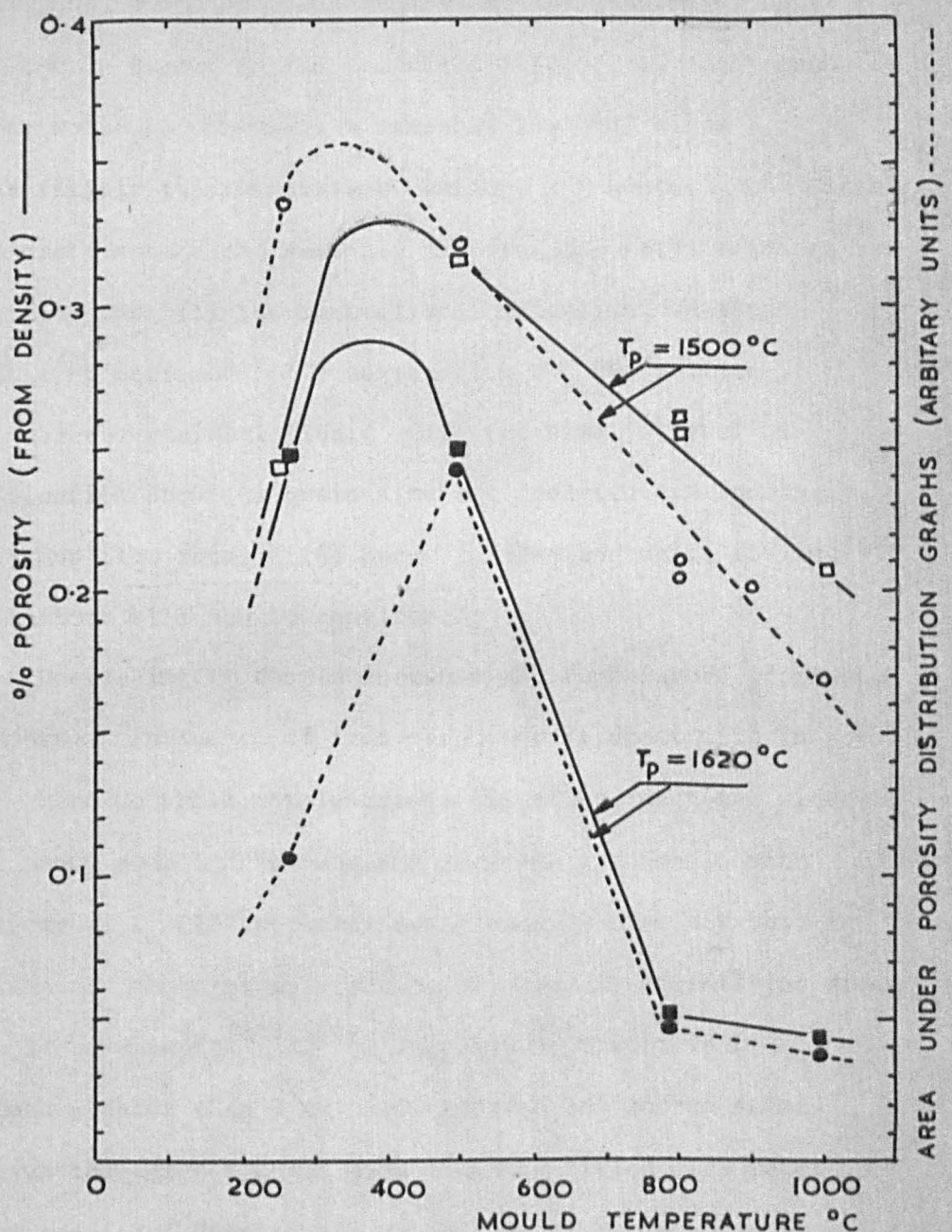

FIGURE 32

POROSITY IN 0·5 cm THICK SPECIMENS OF PK24 ALLOY AS A FUNCTION OF MOULD TEMPERATURE T_m

The observation of decreasing porosity with increasing mould temperature agrees well with the results of other investigators (Section 4.7.) and yet no explanation of this effect can be traced in the technical literature. Any such attempt would be necessarily somewhat involved since T_m affects firstly the temperature gradient and hence L, the width of the pasty zone; and secondly the freezing rate, which in turn influences (1) the mode of solidification, whether dendritic or equiaxed; (2) segregation and the surface tension of the residual liquid, (3) the time interval of solidification Δt; (4) grain size and dendrite arm spacing; (5) viscous flow rates; (6) burst feeding and solid feeding. These factors will now be considered:

Decreasing T_m should increase the temperature gradient. The important influence of this parameter is dealt with in detail later; here we shall merely assess its effect upon the width of the pasty zone L. The maximum gradient attainable with variations of T_m will probably not exceed $30^{\circ}C/cm$ since this is approximately the maximum gradient observed in solidifying steel in a cold sand mould[229,274], which would result in L very much greater than 1 cm. even for the low carbon steel. Thus even the largest mould used would be filled with metal in a pasty condition despite all variations of T_m, so that L cannot be a factor influencing the amount of porosity.

Considering now the affect of the rate of cooling on the observed porosity: if dendrite arm spacing is a direct measure of this rate (Flemings shows that this is true for Al-4.5% Cu alloys[38] and for steels[287] for very widely differing solidification conditions) then the limited data available in Table 8. indicates that a decrease in T_m from 1000 to 300 $^{\circ}C$ increases the freezing rate by almost a factor of 2. Proceeding now to an examination of the various factors dependent on this rate:

Most castings solidified in an equiaxed manner, and although the few that revealed columnar structure tended to have rather higher amounts of porosity, the data is too limited to draw firm conclusions. The effect does not appear to be large.

The greater ease of nucleation of pores due to the segregation of impurities and inclusions into the residual liquid is not likely to be greatly affected by the relatively small changes in solidification rate introduced in these experiments, since all conditions will approximate well to perfect non-equilibrium, described in Section 4.4. Furthermore, it is probable that the alloys are sufficiently impure as to be little affected by further concentration of impurities.

As T_m increases, the consequent reduction in freezing rate should cause Δt, grain size, and dendrite arm spacing to increase porosity. Experimentally however, porosity in general was observed to decrease with increasing T_m so that these factors are either unimportant in these experiments, or are outweighed by other influences. In addition, Bhattacharjya's work[236] demonstrates that porosity is largely independent of Δt when the gas content is small, which is probably true of practically all of the alloys used since the levels of porosity were very small.

The importance of the following two factors is not easy to assess; both would tend to reduce porosity with increasing T_m: (a) The pressure differential across the pasty zone would be lowered during slower freezing because of the slower movement of the liquid during interdendritic feeding, and (b) burst feeding which acts similarly since the metal will remain in a more plastic condition for a longer time with higher values of T_m (although it is possible that the lower shrinkage pressures which accompany slow

solidification may in any case reduce the likelihood of a burst). Neither of these mechanisms can be dismissed on independent grounds but both are thought to make a relatively small contribution to porosity in these experiments because of arguments based upon the distribution of porosity which are discussed in the following paragraphs.

Thus far in this search for a cogent explanation of the effects of pouring and mould temperatures on porosity, out of 11 possible influencing mechanisms, by a series of elimination we are left with 2 parameters which appear to be of prime importance: temperature gradients and solid feeding. Figs. 29. and 30 can be explained qualitatively very satisfactorily assuming only the operation of these two factors:

As mould temperature increases the temperature gradients become less favourable so that porosity is no longer concentrated along the centreline (Figs. 29. and 30.) but is dispersed over the whole casting: the base of the porosity distribution curve widens. This may be stated conversely for as T_m decreases the increased chilling power of the mould produces a progressively thicker sound outer region of the casting. Thus with low T_m values the porosity is initially small (Fig. 32.) corresponding to a chilled structure, and increases with increase in T_m.

Solid feeding is practically inoperative with cold metal but starts to become important at higher temperatures, acting in opposition to the temperature gradients. The overall density measurements reveal that solid feeding rather more than balances the effect of the unfavourable gradients at high temperatures, so that the total porosity falls again above about 400°C (Fig. 32.).

The important feeding mechanism at high temperatures is identified as being solid feeding because of the occurrence of the central dip in the porosity distribution (Figs. 29. and 30).

This clearly reveals the easy collapse of the centre of the flat specimen under the reduced internal pressure (exterior pressure was close to zero since P.K.24 alloy was cast in vacuum), leaving regions of higher porosity on either side of the centreline which are partially supported by the cooler outer edges of the casting.

A comparison of the effects of mould temperature on carbon steels and P.K.24 alloy reveals firstly the absence of a peak in the porosity versus T_m graphs for steels (Fig. 20.), whereas P.K.24 alloy shows a prominent maximum. This may be ascribed to the fact that high temperature alloys gain strength more rapidly as temperature falls, so that solid feeding rapidly becomes inoperative, whereas for steels, which are comparatively weak, solid feeding continues to be an efficient feeding process even at low T_m values. Secondly, at high temperatures porosity decreases more rapidly for P.K.24 than for steels. This may be due to the P.K.24 alloy being much nearer to its solidus temperature (about 1280; liquidus 1310°C).

The effects of mould and pouring temperatures can be seen to be cooperative, for increase of either will favour solid feeding and worsen temperature gradients. This may be expressed quantitatively in terms of the total heat content of the metal-mould system:

$$Q_{Total} = M_1 S_1 \Delta T_s + H M_1 + M_2 S_2 T_m \qquad \ldots(71)$$

where M_1, M_2 are the masses of metal and mould; S_1, S_2 are the specific heats of the metal and mould respectively; H is the latent heat of fusion of the metal. In order to obtain the same thermal conditions for a given casting and mould, therefore, an increase in mould temperature ΔT_m must be accompanied by a corresponding decrease in pouring temperature ΔT_p where

$$\frac{\Delta T_p}{\Delta T_m} = \frac{M_2 S_2}{M_1 S_i} = Z \qquad \ldots(72)$$

where Z is a constant. For the 0.5 cm. section casting, the ceramic mould had a thermal capacity about twice that of the steel or high temperature alloy, so that Z works out to 2 ± 1 for this system.

The relatively small effect of superheat is emphasised by applying equation (71) to a typical ferrous alloy, with mould temperature at 1000°C and superheat 200°C, the relative contributions to the total heat of the system from the mould, latent heat, and superheat are respectively about 21, 7 and 2 K calories, the latter representing less than 7% of the total heat available. These considerations help to understand the small effect of superheat, particularly in the experiments on carbon steels.

The noticeably larger effect of superheat on P.K.24 alloy could be due to other effects which are difficult to evaluate, particularly the possibility of certain efficient pore nuclei being taken into solution at higher temperatures[264].

8.3. Effect of Section Thickness.

The results for all materials studied clearly show that thinner sections are less sound than thicker ones. The causes for this can be sought in terms of (a) the rate of solidification, and (b) the origin of the porosity:

(a) Thicker sections will freeze at slower rates than thicker sections. Ruddle's equation (68) in fact predicts a parabolic relation between the solidification time and the mass of a casting, and this is confirmed reasonably well by the measurements of dendrite arm spacing (Table 8.).

As in Section 8.2., the solidification interval Δt, the grain size and the dendrite arm spacing should all lead to a reduction in porosity as the section thickness decreases. This is contrary to observations so these factors either are not operative, or are outweighed by

other factors. Similarly, solid feeding ought to increase in effectiveness as section thickness decreases because solidification will be completed while the exterior of the casting will still be relatively hot, and therefore sufficiently weak to allow solid feeding, and because of the earlier impinging of the plastic zones on the free surface of the casting, both of which would tend to keep the hydrostatic tension in the trapped liquid region below that required for the nucleation of a pore. These qualitative arguments are considered quantitatively in Section 3.5. Thus solid feeding cannot explain the experimental data; furthermore, in very thin sections of only a few grain diameters or less in width, the concept of imprisoned liquid regions becomes less plausible.

(b) The rate at which feeding liquid can be delivered to regions of a casting at a late stage in solidification is in proportion to the number of available flow channels per unit area, and therefore must be in approximate proportion to the section thickness. However, the requirements for the rate of feeding do not decrease in this linear fashion as section thickness decreases, but are expected to increase rapidly because solidification occurs (i) simultaneously throughout the volume of the casting because of low temperature gradients, and (ii) very rapidly because of the small amount of heat to be extracted (equation 63).

As solidification nears completion, therefore, feeding conditions become very difficult in thin sections, and hydrostatic tension begins to increase. At this stage interdendritic or burst feeding from the direction of the feeder becomes less feasible, but the transverse pressure gradient may suck interdendritic liquid away from the surface of the casting, or if a sound outer skin exists, may cause this to rupture at a weak point, allowing the ingress of air.

Thus it seems likely that the mechanism of formation of porosity changes with section size: as very narrow sections are approached the mechanism changes from nucleation-and-growth in the interior of a liquid-solid mass, to the non-nucleation process of liquid drainage away from a free surface. This mechanism will probably operate under rather small pressure gradients between the exterior and interior of the casting, so that pores will form and grow before the pressure differential has reached the larger values necessary for efficient feeding by other methods: interdendritic (from the feeder), burst or solid feeding. This mode of pore formation would be predicted to yield, therefore, higher levels of porosity than that produced by the nucleation process, in agreement with observations.

The operation of such a process is evident from the appearance of cast specimens of 0.25 and 0.125 cm. thickness (particularly the incompletely filled castings, Figs. 25-27) where surface pores are seen to disappear into a labyrinth of internal passages. Also, when the castings are submerged during density determinations their weight is observed to increase continuously as the pores gradually fill with liquid.

3.4. Effect of Composition.

It has often been assumed that increasing the equilibrium freezing range ΔT_f of an alloy increases its tendency towards greater porosity because of the increased difficulties of feeding through the more extensive pasty zone. The results for Fe-C alloys in Fig. 23. are therefore surprising, since instead of the expected continuous increase of porosity with carbon content, a definite maximum occurs at about 0.7% C.

These observations may genuinely represent the influence of differences in carbon content, although there is the possibility that the results may be heavily influenced by

differences in gas content. An attempt was made to assess this possibility employing the relations listed in Table 3. The equilibrium partial pressures of the gases within a bubble were calculated for the solidus temperatures of each of the steels. The total oxygen analyses were used in these calculations, so that rather higher pressures were deduced since most of this oxygen was chemically bound in inclusions; only the oxygen remaining in solution was available for pore formation. In the absence of analyses for N_2 and H_2 their effect was estimated by assuming the reasonably high concentrations of 0.01 wt.% N_2 and 10 $cm^3/100$ g. H_2 (using conventional units). The total gas pressures for the 0.25, 0.80 and 1.30% C steels work out to be 1.3, 1.8 and 2.9 atmospheres (neglecting the enhancement of these figures by segregation effects, which would increase them all by about the same factor). Taking these results as they stand, the maximum in the porosity-composition curve cannot be explained by differences in gas content.

The few results available in Table 3. indicate that the porosity maximum at 0.7% C can neither be explained by changes in dendrite arm spacing nor grain size. Similarly, no substantial effect can be attributed to the decrease of surface tension with carbon content since most investigators find this to be negligible[73,75,84,343,344].

Values are quoted[293] for the contraction during solidification, α, which indicates a maximum at 0.7% C. Unfortunately these results are based upon very early data which do not appear to be reliable, particularly in the light of more recent refined experiments by Vertman et.al.[294] which show an approximately linear decrease in α from 11.5% to 2.0% as the carbon content increases from 0.15% to 2.0%.

A more plausible theory to explain the existence of the maximum is based upon considerations of the non-equilibrium conditions during freezing.

Conditions intermediate between true equilibrium and non-equilibrium as defined in Section 4.4. could give rise to a maximum in freezing range ΔT_f of about 300°C at 0.7% C as indicated in Fig. 13. This would correspond, of course, to equivalent maxima in difficulty of feeding, and in the amount of final porosity.

There remains the possibility that the presence of eutectic liquid under conditions of non-equilibrium freezing may be causing the fall in porosity above 0.7% C according to Scheuer's theory outlined in Section 4.4. Evidence of some eutectic liquid was observed metallographically in the 1.30% C steel, but the compositions of the steels were too widely spaced to draw firm conclusions.

Thus a closely spaced series of Al-Cu alloys up to 17% Cu was cast, and the peak in porosity determined to be at 0.3% Cu. Although the equilibrium limit of solid solubility is 5.6% Cu, the second phase $CuAl_2$ existed as a practically continuous interdendritic film at 4% Cu, and decreased to trace quantities only at about 1% Cu. At 0.3% Cu no $CuAl_2$ could be detected although clear evidence of non-equilibrium solidification was provided by the heavily cored dendrites.

It seems reasonable to conclude, therefore, that the porosity maxima observed in the Fe-C and Al-Cu systems (and noted by other investigators for other systems - Section 4.4.) are the direct result of a maximum in the freezing range - composition relation as a consequence of non-equilibrium freezing.

8.5. Effect of Taper.

Brinson and Duma[316] observed that the critical taper (assuming that such exists) required to reduce porosity to low levels was below 5° (the smallest angle investigated). The present series of investigations lowers the estimate of the critical taper to below 2°, which corroborates well with

Walters[233] prediction of 1.7° calculated for a skin freezing metal in a cylindrical sand mould, and implies that despite the undoubted greater complexity of the mode of solidification of the 0.25% C steel, the exterior taper imposes a similar taper on the aggregate of the flow paths for the residual liquid.

A further implication is that the formulae based upon the viscous flow of feeding liquid through the dendrite mesh are fundamentally correct.

3.6. Effect of Pressure.

The comparatively large reduction in porosity observed experimentally (Fig. 31.) due to the rather small (absolute) increase in pressure, which was less than only 1 atmosphere, infers that pore formation is easy, and must therefore occur either by a non-nucleation or a non-classical nucleation mechanism. For instance to suppress classical pore nucleation by gas in the interior of a complex inclusion, which is the least stringent classical oondition (Section 2.3.3.), an applied pressure of at least 200 atmospheres would be required.

Since nucleation is easy, then the quantity of porosity is, therefore, governed by growth. Clearly, a gas bubble will expand to 10^5 times its volume as the pressure is decreased from 1 atmosphere to 10μ pressure. This is also predicted approximately by equation 60. Nevertheless, the quantity of porosity in successive castings only decreases by a factor of about 10 as the Ar pressure inside the vacuum chamber is raised. This means that the growth of porosity must be controlled by other effects in addition to the applied pressure, and which are not allowed for in equation 60. These may include:

(a) Equation 60 neglects the effects of shrinkage, This is likely to be important, particularly since the contribution of gas to pore growth is probably small as a result of remelting vacuum-melted stock under vacuum. The applied pressure will add directly to the gas pressure and shrinkage pressure, as indicated in equation 1. In the furthest regions of the pasty zone of the casting P_s may greatly outweigh other pressures so that P_a and P_g become negligible and equation 60 irrelevent.

(b) The already advanced growth of the solid may mechanically limit the expansion of a gas bubble.

(c) There may be porosity present in the casting which is separate from the easily formed variety, and which is nucleated only with difficulty, so that its formation is comparatively unaffected by the small increase in absolute pressure.

8.7. On the Origin of Layer Porosity.

Early authors[339-341] assumed that pores resulted from thermal contraction and were formed in the solid state in a manner analogous to hot tearing. Baker[310,342] effectively proves that pores form at a late stage in freezing; his theory is rather better stated by Cibula[312] who argues that after mass feeding is arrested, further shrinkage imposes tensile stresses on the continuous solid network which tears perpendicularly to the stress, i.e. parallel to the isotherms. If these tears are not healed by the inflow of residual liquid then layers of porosity result.

Baker[223] attempted to test whether microporosity was the result of thermal contraction by casting test pieces in a mould which was designed to accentuate hot tearing tendencies. However, no significant increase in porosity was observed.

The negative result of Baker's critical experiment is substantiated by Cibula's observations[312] that grain

refinement promotes layer porosity but decreases the tendency towards hot tearing, and later[278] that Al-4.5% Cu alloy has little tendency towards microporosity but commonly hot tears. Experiments by Lagowski and Meier[283] on Mg-Zn alloys covering the range of Zn contents from 0 to 30% Zn show clearly that the maxima for the incidence of hot tearing and microporosity are well separated, occurring at 1% and about 6% Zn respectively. Furthermore, the thermal contraction curve has its maximum at 1% Zn indicating that hot tearing is associated with contraction in the solid state, and not with microporosity.

All these observations are substantiated by the elementary consideration that the thermal contraction of the whole casting is likely to produce (if anything) a compressive stress on the internal dendrite mesh because of the larger fall in temperature of the exterior skin compared to the interior. In materials of high thermal conductivity, however, such as Cu and light alloys, the temperature differential between the interior and exterior is in any case likely to be negligible, producing no stress differential.

A new explanation of the origin of layer porosity is therefore required, and a tentative model is proposed and outlined below. It is based not upon thermal contraction as the fundamental driving force, but upon the contraction on solidification.

If we assume Flemings formula (equation 27) for the pressure differential across the mushy zone, and substituting their relation[230] for the radius of the flow channels as a function of time

$$a^2 = (b - 4\lambda t^{\frac{1}{2}})/\pi bn \qquad \ldots(73)$$

then we obtain the pressure differential as a function of time

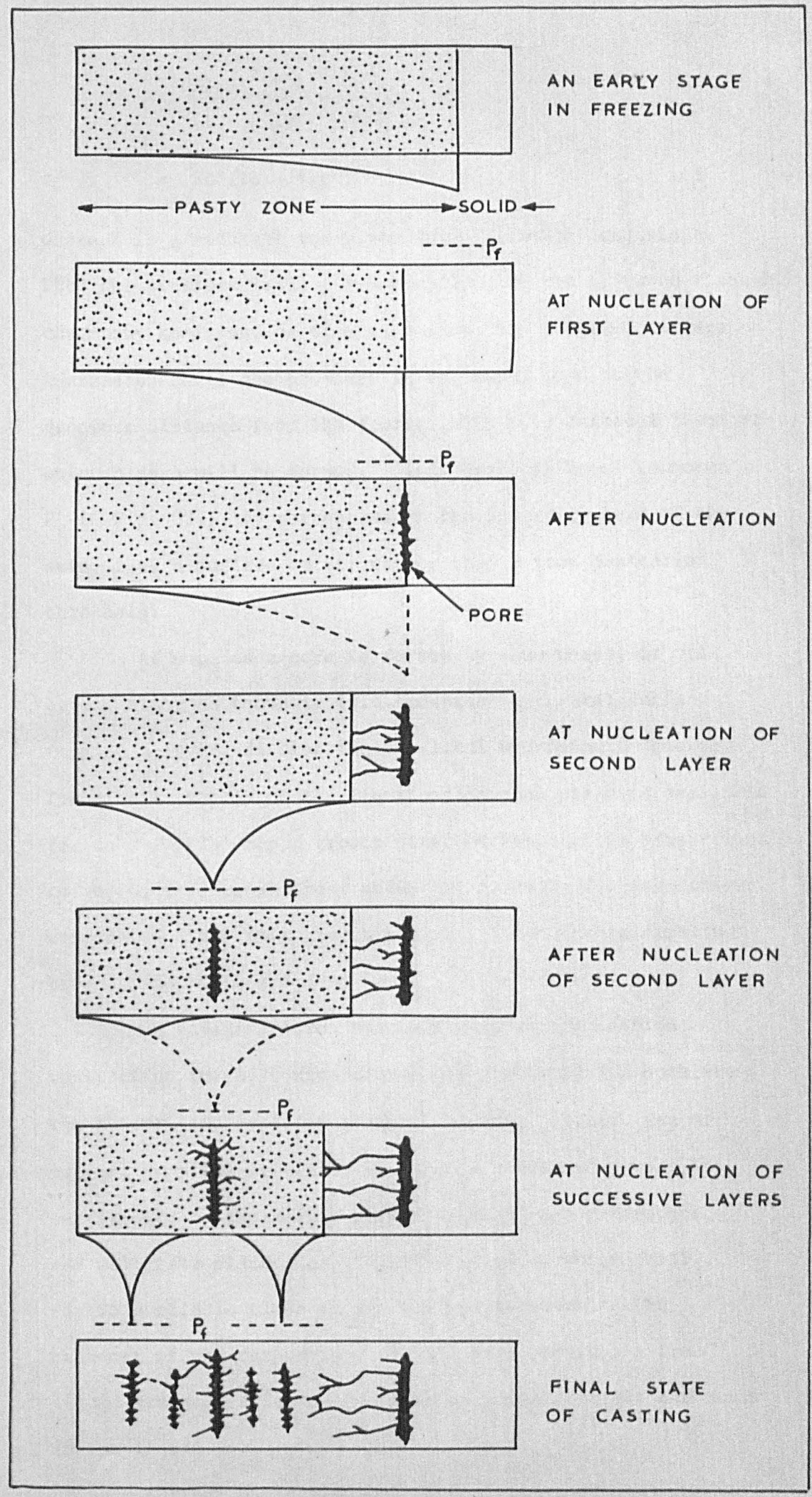

FIGURATIVE REPRESENTATION OF THE ORIGIN OF LAYER POROSITY.

FIGURE 33

$$\Delta P = \frac{32\mu\alpha\lambda^2 L^2\pi^2 b^2 n^2}{(1-\alpha)(B - 4t^{\frac{1}{2}})^2}$$

$$= ZL^2/(b - 4\lambda t^{\frac{1}{2}})^2 \qquad \ldots(74)$$

where Z is a constant for given solidification conditions. Thus the pressure falls parabolically with the distance through the mushy zone, and as time increases, the pressure difference increases, until the pressure in the mushy zone at the greatest distance from the feeder falls to a critical level at which a pore will be formed. This critical level (denoted P_f in Fig. 33.) may correspond to the inward rupture of the skin, i.e. a surface burst, rather than a true nucleation threshold.

As soon as a pore is formed by some means, it will spread along an isobaric (i.e. constant pressure) surface forming a layer, dissipating the local hydrostatic tension. The elastic energy of the liquid-solid mass which is available for this initial rapid growth stage of the pore is proportional to the difference in areas under the pressure distance curves before and after this growth phase. This area is clearly proportional to L x P_f.

As solidification proceeds, the solidification contraction in the centre of the mushy zone is fed both from the feeder, and by fluid (whether residual liquid, gas or vapour) from the direction of the newly created pore. This corresponds to the slower growth phase of the first pore, and will take place along the limited paths which still remain available close to the solidus isotherm. The presence of the outpushings of this pore provides a free liquid surface, adjacent to which no large stresses can occur in the liquid.

Further nucleation and growth events produce further layers until the whole casting is solidified. The final state consists of layers of porosity showing considerable interlinking.

CONCLUSIONS.

Nucleation

1. When the solidus isotherm intersects the surface of the casting at a late stage in solidification, then porosity may occur by the non-nucleation process of growth of pores from surface pinholes.

2. (Nucleation of pores in castings is subject to the following condition being satisfied

$$P_g - P_s = P_f$$

where P_s is the shrinkage pressure (negative), P_g is the total gas pressure in equilibrium with the melt at the point of nucleation, and the fracture pressure, P_f, is a constant depending upon many factors, and in particular, the nucleation mechanism.)

3. (The conclusions of this work must remain tentative while P_f can be only roughly estimated. Furthermore, the maximum value of P_s is not well known because of lack of data on mechanical properties of metals at the melting point[39], and P_g is completely unknown for most low melting point constituents in metals and alloys.

4. Homogeneous nucleation is not a feasible mechanism for the nucleation of pores in castings.

5. Solid, and perhaps liquid, inclusions do not aid nucleation sufficiently to enable heterogeneous nucleation to occur.

6. Complex inclusions consisting of solid and liquid phases (are possible (although perhaps rather difficult) sites for the heterogeneous nucleation of porosity.)

7. Nucleation will occur preferentially at advancing solidification fronts because of (a) high local gas content, (b) probably low surface tension because of (i) concentration of surface active impurities and (ii) the high internal gas pressure.

8. Small bubbles introduced by turbulent pouring and held in suspension in the liquid will not in general survive. If however a bubble does impinge on a well-established solidification front before it dissolves then it will form a very favourable nucleus for porosity.

9. Air trapped in certain exogenous inclusions appears to be capable of a long stable existence in the melt, and able to provide many small bubbles as nuclei for pores.

10. It is possible that cosmic rays may be an important source of porosity in large castings if other nucleation factors are not operative.

11. It is possible that traces of radioactive materials in a batch of metal may be an important source of porosity nucleation.

12. In the absence of suitable nuclei a casting will freeze perfectly sound, despite a total lack of feeding liquid, because of the possibility of solid feeding.

Growth

13. The driving force for the growth of pores during the first few milliseconds is the internal gas pressure and the stored elastic energy in the solid-liquid surroundings, and subsequently gas and shrinkage.

Feeding

14. The reduced pressure in castings may be relieved by as many as five separate feeding mechanisms: liquid-, mass-, interdendritic-, burst- and solid-feeding.

15. Solid feeding is investigated by quantitative theory using elastic-plastic, Bingham, viscous and creep flow models.

16. Experimental evidence is presented supporting this effect of mechanical constraint on porosity.

Effect of the Mode of Solidification on Porosity.

17. Non-equilibrium freezing results in a peak in the freezing range versus composition relation for alloys of a eutectic system, corresponding to a maximum in the porosity-composition relation. This was demonstrated for Fe-C and Al-Cu alloys.

18. A theory of the origin of layer porosity is proposed based on the flow of liquid through the pasty zone.

19. A quantitative relation illustrating the cooperative effects of mould temperature and superheat is proposed.

Note on Appendices.

The appendices 2. to 7. represent a literature survey of data which is pertinent to the theoretical investigation of fracture pressures in liquid metals. A comparison of measurements of the same physical quantity made by different investigators will indicate to the reader how much faith may be placed in the data: a critical assessment of the reliability of each determination would be a vast undertaking and in any case not entirely remove doubt about the presence of trace impurities which may greatly affect all measurements of this kind. Some critical reviews of data on the surface tension of metals do exist,[201] but the general conclusion seems to be that an arithmetic mean of all determinations yields about the best working value. The author does not entirely suscribe to this view and has tended to favour high values for surface tensions in view of the fact that the impurities which are most likely to be present, and which affect surface tension appreciably, and which, furthermore, are most likely to remain undetected (particularly oxygen), mainly lower surface tension.[75]

APPENDIX 1

Cavitation at a Liquid-Liquid Interface

Considering the equilibrium of forces on a bubble at the interface (Fig. 9d)

$$\gamma_{12} \cos \theta_{12} = \gamma_1 \cos \theta_1 + \gamma_2 \cos \theta_2 \qquad \ldots(1)$$

$$\gamma_{12} \sin \theta_{12} = \gamma_1 \sin \theta_1 + \gamma_2 \sin \theta_2 \qquad \ldots(2)$$

Further conditions are (C.f. Fig. 9a.)

$$d_1/r_1 = m_1 = \cos \theta_1 \qquad \ldots(3)$$

$$d_2/r_2 = m_2 = \cos \theta_2 \qquad \ldots(4)$$

and the necessity for the pressure to be everywhere equal inside and immediately outside the bubble

$$P_i - P_e = 2\gamma_1/r_1 = 2\gamma_2/r_2$$

thus

$$\frac{r_1}{r_2} = \frac{\gamma_1}{\gamma_2} \qquad \ldots(5)$$

Since the curved area of a spherical cap is $2\pi r^2(1 - m)$, and its plane area is $\pi r^2 (1 - m^2)$, and its volume $\frac{\pi}{3} r^3 (2 - 3m + m^3)$, then the work required for the creation of this bubble is

$$W = (\text{Area})\gamma + (\text{Volume})(P_e - P_i)$$

$$= \pi r_2^2 \left[2(1-m_2)\gamma_2 + 2(1-m_1)\frac{\gamma_1^3}{\gamma_2^2} - (1-m_2^2)\gamma_{12} \right.$$

$$\left. + \frac{r_2}{3}(2-3m_2+m_2^3)(P_e-P_i) + \frac{r_2}{3}\left(\frac{\gamma_1}{\gamma_2}\right)(2-3m_1+m_1^3)(P_e-P_i) \right]$$

Differentiating with respect to r_2 and equating to zero gives the critical radius, r^*, of the vapour with the second liquid surface,

$$r^* = \frac{2\gamma_2 \left[2(1-m_2) + 2(1-m_1)\left\{\frac{\gamma_1}{\gamma_2}\right\}^3 - (1-m_2^2)\frac{\gamma_{12}}{\gamma_2} \right]}{(P_e-P_i)\left[(2-3m_2+m_2^3) + \frac{1}{2}(2-3m_1+m_1^2)\right]}$$

which corresponds to the peak of the energy-radius relation:

$$W_{max} = \frac{16\pi\gamma_2^3}{3(P_e-P_i)^2}\phi_2$$

APPENDIX 2

Recently Measured Surface Energies of Some Liquid Metals

	Surface Energy ($ergs/cm^2$)	Temp. (^oC)	Ref.
Fe	1700	1550	78
	1835	1550	79
	1880	1535	80
	1860	1550	81,82,83
	1754		84
	1640	1650	85
	1730		86,87
	1735		88
	1670		89
	1710		74
Ni	1660	1400	90
	1760	1470	91
	1720	1500	92
	1900 ± 100	1500	(92 extrap to zero O_2)
	1738	1452	78
	1780	1452	80
	1760	1452	93
	1780	1550	94
	1845	1500	95
	1924	1550	79
	1650	1660	85
Co	1825	1550	78
	1845		96
	1885	1550	97
	1880	1492	80
	1936	1550	79
	1812	1600	94
	1650	1650	85
	1880	1400	90
Al	825	660	98
	860		100
	850	700	101
	543	700	85
	865*	660	102
Cu	1265	1550	96
	1298		103
	1437	1100	104
	1301	1100	105
	1220	1100	85
	1355*	1083	102
	1150	1083	106
	1268	1130	107

APPENDIX 3

Measured Surface Energies of Solid Metals

	Surface Energy ergs/cm^2	Temp. (°C)	Ref.
Fe delta	2090 ± 100	1450	108
	1950 ± 195	1400 - 1535	109
gamma	2130 ± 80	1450	108
	2150 ± 422	1360 - 1400	109
	1950	1100	110
Fe - 2.9% Si	1900 ± 100 (?)	1500	111
Ni	1725 ± 150	1452	112
Cu	1755 ± 89	1083	113
	1650 ± 100	1083	114
	1750 ± 90	1083	115

APPENDIX 4

Some Values of Interfacial Energies between Liquid and Solid Pure Metals.

Metal	Interface Energy ($ergs/cm^2$)	Temp. (^oC)	Ref.
Fe	204	1240	115
	234		117
	(δ) 100 ± 225	1535	*
	(γ) 300 ± 450	1535	*
Ni	255	1133	115
	289		117
Co	234	1160	115
Cu	117	847	115
	347 ± 70	1083	*
Al	93	530	115

* Calculated from the difference between the best values for the surface energies of the solid and liquid.

APPENDIX 5

Some measured surface energies of non-metallic liquids

Liquid (composition wt. %)	Surface Energy γ_{LV} (ergs/cm^2)	Temp. (°C)	Ref.
Si (Pure)	712	1440	118
	750	1550	87
Si (Saturated with Al)	720		119
SiO_2	307	1800	120
SiO_2, 50 MgO	400	1750	121
	390		122
SiO_2, 60 CaO	510	1600	123
	450		122
	480		124
SiO_2, 30 CaO	340		122
	389		124
	455	1600	123
	389	1600	125
SiO_2, 10 CaO, 20 Al_2O_3	205	1345	127
SiO_2, 30 CaO, 15 Al_2O_3	510	1400	121
	486	1450	126
SiO_2, 48 CaO, 45 Al_2O_3	748	1450	126
SiO_2, 33 CaO, 19 FeO	444	1300	203
SiO_2, 42 CaO, 15 P_2O_5	396		124
SiO_2, 37 CaO, 8 CaS	380	1600	123
SiO_2, 24 CaO, 9 CaS, 15 MgO	280	1600	123
SiO_2, CaO, Cr_2O_5 (minimum ?)	345	1600	125
SiO_2, CaO, V_2O_5 (minimum ?)	270	1600	125
SiO_2, 5 CaO, 35 MgO	460	1500	121
SiO_2, 41 CaO, 34 Al_2O_3, 10 MgO	473	1600	128
SiO_2, 47 CaO, 14 Al_2O_3, 4 MgO	591	1450	196
SiO_2, 9 CaO, 27 MnO, 10 CaS	290		129
SiO_2, 68 FeO	409	1410	130
	430		122
SiO_2, 65 FeO, 5 Fe_2O_3	403	1370	131
SiO_2, 24 FeO, 31 MnO	400	1400	131
SiO_2, 30 Al_2O_3, 25 MnO	280	1510	132
FeO	590	1420	131
	585	1410	130
	619	1420	136
FeO, 8 Fe_2O_3	500	1370	131
FeO, 16 Fe_2O_3, 7.4 CaO	470	1375	131
FeO, 7 Al_2O_3	604	1410	130
FeO, 22 CaO	573	1410	130
FeO, 3 Cr_2O_3	588	1410	130
FeO, 10 MnO	555	1410	130
FeO, 18 TiO_2	510	1410	130

Some measured surface energies of non-metallic liquids (Cont'd.)

Liquid (composition wt. %)	Surface Energy γ_{LV}(ergs/cm^2)	Temp. (°C)	Ref.
FeS	585	1500	133
	380	1193	134
	(390)	1300	135
	479	1193	136
Ni_3S_2	510,570	1300	135
Cu_2S	467	1130	136
	410	1130	137
P_2O_5	60	100	136
MnO	653	1750	138
	613	1750	136
CoO	555	1800	138
	621	1800	136
Nb_2O_5	220	1500	139
Al_2O_3	700	2050	138
	690	2050	120
	917	2050	136
Al_2O_3, 50 CaO	700	1550	121
Na_2O .$2SiO_2$ (Sodium silicate glass)	292	1300	140
CaF_2	274	1550	141
AgCl	(109)	600	142
$BaCl_2$	171	960	142
$CaCl_2$	152	782	142
CsCl	87	700	142
CuCl	92	450	137
KCl	95.8	800	142
LiCl	131	700	142
NaCl	114	800	142
$PbCl_2$	127	600	142
RbCl	95.7	750	142
$SnCl_2$	(78.8)	500	142

Literature survey of surface tensions of liquid glasses: (140) and (143).

APPENDIX 6

Some measured surface energies of non-metallic solids.

Solid	Surface Energy (ergs/cm^2)	Temp. ($^\circ$C)	Ref.
Al_2O_3	905 (940) 1112 (962)	1850 (1500) -273 (1500)	144 145
ZrO_2	590 (625) 797 (647)	1850 (1500) -273 (1500)	144 145
ThO_2	470	-273	145
MgO	1000 1200 (1030) 1090 (900)	 -196 (1500) -273 (1500)	146 147 145
SiO_2	290 $\pm$ 10	1100-1300	148
ZnO	610	-273	145
CdO	530	-273	145
CaF_2	450	-196	147
Si	1240	-196	147
Si_3N_4	1100	1200	78
$MoSi_2$	1165	1100	78
Graphite (Basal Plane)	1590 (minimum) 1200		149 150
TiC	1930 (minimum)		149
VC	1675 $\pm$ 500	1100	145
TaC	1290 $\pm$ 390	1100	145
ZrC	800 $\pm$ 250	1100	145
SiC	840	1200	78

Figures in brackets signify values corrected to 1500°C assuming $\partial\gamma / \partial T$ = 0.1 ergs/cm^2/$^\circ$C approximately.

APPENDIX 7

Contact Angles between various solids and liquids.

Liquid	Solid	θ°	Temp. ($^{\circ}$C)	Ref.
Fe	Al_2O_3	141	1550	88
		141		74
		128	1550	78
		120	1650	99
		100-148		73
		141	1550	151
	MgO (Polycryst.)	123,130	1550	151
	(single crystal)	117		152
	ZrO_2	92,111,102	1550	151
	BeO	120	1650	99
	ZrC	140	1500	153
		45	1490	154
	TiC	132	1500	153
		28	1490	154
	VC	20	1490	154
	NbC	25	1490	154
	TaC	23	1490	154
	Cr_2C_3	0	1490	154
	MO_2C	0	1490	154
	WC	0	1490	154
	Graphite	60	1540	149
Ni	Al_2O_3	120	1400	156
	(Polycrystal)	128,133,141	1500	151
		148 (at zero O_2)	1500	92
		138	1475	78
		121,140,136	1520	99
	Al_2O_3 (single crystal)	108	1500	95
	ZrO_2	118,131,120	1500	151
	TiO_2	105,146,121	1500	151
	ThO_2	132,134	1500	151
	MgO	132,152,132	1500	151
		127	1470	99
	BeO	110	1470	99
	TaB_2	50	1480	155
	CrB_2	20	1480	155
	ZrC	24	1380	154
	NbC; TaC	17	1380	154
	Cr_2C_3; MO_2C	0	1380	154
	VC	17	1380	154
		13	1400	157
	TiC	4		149
		48	1300	158
		23	1380	154
		20	1400	157
		37	1500	156
		0	1500	161
		17,30,32	1450	151
	Graphite	90,68,86		151
		59,62		149
	Cr_2C_3	0	1500	161
		0	1380	154
	NbC	21.2	1450	157
	BeC	90,75,92	1500	151
	B_4C	90	1780	176
	WC	0		156,154
	TiB_2	100-38	1480	161
	Mo_2B_5	8	1480	161

APPENDIX 7 (Cont'd)

Liquid	Solid	Contact Angle (θ°)	Temp. ($^{\circ}$C)	Ref.
Co	Al_2O_3	138,141,142	1520	99
		130	1550	159
		120	1500	156
	MgO	123	1500	99
	BeO	110,117	1470	99
	TiC	25	1420	154,151
	ZrC	36	"	154
	HfC	40	"	"
	VC	13	"	"
	NbC	14	"	"
	TaC	13	"	"
	Cr_2C_3; Mo_2C; WC	0	"	"
	Graphite	36,60	1495	149
Cu	Al_2O_3	170	1100	78
	Al_2O_3; MgO	100	1150	77
	HfC	134	1100	154
	TiC	112	1100	154
		148	1500	153
		108	1100	145
		17	1300	158
	MoC	148	1500	153
	Mo_2C	18	1100	154
	NbC	148	1500	153
	$NbC_{0.97}$	70	1500	153
	CrC	148	1500	153
	Cr_3C_2	47	1100	154
	VC	148	1500	153
		54	1090	145
	$VC_{0.88}$	50	1100	154
	ZrC	148	1500	153
		140	1100	145
		127	1100	154
	TaC	75	1100	145
		78	1100	154
	WC	30	1100	145
		20	1100	154,178
	Diamond	145	1150	160
	B_4C	130,17	1000	179
	TiB_2	156	1080	155
	ZrB_2	130	1080	155
	VB_2	150	"	"
	NbB_2	135	"	"
	TaB_2	80	"	"
	CrB_2	50	1300	"
	MoB_2	10	1300	"
Al	Al_2O_3	170	940	145
		148	970	145
		85	1255	145
	Diamond	150	800	160
		75	1000	160
	TiC	118	700	155
	B_4C	117.5	600-670	179
	Al_4C_3	104	1000	180
Zn	TiC	120	550	155
	B_4C	120	540-620	179

APPENDIX 7 (Cont'd).

Liquid	Solid	Contact Angle (θ°)	Temp. (°C)	Ref.
	WC	120-30	500-1300	145
Sn	Al_2O_3	162	800	78
	Diamond	125	1150	160
	Graphite	150	1150	160
	SiC	162	800	78
	Si_3N_4	168	800	78
	MoS_2	170	800	78
Ag	Al_2O_3	144	1000	161
	Diamond	120	1000	160
	MgO	136	975	145
	ThO_2	90	1000	145
	ZnO	101	980	145
	CdO	113	970	145
	TiC	108	980	145
	TaB_2	118	1300	161
Al_2O_3	Graphite	128	2100	164
	TaC; ZrC; TiN; ZrB_2	~40	2100	164
50 Al_2O_3, 50 CaO	MoC; NbC; CrC; VC; ZrC; TiC	~41	1500	153
SiO_2; 40 CaO, 20 Al_2O_3	MoC; NbC; TiC	~31	1500	153
SiO_2, 16 Na_2O, 10 B_2O_3 etc.	Graphite	158	1000	163
SiO_2, 17 Na_2O, 5 CaO 4 MgO, 2 Al_2O_3	Al_2O_3	7	1200	165
	50 SiO_2, 50 Al_2O_3	30	1200	165
	SiO_2	0 (?)	1200	165
	Mullite	7	1200	165
FeO	MgO (single crystal)	21		152
Na_2O. 2 SiO_2 (Saturated with Fe_3O_4	Fe_3O_4	2 ± 1	1000	162
	Graphite	166	1020	163
Bi	TiC	138-122	300-600	145
	WC	140-52	700-1100	145
	UC	140-93	300-700	145
Pb	TiC	152-90	400-1000	145
	B_4C	121-113	225-395	179

REFERENCES.

1. Allen, N.P., J.Inst. Metals 1932 49 317-346.
1933 51 233-303, 52 193-220.

2. Whittenberger, E.J., Rhines, F.N., J.Metals 1952 4 409-420.
Trans. Met. Soc. AIME 1952 194 409-420.

3. Fisher, J.C., J.Appl. Phys. 1948 19 1062-67.

4. Wakeshima, H., J.Phys.Soc. Japan 1961 16 6-14.

5. Temperley, H.N.V., Proc. Phys. Soc. 1947 59 119.

6. Bernath, L., Ind.Eng.Chem. 1952 44 1310 13.

7. Döring, W., Z.Phys.Chem. 1937 (B) 36 371.
1938 (b) 38 292.

8. Blake, F.G., "The Tensile Strength of Liquids",
Technical Memorandum No.9. June 1949.
Acoustics Research Lab., Harvard University, Mass.

9. Kundt, A., Ann. Physik 1881 12 533-50. Int. Crit. Tables 4 475.

10. Turpin, M.L., Elliott, J.F., J.Iron Steel Inst. 1966 204 217-225.

11. Chalmers, B., "Principles of Solidification" 1964 Wiley, U.S.A.

12. Schener, E., Foundry Trade J., 1948 85 (1671) 245-248.
(1672) 273-276, 280.

13. Fletcher, N.H., J.Chem. Phys. 1963 38 237-40.

14. Chakraverty, B.K., Pound, G.M., Acta Met. 1964 12 851-60.

15. Kramer, J.J., Tiller, W.A., J. Chem. Phys. 1965 42 257-262.

16. Antonenko, V.I., Kozhemrov, U.A., Izv. VUZ Chern.Met. 1965 (11) 14-19
Ershov G.S., Izv.Akad.Nauk SSSR OTN Metall. 1965 (1) 78-81.
Kamyshov, V.M., Esin, O.A., Chuchmarev, S.K., Izv. VUZ Chern. Met.
1964 (7) 24-28.

17. Frenkel, J., "Kinetic Theory of Liquids" 1946 Dover.

18. Fürth, R., Proc. Camb. Phil. Soc. 1941 37 252-290.

19. Kagan, Yu, Russ.J.Phys.Chem. 1960 34 92-101.

20. Portevin, A.M., Trans.Amer.Found.Soc. 1952 60 109-124.

21. Vallet, P., Iron and Steel 1955 28 463-67.

22. Bogdandy, L. von, "Steelmaking - Chipman Conference 1962"
M.I.T. Press 1965. Editor, J.F. Elliott.

23. Fremunt, P., Slevarenstvi 1964 12 (8) 302-7.

24. Gernez, M., Phil. Mag. 1867 33 479.

25. Harvey, E.N., J. Cellular Comp. Physiol 1944 24 123.

26. Turkdogan, E.T., Trans.Met. Soc. AIME 1965 233 (12) 2100-12.

27. Glaser, D.A., Phys. Rev. 1953 91 762.

28. Hahn, B., Fischer, J., Rev. Sci. Instr. 1957 28 656.

29. Lieberman, D.V., Phys. Fluids 1959 2 466-468.

30. Hahn, B. Il Nuovo Cimento 1961 22 650-653.

31. Hahn, B., Peacock, R.N., Nucl.Instr. Methods 1963 20 133-134.

32. Sette, D., Wanderlingh, F., Phys. Rev. 1962 125 409-417.

33. Seitz, F., Phys. Fluids 1958 1.2.

34. Tenner, A.G., Nucl. Instr. Methods 1963 22 1-42.

35. Mullins, J.H., Alyea, E.D., Gallagher, L.R., Chang. J.K., Teem, J.M., Bull. Amer. Phys. Soc. 1957 2 175.

36. Montgomery, D.J., "Cosmic Ray Physics" Princeton Univ. Press, New Jersey, 1949.

37. Damask, A.C., Dienes, G.J., "Point Defects in Metals" 1963 Published by Gordon and Breach, N.Y.

38. Bower, T.F., Brody, H.D., Flemings, M.C., "Effects of Solidification Variables on the Structure of Al-base Ingots", Contract No. DA-19-020-ORD-5706 (A) Annual Report June 1964. M.I.T. Trans. Met. Soc. AIME 1966 236 1157-1165.

39. Campbell, J., Trans. Met. Soc. AIME 1967. 239 (2) 138-142

40. Briggs, L.J., J.Appl. Phys. 1950 21 721; 1953 24 488
Science 1950 112 427; 1951 113 483
J.Chem.Phys. 1951 19 970.

41. Ransley, C.E., Neufeld, H., J.Inst.Metals 1948 74 599-620, 781-786.

42. Eichenauer, W., Pebler, A., Z. Metall. 1957 48 373.

43. Opie, W.R., Grant, N.J., Trans. Met. Soc. AIME 1950 188 1237.

44. Eichenauer, W., Hattenbach, K., Pebler, A., Z. Metall. 1961 52 682-684.

45. Busk, R.S., Bobalek, E.G., Trans. Met. Soc. AIME 1947 171 261.

46. Sauerwald, F., Z. anorg. Chem. 1949 258 27.

47. Winterhager, H., Alum. Archiv. 1938 12 7.

48. Röntgen, P. Möller, F., Metallwirtschaft 1934 13 81, 87.

49. Bever, M.B., Floe, C.F., Trans. Met. Soc. AIME 1944 156 149-159.

50. Hofmann, W. von, Schneider, H.J., Giesserei Techn. Wiss. 1960 28 1567.

51. Weinstein, M., Elliott, J.F., Trans. Met. Soc. AIME, 1963 227 285-286.

52. Luckenmeyer-Hasse, L., Schenk, H., Arch. Eisenh. 1932 6 209-214.

53. Lakomskii, V.I., "Gases in Cast Metals" Ed. B.B. Gulyaev 1965 251-255.

54. Sieverts, A., Krumbaar, W., Jursisch ; Z. Phys. Chem. 1911 77 591-613.

55. Liang, H., Bever, M.B., Floe, C.F., Trans. Met. Soc. AIME, 1946 167 395-403.

56. Bagshaw, T., Engledow, D., Mitchell, A., J.Iron Steel Inst., 1965 203 160-165.

57. Busch, T., Dodd, R.A., Trans. Met. Soc. AIME 1960 218 488-490.

58. Briggs, H.B., Johnson, J.B., Mason, W.P., J. Acoust. Soc. Amer. 1947 19 664.
Thorndike, A.M., Scientific Res. & Dev. Section C-4. Rep. No. 81496.

59. "Gmelins Handbuch der anorganischen Chemie. Kobalt, Teil A. Erganzungsband" Verlag Chemie, Weinheim, 1961.

60. Bagshaw, T., Mitchell, A., J. Iron Steel Inst., 1966 204 87-90.

61. Sieverts, A., Zapf. G., Moritz, H., Z.Phys.Chem. 1938 183 19

62. Burdese, A., Metallurgia Ital. 1955 47 357 366.

63. Pehlke, R.D., Elliott, J.F., Trans. Met. Soc. AIME 1960 218 1088-1101.

64. Dodd, R.A., Gokcen, N.A., Trans. Met. Soc. AIME 1961 221 233-236.

65. Tankis, S., Gokcen, N.A., Trans. A.S.M., 1961 53 843-852.

66. Dastur, M.N., Chipman, J., Trans. Met. Soc. AIME 1949 185 441-445.

67. Averin, V.V., Polyakov, A. Yu., Samarin, A.M.
Izv. Akad. Nauk SSSR OTN 1957 (8) 120-122.

68. Tankins, E.S., Gokcen, N.A., Belton, G.R., Trans. Met. Soc. AIME 1964 230 820-827.

69. Epstein, H., Chipman, J., Grant, N.J., Trans. Met. Soc. AIME 1957 209 597-608.

70. Parlee, N.A., Foundry 1956 84 Aug. 80-87.

71. Banya, S., Matoba, S., 1959 "Physical Chemistry of Process Metallurgy" Pt. 1. Vol. 7. Interscience, N.Y.

72. Chipman, J. "Basic Open Hearth Steelmaking" 2nd Edition, N.Y. 1951.

73. Halden, F.A., Kingery, W.D., J. Phys. Chem. 1955 59 557.

74. Tsarevskii, B.V., Popel, S.I., Fiz. Khim. Osnovy Proizv. Stali., 1961, 97-105.

75. Wang Ching-T'ang, Karasev, R.A., Samarin, A.M.
Fiz. Khim. Osnovy. Proizv. Stali, Moscow 1961, 106-111.

76. Kurochkin, K.T., Baum, B.V., Borodulin, E.K., Fiz. Met. Metall. 1963 15 (3) 461-462.

77. Eremenko, V.N., Naidich, Yu. V., Nosonovich, A.A., Z. Fiz. Khim. 1960 34 (5) 1018-1020, (6) 1186-1189.

78. Allen, B.C., Kingery, W.D., Trans. Met. Soc. AIME 1959 215 30-36.

79. Kozakevitch, P., Urbain, G., J. Iron Steel Inst. 1957 186 167-173.

80. Allen, B.C., Trans. Met. Soc. AIME 1963 227 1175-1183.

81. Kurochkin, K.T., Baum, B.A., Borodulin, E.K., 1963 Fiz. Met. Metall. 15 (3) 461-462.

82. Baum, B.A., Kurochkin, K.T., Umrikhin, P. V., Phys. Met. Metall. 1961 11 (6) 139-140. Izv. A.N. Met. i Toplivo 1961 (3) 82-89.

83. Volkov, S.E., Mchedlishvili, V.A., Samarin, A.M., Docklady Akad. Nauk SSSR 1963 149 (5) 1131-1133.

84. Dyson, B.F., Trans. Met. Soc. AIME 1963 227 1098-1102.

85. Monma, K., Suto, H., Trans. Japan Inst. Met. 1960 1 Oct. 69-76.

86. Popel, S.I., Tsarevsky, B.V., Dzhemilev, N.K., Fiz. Met. Metall. 1964 18 (3) 468-470.

87. Dzhemilev, N.K., Popel, C.I., Tsarevskii, B.V., Fiz. Met. Matall. 1964 18 (1) 83-87.

88. Smirnov, L.A., Popel, S.I., Tsarevskii, B.V., Izv. VUZ Chern.Met. 1965 (3) 10-14.

89. Vishkarev, A.F., Kryakovskii, Yu. V., Bliznyukov, S.A., Yavoiskii, V.I., Izv. VUZ Chern. Met. 1962 (3) 60-66.

90. Tumanov, V.I., Funke, V.F., Belen'yaya L.I., Usol'teva, L.P., Izv. Akad. Nauk. SSSR Met i Toplivo 1962 (Tekhn) (6) 43-48.

91. Kingery, W.D., Humenik, M., J.Phys.Chem. 1953 57 359.

92. Eremenko, V.N., Naidich, Y.V., Izv. Akad. Nauk SSSR Met. i Toplivo 1960 2 53-55.

93. Eremenko, V.N., Nizhenko, V.I., Ukrain. Khim. Zhur. 1964 30 (2) 125-132.

94. Eremenko, V.N., Nizhenko, V.I., Ukrain. Khim. Zhur. 1960 26 423-428.

95. (Armstrong, W.M., Chaklader, A.C.D., Clarke, J.F., J.Amer.Ceram.Soc. 1962 45 115-118.
(Clarke, J.F., M.S. Thesis, Univ. Br. Columbia, 1959.

96. Fesenko, V.V., Vasiliu, M.I., Eremenko, V.N., Zhur. Fiz. Khim. 1962 36 (3) 518-520.
Russ. J. Phys. Chem. 1962 36 269-271.

97. Eremenko, V.N., Naidich, Yu. V., Vasiliu, M.I., Izv. Akad. Nauk SSSR (Otdel Tekhn) Met. i Gornoe Delo 1963 5 64-66.

98. Davies, V. de L., West, J.M., J.Inst. Metals 1963-64, 92 (7) 208-210.

99. Eremenko, V.N., Ivashchenko, Yu N., Nizhenko, V.I., Fesenko, V.V., Izv. Akad. Nauk SSSR Otd. Tekh. Nauk 1958 7 144-146.

100. Korolkov, A.M., "Casting properties of metals and alloys" Consultants Bureau Trans. 1960.

101. Kubichek, L., Izv. Akad. Nauk SSSR Met i Topl. 1959 (Tekhn) (2) 96.

102. Naidich Yu, V., Eremenko, V.N., Phys. Met. Metall. 1961 11 (6) 62.

103. Kozakevitch, P., Chatel, S., Urbain G., Sage, M., Rev. Mét. 1955 52 139-160.

104. Lauerman, I., Sauerwald, F., Z. Metallk. 1964 55 (10) 605-612.

105. Metzger, G., Z. Phys. Chem. 1959 211 1.

106. Calverley, A., Proc. Phys. Soc. 1957 70B 1040.

107. Belforti, D.A., Lepie M.P., Trans. Met. Soc. AIME 1963 227 80-83.

108. Hondros, E.D., Proc. Roy. Soc. 1965 286A 479-498.

109. Price, A.T., Holl, H.A., Greenough, A.P., Acta Met. 1964 12 49-58.

110. Mazanec, K., Kamenska, E., Phys. Met. Metall. 1961 12 (1) 79-83.

111. Jones, H., Leak, G.M., Acta Met. 1966 14 21-27.

112. Hayward, E.R., Greenough, A.P., J.Inst.Metals 1960 88 217.

113. Hoage, J.H., Hanford Atomics 1963 H.W. 78132.

114. Udin, H., Trans. Met. Soc. AIME 1951 191 63.

115. Pranatis, A., Pound, M., Trans.Met.Soc. AIME 1955 203 664.

116. Turnbull, D., J.Appl.Phys. 1950 21 1022-1028.

117. Ward, R.G., J. Australian Inst. Metals. 1965 10 (3) 278.

118. Shashkov Yu, M., Kolesnikova, T.P., Russ. J. Phys. Chem. 1963 37 (6) 747-748.

119. Gel'd, P.V., Petrushevskii, M.S., Izv. Akad. Nauk SSSR Otd. Tekh. Nauk 1961 (3) 160.

120. Kingery, W.D., J. Amer. Ceram. Soc. 1959 42 6-10.

121. Popel, S.I., Esin, O.A., Russ. J. Inorg. Chem. 1957 11 (3) 252-269.

122. King, T.B., Symposium Phys. Chem. of Melts 1953 Inst. Mining Metallurgy, London.

123. Panov, A.S., Kulikov, I.S., Tsylev, L.M., Russ. J. Phys. Chem. 1962 36 722-723.

124. Cooper, C.F., Kitchener, J.A., J. Iron Steel Inst. 1959 193 48-55.

125. Swisher, J.H., McCabe, C.L., Trans. Met. Soc. AIME 1964 230 1669-1675.

126. Kozakevitch, P., "Liquids; structure, properties, solid interactions" Hughel, T.J., 1965, Elsevier, Amsterdam.

127. Ermolaeva, E.V., Ogneupory 1955 20 221-228.

128. Smolyarenko, V.D., Yakushev, A.M., Edneral, F.P., Izv. VUZ Chern. Met. 1965 (3) 36-41.

129. Mikiashvili, S.M., Soobshch. Akad. Nauk Gruz SSR 1962 29 (5) 549-554.

130. Kozakevitch, P.P., Kononenko, A.F., Russ. J. Phys. Chem. 1940 14 1118.

131. Popel, S.I., Esin, O.A., Zhur. Fiz. Khim. 1965 30 1193.

132. Mikiashvili, S.M., Samarin, A.M., Tsylev, L.M., Izv. Akad. Nauk SSSR Otdel Tekh. Nauk 1957 4 54-62.

133. King, T.B., J. Soc. Glass Tech . 1951 35 241-259.

134. Leonteva, A.A., J. Colloids USSR 1949 11 (3) 176-177.

135. Kheifets, B.L., Sheinin, A.B., Zhur. Prikl. Khim. 1959 32 1039-1042.

136. Sokolov, O.K., Izv. Akad. Nauk SSSR Otdel Tekh. Nauk Metall. 1965 (1) 97-103.

137. Boni, R., Derge, G., J. Metals 1956 8 53-64.

138. Lepinskikh, V.M., Esin, O.A., Teterin, T.A., Zhur. Neorgan, Khimii 1960 5 (3) 642.

139. Manakov, A.I., Esin, O.A., Lepinskikh, B.M., Russ. J. Phys. Chem. 1962 36 1257-1259.

140. Appen, A.A., Schischow, K.A., Kayalov, S.S., Silikat Tech. 1953 4 104-105.

141. Evseyev, P.P., Filipov, A.F., Izv. VUZ Chern. Met. 1965 (3) 70-73.

142. Int. Crit. Tables 1930 Nat. Research Council, U.S.A.

143. Mitchell, D.W., Mitoff, S.P., Zackay, V.F., Pask, J.A., Glass Ind. 1952 33 515-523.

144. Kingery, W.D., J. Amer. Ceram. Soc. 1954 37 42-45.

145. Livey, D.W., Murray, P., J. Amer. Ceram. Soc. 1956 39 363. Plansee Proc. Chapter 32 (Ed. F. Benesovsky) 1956.

146. Jura, G., Garland, C., J. Am. Ceram. Soc. 1952 74 6033.

147. Gilman, J.J., J. Appl. Phys. 1960 31 2208-2218.

148. Parikh, N., J. Amer. Ceram. Soc. 1958 41 18.

149. Humenik, M., Whalen, T.J., "Cermets" Chapter 1. Editors: Tinklepaugh, J.R. and Crandall, W.B., Reinhold Publishing Co. 1960.

150. Patterson, W., Ammann, D., Engler, S., Giesserei Techn.-Wiss. Beiheft 1958 10 1037.

151. Humenik, M.H., Kingery, W.D., J. Amer. Ceram. Soc. 1954 37 18-23.

152. Armstrong, W.M., Chaklader, A.C.D., Rose, D.J., Trans. Met. Soc. AIME 1963 227 1109-1115.

153. Kamyshov, V.M., Esin, O.A., Chuchmarev, S.K., Zh. Fiz. Khim. 1966 40 262-263.

154. Ramqvist, L., Int. J. Powder Met. 1965 1 (4) 2-21.

155. Ereremenko, V.N., Naidich, Yu, V., Russ J. Inorg. Chem. 1959 4 (9) 931.

156. Tumanov, V.I., Funke, V.F., Belenkaya, L.I., Russ. J. Phys. Chem. 1962 36 847.

157. Tumanov, V.I., Funke, V.F., Belenkaya, C.I., Soviet Powder Met., 1963 5 (17) 376-378.

158. Whalen, T.I., Humenik, M., Trans. Met. Soc, AIME 1960218·952-956

159. Eremenko, V.N., Nizhenko, V.I., Russ. J. Phys. Chem. 1961 35 (6) 638-640.

160. Naidich, Yu, V., Kolesnichenko, G.A., Soviet Powder Met. 1964 (3) 191-195.
1963 1 (13) 35-38.

161. Eremenko, V.N., Naidich, Yu, V., "The Wetting of Refractory Compounds with Liquid Metals", Akad. Sci. Ukrain. SSr., Kiev. 1958.

162. Cline, R.W., Fulrath, R.M., Pask, J.A., J. Amer. Ceram. Soc. 1961 44 423-428.

163. Ellefson, B.S., Taylor, N.W., J. Amer. Ceram. Soc. 1938 21 193,205.

164. Bartlett, R.W., Hall, J.K., Bull. Amer. Ceram. Soc. 1965 44 444-448.

165. Comeford, J.E., Hursh, R.K., J. Amer. Ceram. Soc. 1952 35 130-134.

166. Popel, S.I., Esin, O.A., Geld, P.V., Dokl. Akad. Nauk SSSR 1950 74 (6) 1097-1100.

167. Esin, O.A., Nikitin, Y.P., Popel, S.I., Dokl. Akad. Nauk SSSR 1952 83 (3) 431.

168. Kozakevitch, P., Urbain, G., Sage, M., Rev. Mét. 1955 52 139,161. (Transl. in Iron Coal Trade Rev. 1955 170 963).

169. Mori, K., Fajimura, T., Tetsu-to-Hagane 1955 41 495-500.

170. Mikiashvili, S.M., Samarin, A.M., Tsyler, L.M., Akad. Nauk SSSR Otdel. Tekh. Nauk 1957 4 54-62.

171. Popel. S.I., Esin, O.A., Konovalov, G.F., Smirnov, N.S., Dokl. Akad. Nauk SSSR 1957 112 104-106.

172. Yakobashvili, S.B., Frumin, I.I., Avtom. Svarka 1961 10 (103) 14-19.

173. Yakobashvili, S.B., Avtom. Svarka 1962 8 (113) 38-43.

174. Smolyarenko, V.D., Yakushev, A.M., Edneral, F.P., Izv. VUZ Chern. Met. 1965 (3) 36-41.

157. Bobkova, O.S., Petukhov, V.S., Zheladnov, V.I., Sbornik Trudov Tsniichm. Teoria Metall. Protsessov 1965 40 35-40.

176. Hamijan, H., Lidman, W., J. Amer. Ceram. Soc. 1952 35 44.

177. Baxter, J., Roberts, A., Powder Metallurgy Symposium, London, Iron & Steel Inst., 1954 p. 63.

178. Garland, J., Norton, L., J. Metals 1952 4 1051.

179. Samsonov, G.V., Markovskii, L. Ya., Zhigach, A.F., Balyashko, M.G., Boron, Its Compounds and Alloys, Izd. A N UkrSSR, Kiev 1960.

180. Belyaev, A.I., Zhemchuzhina, E.A., Surface Phenomena in Metallic Processes, Metallurgizdat, Moscow 1952.

181. Shafrin, E.G., Zisman, W.A., Advan.Chem.Ser. 1964 43 145-157.

182. Sullivan, E.L., Hardy, B.W., Holland, C.P., Am. Inst. Chem. Engrs. J. 1964 10 (6) 848-854.

183. Joutz, P.D., Myers, J.E., Am.Inst.Chem.Engrs.J.1960 6 34-38.

184. Newman, P.C., Whelan, P.F., Nature (London), 1952 169 326.

185. Hsu, Y.Y., J. Heat Transfer, 1962 84 207-216.

186. Outhwaite, J.G., "Gases in Liquid Metals", Ph.D. Thesis, Birmingham University 1961.

187. Lieberman, L., J. Appl. Phys. 1957 28 205-211.

188. Epstein, P.S., Plesset, M.S., J. Chem.Phys. 1950 18 1505-1509.

189. Plesset, M.S., Zwick, S.A., J.Appl.Phys. 1954 25 493-500.

190. Forster, H.K., Zuber, N., J.Appl.Phys. 1954 25 474.

191. Birkhoff, G., Margulies, R.S., Horning, W.A., Phys. Fluids 1958 1 201-204.

192. Barlow, E.J., Langlois, W.E., I.B.M. J. Res. Develop. 1962 6 239-237.

193. Zadumkin, S.N., Russ.J.Phys.Chem. 1961 35 (12) 1397-1398.

194. Reiss, H., Wilson, I.B., J. Colloid. Sci. 1948 3 551-561.

195. Byers, H.R., Chary, S.K., Z.Angew Math.Phys. 1963 14 428-433.

196. Shcherbakov, L.M.,

Issled. v. Obl. Poverkhn. Sil, Akad Nauk SSR Inst. Fiz. Khim., Sb. Dokl. na Vtoroi Konf., Moscow 1962 17-25. (Published 1964) Chem. Abs. 56 972, 9451.

197. Shcherbakov, L.M., Rykov, V.I., Kolloid Zhur. 1961 23 221-227.

198. Kirkwood, J.G., Buff, F.P., J.Chem.Phys. 1949 17 338.

199. Buff, F.P., J.Chem.Phys. 1951 19 1591-1594
1955 23 419-427.

200. Bellemans, A., Physica 1963 29 (5) 548-554.

201. Flint, O., J. Nuclear Mat. 1965 16 233-248.

202. Dean, R.B., J.Appl.Phys. 1944 15 (5) 446-451.

203. Hanson, D., Pell-Walpole, W.T., "Chill-Cast Tin Bronzes" 1951 Arnold, London.

204. Hudson, F., Trans.Amer.Found.Soc. 1965 73 65-83.

205. Dehaven, J., Davis, J.A., Eastwood, L.W., Trans.Am. Found.Soc. 1945 53 180-9.

206. Flinn, R.A., Trans.Amer. Found.Soc. 1956 64 665-7.

207. Savic, P., Gosnell, J.W., Can.J.Chem.Engr. 1962 40 238-45.

208. Tolubinskii, V.I., Chem.Abs. 1963 59.1 227.

209. Stralen, S.J.D. van, Physics 1963 29 (6) 502-16.

210. Davies, V. de L., J.Inst.Metals 1963-64 92 127;
1964-65 93 10.

211. Rayleigh (Lord), Phil. Mag. 1917 34 94-98.

212. Silver, R.S., Engineering 1942 154 501-2.

213. Blake, F.G., "The Onset of Cavitation in Liquids: I" Tech. Memo No.12. Acoustics Research Lab., Harvard Univ. 1949.

214. Ruddle, R.W., "The Solidification of Castings" Inst. Metals Monograph No.7. 1957. Revised 2nd Edition.

215. Ramqvist, L., Powder Met. 1966 9 (17) 1-25.

216. Nelson, R.S., Mazey, D.J., Barnes, R.S.., Phil. Mag. 1965 11 (109) 91-111.

217. Hoffman, R.D., Myers, R.R., Trans.Soc.Rheol. 1961 5 317:
1962 6 197-207.

218. Parsons, D.E., Trans.Amer.Found.Soc. 1963 71 433-53.

219. Heide, O., "Porosity in Steel Castings" 26th Int. Foundry Congress 1959 Paper No. C-13. Transl. by Br. Steel Castings Research Assocn. No. 145/CMH. 1960.

220. Schwartz, A.M., Rader, C.A., Huey, E., Advan.Chem.Ser. 1964 43 250-267.

221. Koida, N.U., Bukhbinder, M.A., Russ.J.Phys.Chem. 1962 32 637-640.

222. Barrer, R.M., Disc. Farad. Soc. 1948 3 61-72.

223. Adam, N.K., Disc. Farad. Soc. 1948 3 5-11.

224. Sullivan, R.R., Hertel, K.L., Advan.Colloid. Science 1 1942 37-72.

225. Carman, P.C., Disc. Farad. Soc. 1948 3 72-77.

226. Reekle, J., Aird, J., Nature 1945 156 367-368.

227. Wallace, J.F., (ed.), "Fundamentals of Risering Steel Castings" 1960 Steel Founders' Soc., Cleveland, Ohio.

228. Baker, W.A., J. Inst. Metals 1945 71 165-204.

229. Pellini, W.S., Trans.Amer.Found.Soc. 1953 61 61-80.

230. Piwonka, T.S., Flemings, M.C., Trans.Met.Soc. AIME 1966 236 1157-65.

231. Singer, A.R.E., Cottrell, S.A., J.Inst.Metals 1947 73 33-54.

232. Brown, R.L., "Powders in Industry" Soc.Chem.Ind. Monograph No. 14. 1961 150-166.

233. Walter, W.P., Adams, C.M., Taylor, H.F., Trans.Amer. Found. Soc. 1956 64 658-64.

234. Reynolds, O., Mem.Manch.Lit. and Phil.Soc. 1878 17 159, 1882 7 1.
Papers on Mechanical & Physical Subjects, Cambridge 1901 2 573.

235. Liddiard, E.A.G., J.Inst.Metals 1945 71 631-4; 653-4.

236. Prandtl, L., Teitjens, O.G., "Fundamentals of hydro- and aero-dynamics", McGraw Hill, New York 1934 pp. 189-223.

237. Neufville, A. de., "The Dying Vortex" 5th Midwestern Conf. on Fluid Mechanics 1957 (Pub. Ann Arbor 1957) pp. 365-375.

238. Svensson, N.L., J.Appl.Mech. 1958 25 (1) 89-96.

239. Ruddle, R.W., Trans.Amer.Found.Soc. 1960 68 685-90.

240. Chamberlain, B., Sulzer, J., Trans.Amer.Found.Soc., 1964 46 (4) 600-607.

241. Jackson, R.S., Foundry Trade J. 1956 100 487-93.

242. Atkins, A.G., Silverio, A., Tabor, D., J.Inst. Metals 1966 94 369-378.

243. Mackenzie, J.D., Shuttleworth, R., Proc.Phys.Soc. 1949 62B 833-52.

244. Nussey, I.D., Int.J.Mech.Sci. 1964 6 263-72.

245. Sellars, C.M., Tegart, W.J.McG., Rev. Mét. 1966

246. Flemings, M.C., Uram, S.Z., Taylor, H.F., Trans.Amer. Found. Soc. 1960. 68 670-84.

247. Eger, W., "Giessereikunde für Eisen und Stahl", Berlin 1954 Volk u. Wissen Verlag. 428.

248. Fox, F.A., J.Inst.Metals 1945 71 415, 630.
Metal Industry, 1944 64 101, 144.

249. Engler, S., Z.Metallk. 1965 56 (6) 327-35.

250. Köchling, H., Freiberg, Forschungsh, 1964 (B84) 69-104.

251. Guillet, L., Galibourg, J., Ballay, M., Rev. Mét. 1925 22 253.

252. Cowan, W.A., J.Inst.Metals 1928 29 53-8.

253. Ohmann, H., "Allgemeine und Praktische Metallkunde" Leipzig 1955 Fachbuchverlag 193.

254. Poetter, H., Iron and Steel 1956 29 443-5.

255. Balewsky, A., Dimov. I., 33rd Int.Foundry Congress. Dec. 1966.

256. Beeton, (Mrs.) "Household Management" Dobson (London) 1963.

257. Deoras, B.R., Kondič, V., Foundry Tr. J. 1956 100 361-4, 6.

258. Metcalf, G.D., J.Inst.Metals 1945 71 618-9.

259. Ransley, C.E., Talbot, D.E.J., Z.Metallk. 1955 46 328.

260. Smialowski, M., "Hydrogen in Steel" Pergamon Press 1962 London, p. 279.

261. Briggs, H.B., Johnson, J.B., Mason, W.P., J.Acoust.Soc. Amer. 1947 19 664.

262. Brondyke, K.J., Hess, P.D., Trans.Met.Soc. AIME 1964 230 1542-6.

263. Abramov, O.V., Teumin, I.I., Phys.Met.Metall. 1964 17 (5) 146-9.

264. Bogdanov, M.T., Russ. Castings Production 1962 (7) 330-4.

265. Bracale, C., Trans.Amer.Found.Soc. 1962 70 223-52.

266. Flemings, M.C., Trans.Amer.Found.Soc. 1960 68 330.

267. Flemings, M.C., Taylor, H.F., Trans.Amer.Found.Soc., 1959 67 734-7.

268. Flinn, R.A., Mielke, C.R., Trans.Amer.Found.Soc. 1959 67 385-92.

269. Flinn, R.A., Kunsmann, H.G., Trans.Amer.Found.Soc. 1961 69 208-220.
1962 70 1295-1309.

270. Murthy, K., Seshadri, M., Ramachandran, A., Trans.Amer. Found.Soc. 1965 73 502-8.

271. Johnson, W.H., Bishop, H.F., Pellini, W.S., Trans.Amer. Found.Soc. 1954 62 243-51.

272. Green, R.D., Trans.Amer.Found.Soc. 1960 68 245-52.

273. Johnson, W.H., Kura, J.G., Trans.Amer.Found.Soc. 1959 67 535-52.

274. Bishop, H.F., Myskowski, E.T., Pellini, W.S., Trans.Amer. Found.Soc. 1951 59 171, 435-450.

275. Czikel, J., Freiberger Forschungshefte 1960 B45 7-20. Brit. Steel Castings Research Assoc. Transl. No. 202/CMM. 1961.

276. Bardot, M., Fonderie 1952 83 3207-26.

277. Eastwood, L.W., Davis, J.A., Amer.Foundryman 1946 9 (4) 148-155.

278. Jay, R., Cibula, A., Foundry Tr.J. 1956 101 131.

279. Lees, D.C.G., J.Inst.Metals 1946 72 343-64.

280. Scheil von E., Z. Metallk. 1942 34 70-72.

281. Pfann, W.G., J. Metals 1952 4 747-53.

282. Gulliver, G.H., J.Inst. Metals 1913 9 120-53;
1914 11 252-73;
1915 13 263-91.

283. Lagowski, B., Meier, J.W., Trans.Amer.Found.Soc. 1964 72 561-74.

284. Pollard, W.A., Trans.Amer.Found.Soc. 1964 72 587-99.

285. Budgen, N.F., J.Inst.Metals 1929 42 119-40.

286. Bhattacharjya, A.K., Ph.D. Thesis, Industrial Metallurgy Dept., Univ. Birmingham, 1963.

287. Flemings, M.C., Barone, R.V., Uram, S.Z., Taylor, H.F., Trans.Amer.Found.Soc. 1961 69 422-35.

288. Chalmers, B., Newkirk, J., Unpublished work quoted in reference 11.

289. Uhlmann, D.R., Chalmers, B., Jackson, K.A., J.Appl.Phys. 1964 35 2986-2993.

290. Kramer, J.J., Bolling, G.F., Tiller, W.A., Trans.Met. Soc. AIME 1963 227 374.

291. Simonik, S., Trans.Amer.Found.Soc. 1962 70 622-631.

292. Jackson, W.J., J.Br.Steel Castings Res. Assoc. 1962 June 67.

293. Matushka, B., 26th Int. Foundry Congress, Madrid, 1959 Paper 16.

294. Vertman, A.A., Filippov, E.S., Samarin, A.M., Izvest. VUZ Chern.Met. 1964 (7) 19-23.

295. Ruddle, R.W., J.Inst.Metals 1950 77 1-59.

296. Present, H., Rosenthal, H., Trans.Amer.Found.Soc. 1961 39 70-72.

297. Adams, C.M., Metal Progress 1956 69 (5) 58-60.

298. Tedds, D.F.B., Br. Foundryman 1959 52 10-17.

299. Berry, J.T., Watmough, T., Trans.Amer.Found.Soc. 1961 69 11.

300. Briggs, C.W., Taylor, H.F., Foundry Tr.J. 1953 95 413-22.

301. Finch, S.L., Jazwinski, S.T., Foundry Tr.J., 1945 77 221.

302. Jamschanow, P.I., Symp. High Grade Steel Castings, Berlin 1955. Br. Steel Castings Res. Assoc. Transl. No. 66/EW. 1958.

303. Balewsky, A.T., Dimov, T., Br. Foundryman 1965 78 (7) 280-3. 33rd Int. Foundry Congress, New Delhi, 1966.

304. Uram, S.Z., Flemings, M.C., Taylor, H.F., Trans.Amer. Found.Soc. 1959 66 129-34.

305. Parker, R.T., Cox, G.M., Turner, A.N., J.Inst.Metals 1947 73 175-96.

306. Hanson, D., Slater, I., J.Inst.Metals 1935 56 103.

307. Babington, W., Kleppinger, D.H., A.S.T.M. Proc. 1951 51 169.

308. Gulyaev, B.B., Makelskii, M.F., Nazarenko, V.O., Lit. Proizv. 1960 12 33-4.

309. Colling, D.A., Adhearn, P.J., Flemings, M.C., Trans. Amer.Found.Soc. 1962 70 1083-94.

310. Liddiard, E.A.G., Baker, W.A., Trans.Amer.Found.Soc. 1945 53 54-65.

311. Cibula, A., Rundle, R.W., J.Inst.Metals 1949/50 76 361-76.

312. Cibula, A., Foundry Tr. J. 1955 93 713-26.

313. Calvert, D.S., Br. Non Ferrous Res. Assocn. Unpublished.

314. Irani, D., Department of Industrial Metallurgy.

315. Sullivan, E.J., Adams, C.M., Taylor, H.F., Trans.Amer. Found.Soc. 1957 65 394-401.

316. Brinson, S.W., Dumas, J.A., Trans.Amer.Found.Soc. 1942 50 657.

317. Wlodawer, R., Foundry Tr. J., 1963 114 (2) 251-9. (3) 283-9.

318. Hudson, F., Wood, D.R., Gregg, J.F., Proc.Inst.Br. Found. 1958 51 469.

319. Myskowski, E.T., Bishop, H.F., Pellini, W.S., Trans.Amer. Found.Soc. 1953 61 302-8.

320. Jagaciak, J., Jones, J.W., Foundry Tr.J. 1956 101 595-606. Coll.Aer. Rep. No.91. Sept. 1955.

321. Dimitrovich, A.M., Butsel, K.T., "Gases in Cast Metals" Edited by B.B. Gulyaev. Consultants Bureau, N.Y., 1965. pp. 128-132.

322. Avraamov, Yu. S., Semenov, V.M., Levin, I.Ya., Izv. VUZ. Chern. Met. 1966 9 (7) 129-32.

323. Czyzewski, H., Light Metal Age 1951 9 (11/12) 24,26.

324. Ljungberg, I., Gummeson, P.U., Prec. Met. Moulding 1959 17 30-31, 58.

325. Weins, M.J., Bottom, J.L.S. de., Flinn, R.A., Trans.Amer. Found.Soc. 1964 72 832.

326. Trojan, P.K., Weins, M.J., Flinn, R.A., Trans.Amer. Found.Soc. 1963 71 656-70.

327. Flinn, R.A., Kunsmann, H., Trans.Amer.Found.Soc. 1961 69 208-220.

328. Kulcinksi, G.L., Wagner, P., Cowder, L.R., J. Less Common Metals 1964 7 (5) 383-92.

329. Abrahams, C.J., Lavender, J.D., Br.Foundryman 1965 58 Feb. 66-73.

330. Smolen, H., Rosenthal, H., Trans.Amer.Found. Soc. 1959 67 257-262.

331. Hilliard, J.E., Cahn, J.W., Trans.Met.Soc.AIME 1961 221 344-52.

332. Cladman, T., Woodhead, J.H., J.Iron Steel Inst. 1960 194 189-93.

333. Burrill, E.A., Non-Destructive Testing 1955 13 (3) 19-21.

334. Trillat, J.S., Met. Reviews 1956 1 p.3.

335. Sharpe, R.S., "X-Ray Microscopy and Microradiography" p. 590. Cosslett, U.E., Engstrom, A., Pattee, H.H., Academie Press, N.Y., 1957.

336. Busk, R.S., Proc. ASTM 1942 42 1076-87.

337. Tzavaras, A.A., Flemings, M.C., Trans.Met.Soc. AIME 1965 233 355-9.

338. Ruddle, R.W., Br. Foundryman 1957 50 (12) 605-15.

339. Jones, W.R.D., Metal Industry 1944, Sept. 8. 65 146-149.

340. Jones, W.R.D., J.Inst. Metals 1945 71 649-650.

341. Dobkin, E., Foundry 1946 74 (10) 98-101, 178, 180, 182.

342. Baker, W.A., "Non-Ferrous Foundry Metallurgy, pp. 108-158 Ed. A.J. Murphy, Pergamon Press, London.

343. Eremenko, V.N., Ivashchenko, Yu. N., Bogatyrenko, B.B., "The Role of Surface Phenomena in Metallurgy" 1961 pp. 37-40.

344. Kozakevitch, P., Chatel, S., Sage, M., Compt. Rend. Acad. Sci., Paris 1953 236 2064.